

# Bayesian Penalized Transformation Models: Structured Additive Location-Scale Regression for Arbitrary Conditional Distributions

---

Johannes Brachem \*<sup>1</sup>, Paul F. V. Wiemann <sup>2</sup> and Thomas Kneib <sup>1</sup>

<sup>1</sup>Chair of Statistics, Georg-August-University Göttingen

<sup>2</sup>Department of Statistics, University of Wisconsin-Madison

April 9, 2024

## Abstract

Penalized transformation models (PTMs) are a novel form of location-scale regression. In PTMs, the shape of the response's conditional distribution is estimated directly from the data, and structured additive predictors are placed on its location and scale. The core of the model is a monotonically increasing transformation function that relates the response distribution to a reference distribution. The transformation function is equipped with a smoothness prior that regularizes how much the estimated distribution diverges from the reference distribution. These models can be seen as a bridge between conditional transformation models and generalized additive models for location, scale and shape. Markov chain Monte Carlo inference for PTMs can be conducted with the No-U-Turn sampler and offers straightforward uncertainty quantification for the conditional distribution as well as for the covariate effects. A simulation study demonstrates the effectiveness of the approach. We apply the model to data from the Fourth Dutch Growth Study and the Framingham Heart Study. A full-featured implementation is available as a Python library.

---

\*Corresponding author: [brachem@uni-goettingen.de](mailto:brachem@uni-goettingen.de)

# 1. Introduction

We consider the location-scale regression model

$$Y = \mu(\mathbf{x}) + \sigma(\mathbf{x})\varepsilon \quad (1)$$

for a univariate, absolutely continuous response  $Y$ . The location  $\mu(\mathbf{x}) \in \mathbb{R}$  and scale  $\sigma(\mathbf{x}) \in \mathbb{R}_{>0}$  depend on a vector of covariate observations  $\mathbf{x}$ . We write both terms as depending on the same vector  $\mathbf{x}$  only for notational convenience; in practice different covariates can be used in the two terms. The residual  $\varepsilon$  is assumed to have expectation zero and variance one. This model is a powerful tool for accounting for heteroscedasticity and opens up possibilities for insight not only into how covariates relate to the mean of a response, but also its scale. For both frequentist and Bayesian inference, the model is generally completed by assuming a parametric distribution for the residual term; most commonly the standard normal distribution. In this paper, we introduce penalized transformation models (PTMs) as a way to relax this assumption. The approach can be seen as a conditional transformation model (CTM, [Hothorn et al., 2014](#)) with a modified transformation function. In PTMs, the residual's cumulative distribution function (CDF) is specified as  $F_\varepsilon(\varepsilon) = F_Z(h(\varepsilon))$ , where  $h : \mathbb{R} \rightarrow \mathbb{R}$  is a monotonically increasing and at least once differentiable function that transforms the residual to follow a reference distribution with continuous CDF  $F_Z : \mathbb{R} \rightarrow [0, 1]$ . This construction directly implies a definition of the conditional probability density of the response via the change of variables theorem as

$$f_Y(y|\mathbf{x}) = \frac{\partial}{\partial y} F_Z \left( h \left( \frac{y - \mu(\mathbf{x})}{\sigma(\mathbf{x})} \right) \right) = f_Z(h(\varepsilon)) \left| \frac{\partial}{\partial \varepsilon} h(\varepsilon) \right| \frac{1}{\sigma(\mathbf{x})}, \quad (2)$$

where  $f_Z$  denotes the density of the selected reference distribution. We denote by  $\varepsilon$  both the random variable and the observed residual, depending on context. If we choose the standard normal distribution as the reference distribution and the identity function for  $h$ , so that  $F_\varepsilon(\varepsilon) = \Phi(\varepsilon)$ , the model falls back to the normal location-scale model  $Y \sim \mathcal{N}(\mu(\mathbf{x}), \sigma(\mathbf{x})^2)$ . Since it allows the model to deviate from the reference distribution, the transformation function  $h$  is a major focus of inference in PTMs. We construct it around a monotonically increasing penalized spline (see [Lang & Brezger, 2004](#); [Pya & Wood, 2015](#)), giving the model its full name.

**Motivation.** The development of PTMs is motivated by the observation that the residual distribution implies a form for the response's conditional distribution, and assuming a parametric residual distribution can easily prove too restrictive in practice. [Figure 1](#) shows two examples of such cases. Consider a true data-generating process  $Y = \beta_0 + \beta_1 x_1 + \beta_2 x_2 + \varepsilon$ , where  $\varepsilon \sim \mathcal{N}(0, 1)$ . If we do not observe  $x_2$ , we may fit a reduced model  $Y = \beta_0 + \beta_1 x_1 + \varepsilon$  using the available data under the assumption that  $\varepsilon \sim \mathcal{N}(0, \sigma^2)$ . It is well known that, if  $x_1$  and  $x_2$  are uncorrelated or  $\beta_2 = 0$ , we can still obtain unbiased estimates for  $\beta_1$  in this model. However, the model also defines a conditional distribution for the response, in this case  $Y|x_1 \sim \mathcal{N}(\beta_0 + \beta_1 x_1, \sigma^2)$ , and this conditional distribution can be wrong if  $\beta_2 \neq 0$  and  $x_2$  is not included – even if the true residual

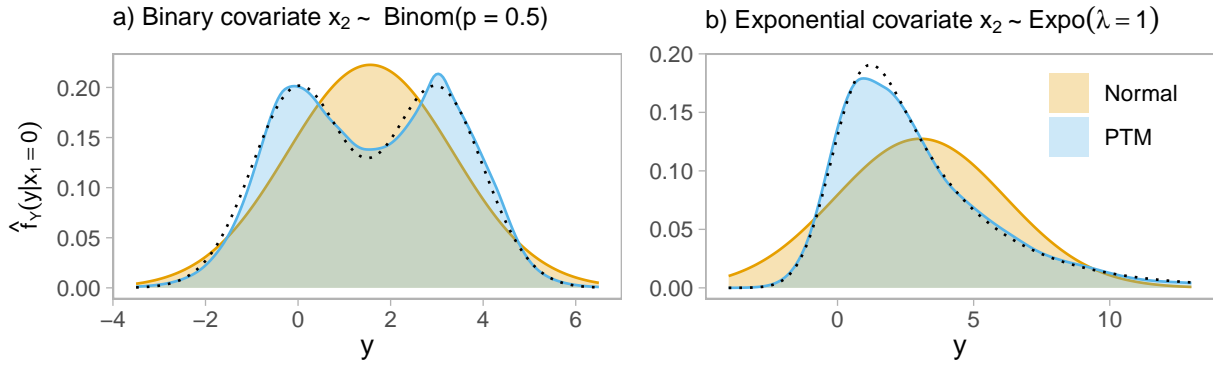


**Figure 1** Conditional densities of  $Y$  given  $x_1 = 0$  in the model  $Y = \beta_0 + \beta_1 x_1 + \varepsilon$ , with a gaussian error distribution (Normal model, yellow), and a nonparametrically estimated error distribution (PTM, blue). The models were fitted on the same data, generated from  $Y = x_1 + 3x_2 + \varepsilon$  with  $\varepsilon \sim \mathcal{N}(0, 1)$ , where  $x_1 \sim \mathcal{U}(-2, 2)$  and  $x_2$  was generated as shown in the panel titles. The dotted line show the true conditional density given  $x_1 = 0$  with  $x_2$  integrated out. The models were fitted on 1000 observations.

distribution is normal. In panel a), a binary  $x_2$  induces a bimodal conditional distribution, and in panel b) an exponentially distributed  $x_2$  induces a right-skewed conditional distribution. To obtain an accurate representation of the response’s conditional distribution given  $x_1$ , we can reparameterize the model to  $Y = \beta_0 + \beta_1 x_1 + \tilde{\varepsilon}$ , where  $\tilde{\varepsilon} = \beta_2 x_2 + \varepsilon$  denotes a residual that includes  $x_2$ , and infer the distribution of  $\tilde{\varepsilon}$  directly from the data.

As an illustrative example, take the “dutch boys” dataset provided in the R package `gamlss.data` (Stasinopoulos et al., 2021). It consists of cross-sectional measurements of the body mass index (BMI) and age of dutch boys between the ages 0 and 21 years. The data originates from the Fourth Dutch Growth Study (Fredriks, van Buuren, Wit, et al., 2000; Fredriks, van Buuren, Burgmeijer, et al., 2000). When analyzing this data, it is not only the average BMI of the subjects that is of interest. On the contrary, to assess public health, it is important to gain insight into obesity and underweight. When modeling the BMI conditional on age, we can translate this interest into specific questions about the quantiles of the conditional distribution of BMI given subjects’ age, and under the assumption of a normal distribution for the residuals in a regression model, such conditional quantiles are easily derived. However, as Figure 2 shows, a visual inspection of these conditional quantiles alongside a scatterplot of the data suggests that both the 0.01 and 0.99 quantile are heavily underestimated in the normal model. A penalized transformation model yields a right-skewed conditional distribution (panel c), which leads to a considerable improvement (panel b). In Section 5.1, we describe the analyses in detail, including a comparison to quantile regression.

**Related literature.** Penalized transformation models provide a bridge between generalized additive models for location, scale, and shape (GAMLSS, Rigby & Stasinopoulos, 2005) and conditional transformation models (CTMs, Hothorn et al., 2014, 2018). In GAMLSS, we assume a parametric distribution for the response’s conditional distribution given the covariates, and relate one or more of this distribution’s parameters to covariates. In CTMs, the response’s conditional CDF is specified nonparametrically as  $F_Y(y|\mathbf{x}) = F_Z(h(y|\mathbf{x}))$ , with inference and

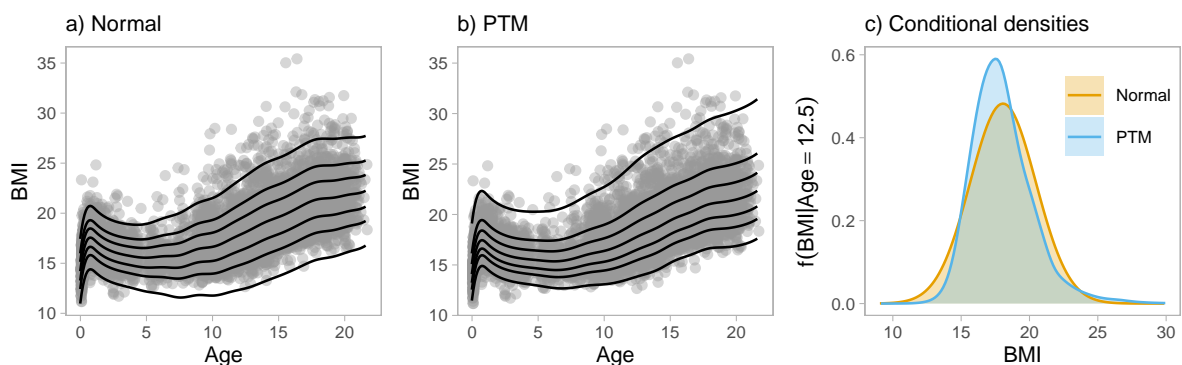


**Figure 2** Panels a) and b) show quantile curves for the “dutch boys” data implied by a normal location-scale model and a location-scale penalized transformation model (PTM), respectively. The curves refer to the probability levels 0.01, 0.1, 0.25, 0.5, 0.75, 0.9, and 0.99. Panel c) shows the conditional distributions implied by the two models for a fixed age of 12.5 years.

modeling focused on the conditional transformation function  $h(y|\mathbf{x})$ . This function is additively decomposed as  $h(y|\mathbf{x}) = \sum_{j=1}^J h_j(y|\mathbf{x})$ , and the partial transformation functions  $h_j$  are parameterized as tensor product splines  $h_j(y|\mathbf{x}) = (\mathbf{a}_j(y)^\top \otimes \mathbf{b}_j(\mathbf{x})^\top)^\top \boldsymbol{\gamma}_j$ , where  $\otimes$  denotes the Kronecker product. Depending on the researcher’s choice for the bases  $\mathbf{a}_j(y)$  and  $\mathbf{b}_j(\mathbf{x})$ , CTMs can capture all moments of the conditional response distribution dependent on covariates. They can provide great flexibility, but their interpretability is limited. PTMs occupy a middle ground, offering a conditional response distribution with location and scale parameters, while the distribution’s shape is specified nonparametrically. Bayesian formulations and inference for GAMLSS and CTMs were developed by Umlauf et al. (2018) and Carlan et al. (2023), respectively.

Siegfried et al. (2023) recently presented transformation additive models for location and scale (TAMLS). Like PTMs, these models can be viewed as hybrids of GAMLSS and CTMs. In TAMLS, the response’s conditional distribution is set up as  $F_Y(y|\mathbf{x}) = F_Z(\mu(\mathbf{x}) + \sigma(\mathbf{x})^{-1}h(y))$ , and the transformation function  $h$  is parameterized with Bernstein polynomials. When written instead as  $h(y) = \sigma(\mathbf{x})^{-1}\mu(\mathbf{x}) + \sigma(\mathbf{x})z$ , where  $z \sim F_Z$ , it becomes evident that  $\mu(\mathbf{x})$  and  $\sigma(\mathbf{x})$  reflect the location and scale of the transformed response  $h(y)$ . The transformation function in TAMLS thus resembles the link function of a generalized additive model, whereas they can be interpreted directly on the level of the response in PTMs. In Section A of the supplemental materials, we illustrate this point with additional detail.

Beyond the family of transformation models, Hanson & Johnson (2002) and Leslie et al. (2007) set up response-level models similar to (1) with flexible nonparametric estimates for the residual distribution. Specifically, Hanson & Johnson (2002) use a mixture of Polya trees, and Leslie et al. (2007) use a Dirichlet process mixture prior. Both limit their exploration to purely linear covariate effects. In comparison to Dirichlet process mixture priors, a big appeal of penalized transformation models lies in their reduced complexity: instead of thinking about an infinite-dimensional mixture, organized in a three-levelled hierarchy, PTMs allow researchers to think

about a single transformation function that resembles the well-known quantile-quantile plots. As a welcome byproduct of their conceptual sparsity, PTMs are straightforward to set up and fit to data - in fact, they can be thought of as a drop-in replacement for gaussian location-scale regression.

**Contributions.** In this paper, we make the following contributions:

- In Section 2, we develop a transformation model specifically tailored for providing a maximum of interpretability for the conditional response distribution. The transformation function regulates the model’s deviation from the base model, usually a gaussian location-scale model. We show how the model can be extended to cover count responses and censored responses.
- In Section 3, we provide details on our fully Bayesian Markov chain Monte Carlo inference using the No-U-turn sampler (NUTS, Hoffman & Gelman, 2014) and provide computational details.
- In Section 4, we present extensive simulation studies to assess the performance of PTMs for recovering a wide range of different residual distributions and obtaining unbiased and efficient estimates for nonlinear location and scale effects. We compare PTMs to Gaussian location-scale regression, quantile regression, and conditional transformation models.
- In Section 5, we apply the model to data from the Fourth Dutch Growth Study and the Framingham Heart Study, showcasing its usage and providing additional contrasts to quantile regression and conditional transformation models.
- In Section 6, we lay out future developments based on PTMs and conclude the paper.
- We provide a feature-rich open source implementation in the Python library `liesel-ptm`. The library is described in Section B.3 of the supplemental materials.

## 2. Penalized Transformation Models

The basic model formulation is given by (1), with  $\mathbb{E}(\varepsilon) = 0$ ,  $\text{Var}(\varepsilon) = 1$ , and the residual distribution given by  $F_\varepsilon(\varepsilon) = F_Z(h(\varepsilon))$ , where  $h$  is the transformation function and  $F_Z$  is the CDF of the reference distribution. We assume that the reference distribution is specified in standardized form with expectation zero and variance one.

### 2.1. Transformation function

We set up the transformation function  $h$  around a monotonically increasing B-spline (Pya & Wood, 2015). At the far ends, where no information is available from the data, the function smoothly transitions to a linear function with slope one. In these linear function segments, the model thus falls back to a location-scale model for the family of the reference distribution. Figure 3 shows two illustrations of the transformation function and its derivative using two

sets of arbitrarily chosen parameters in the spline segments. In the following, we first state the transformation function once in full before elaborating on the construction of its individual parts. The full transformation function is given by

$$h(\varepsilon) = \alpha + \begin{cases} \varepsilon + \text{spline}(a - \lambda) - (a - \lambda) & \text{if } \varepsilon \in (-\infty, a - \lambda) & \text{(linear),} \\ \frac{\varepsilon}{\lambda} \left[ a - \frac{\varepsilon}{2} + \left( \lambda - a + \frac{\varepsilon}{2} \right) \cdot \frac{\partial}{\partial a} \text{spline}(a) \right] + A & \text{if } \varepsilon \in [a - \lambda, a) & \text{(transition),} \\ \text{spline}(\varepsilon) & \text{if } \varepsilon \in [a, b] & \text{(core),} \\ \frac{\varepsilon}{\lambda} \left[ \frac{\varepsilon}{2} - b + \left( \lambda + b - \frac{\varepsilon}{2} \right) \cdot \frac{\partial}{\partial b} \text{spline}(b) \right] + B & \text{if } \varepsilon \in (b, b + \lambda] & \text{(transition),} \\ \varepsilon + \text{spline}(b + \lambda) - (b + \lambda) & \text{if } \varepsilon \in (b + \lambda, \infty) & \text{(linear),} \end{cases} \quad (3)$$

where  $\lambda \in \mathbb{R}_{>0}$ ,  $a < b$ , and  $a, b, A, B \in \mathbb{R}$ . The parameter  $\alpha \in \mathbb{R}$  is an intercept. For a given sample  $\varepsilon_1, \dots, \varepsilon_N$ , and assuming the remaining parameters to be fixed, it can always be chosen to ensure that the sample mean of the transformed residuals  $h(\varepsilon_1), \dots, h(\varepsilon_N)$  is zero. We elaborate on this point in Section 3.2.

**Core segment.** The increasing spline with real-valued parameters  $\boldsymbol{\delta}^\top = [\delta_1, \dots, \delta_{J-1}]$  and  $\omega \in \mathbb{R}_{>0}$  at the core of the transformation is specified as

$$\text{spline}(\varepsilon) = \frac{\omega}{s(\boldsymbol{\delta})} \sum_{j=1}^J B_j(\varepsilon) \left( \sum_{\ell=2}^j \exp(\delta_{\ell-1}) \right), \quad (4)$$

where  $B_j(\varepsilon)$  is a third-order (cubic) B-spline basis evaluation. This B-spline relies on  $J + 4$  knots  $k_{-2} < k_{-1} < k_0 < \dots < k_J < k_{J+1}$ , where  $k_1, \dots, k_{J-2}$  are called the interior knots. The spline is strictly monotonically increasing for  $\varepsilon \in [k_1, k_{J-2}]$ . We use this observation to define the transformation function's core-segment by setting  $a = k_1$  and  $b = k_{J-2}$ . We use equidistant knots, i.e.  $d = k_{j+1} - k_j$  for all  $j = -2, -1, \dots, J$ . In practice, the choice of specific boundary knot locations  $a$  and  $b$  is important, because the transformation function is most flexible in the interval  $[a, b]$ . We describe our procedure for finding sensible knots in Section 3.2. The derivative of (4) is a B-spline of order 2 (see Eilers & Marx, 2021), given here by

$$\frac{\partial}{\partial \varepsilon} \text{spline}(\varepsilon) = \frac{\omega}{s(\boldsymbol{\delta}) \cdot d} \sum_{j=2}^J B_j^{(2)}(\varepsilon) \exp(\delta_{j-1}).$$

This function uses the same knots as (4), so to keep the correspondence of basis evaluations to knots consistent, we let the index of the sum start at  $j = 2$ . The term  $\omega/s(\boldsymbol{\delta})$  in (4) gives us fine-grained control over the scale of the transformation.

**Proposition 2.1** (Average slope of a monotonically increasing B-spline). *Let  $f : \mathbb{R} \rightarrow \mathbb{R}$  be a monotonically increasing B-spline  $f(\varepsilon) = \sum_{j=1}^J B_j(\varepsilon) \left( \sum_{\ell=2}^j \exp(\delta_{\ell-1}) \right)$  with bases of order 3, on an equidistant knot base  $k_{-2} < k_{-1} < k_0 < \dots < k_J < k_{J+1}$ , and with parameters  $\boldsymbol{\delta} \in \mathbb{R}^{J-1}$ . Let  $a = k_1$*

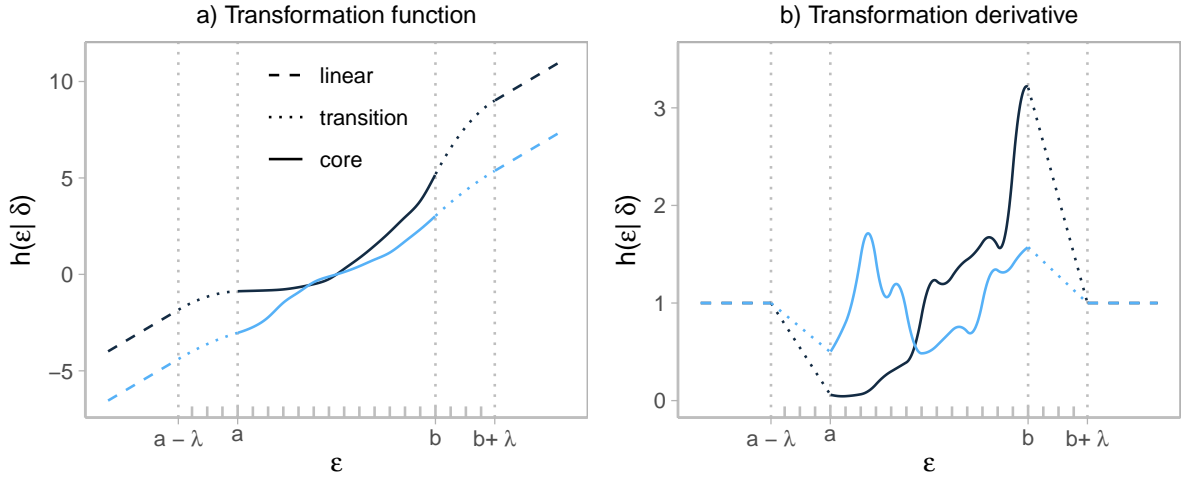


**Figure 3** Two examples for possible transformation functions and their derivative given the same fixed knot sequence. The knots are shown by grey upticks on the x-axis. Light grey vertical lines mark the boundaries of the function segments.

and  $b = k_{J-2}$  denote the boundary knots. Then the average slope of  $f$  over the interval  $[a, b]$  is given by

$$s(\boldsymbol{\delta}) = \frac{1}{b-a} \int_a^b \frac{\partial}{\partial \varepsilon} f(\varepsilon) d\varepsilon = \frac{1}{b-a} \sum_{j=1}^{J-3} \left( \frac{\exp(\delta_j) + \exp(\delta_{j+2})}{6} + \frac{2 \exp(\delta_{j+1})}{3} \right). \quad (5)$$

*Proof.* The proof is given in Section B.1 of the supplemental materials. □

From Proposition 2.1, it follows immediately that the average slope of  $f(\varepsilon)/s(\boldsymbol{\delta})$  over the interval  $[a, b]$  is one. Note also that we assume  $\text{Var}(\varepsilon) = 1$ . We use these observations to stabilize the variance of the transformed residuals. For  $\omega = 1$ , dividing by  $s(\boldsymbol{\delta})$  in (4) ensures that the variance of the transformed residuals is close to one for all  $\boldsymbol{\delta}$ . The scalar  $\omega$  can allow the model to correct for small deviations from variance one. In our simulation studies, we explore the effect of different priors and specifications for  $\omega$ , including  $\omega = 1$  fixed, a constant prior for  $\omega$ , and two different informative priors for omega, centered on one. The details are given in Section 4.

**Transition segments.** The transition segments are defined such that their respective derivatives are linear functions providing smooth transitions between slope one in the linear boundary segments to the slope of the core segment at  $a$  and  $b$ , respectively. This behavior is visible in panel b) of Figure 3. The constant  $\lambda \in \mathbb{R}_{>0}$  defines the width of the transition intervals. It can be chosen as  $\lambda = v(b-a)$ , where  $v \in \mathbb{R}_{>0}$  indicates the width of the transition interval relative to the interior knot range  $b-a$ . We use a default value of  $v = 0.3$  in the remainder of this work. The constants  $A$  and  $B$  induce vertical shifts, ensuring that the function values at the segment

boundaries align. They are given by

$$A = \text{spline}(a) - \frac{a}{\lambda} \left[ \frac{a}{2} + \left( \lambda - \frac{3a}{2} \right) \cdot \frac{\partial}{\partial a} \text{spline}(a) \right], \text{ and}$$

$$B = \text{spline}(b) - \frac{b}{\lambda} \left[ -\frac{b}{2} + \left( \lambda - \frac{3b}{2} \right) \cdot \frac{\partial}{\partial b} \text{spline}(b) \right].$$

**Derivative, monotonicity.** The derivative of the transformation function (3) is

$$\frac{\partial}{\partial \varepsilon} h(\varepsilon) = \begin{cases} 1 & \text{if } \varepsilon \in (-\infty, a - \lambda) & \text{(linear),} \\ (1 - \frac{a-\varepsilon}{\lambda}) \cdot \frac{\partial}{\partial a} \text{spline}(a) + \frac{a-\varepsilon}{\lambda} & \text{if } \varepsilon \in [a - \lambda, a) & \text{(transition),} \\ \frac{\partial}{\partial \varepsilon} \text{spline}(\varepsilon) & \text{if } \varepsilon \in [a, b] & \text{(core),} \\ (1 - \frac{\varepsilon-b}{\lambda}) \cdot \frac{\partial}{\partial b} \text{spline}(b) + \frac{\varepsilon-b}{\lambda} & \text{if } \varepsilon \in (b, b + \lambda] & \text{(transition),} \\ 1 & \text{if } \varepsilon \in (b + \lambda, \infty) & \text{(linear).} \end{cases} \quad (6)$$

The function  $h$  as specified in (3) is strictly monotonically increasing in  $\varepsilon$ , as formalized in the following theorem.

**Theorem 2.1** (Monotonicity of the transformation function). *Let the function  $h : \mathbb{R} \rightarrow \mathbb{R}$  be given by (3), with  $\text{spline}(\varepsilon)$  as in (4). Then  $h$  is strictly monotonically increasing in  $\varepsilon$ ; that is, for all  $\varepsilon_1, \varepsilon_2 \in \mathbb{R}$  with  $\varepsilon_1 < \varepsilon_2$ , we have  $h(\varepsilon_1) < h(\varepsilon_2)$ .*

*Proof.* The proof is given in Section B.2 of the supplemental materials. □

## 2.2. Prior specifications

**Prior for  $\delta$ .** When specifying a prior for the shape parameters  $\delta = [\delta_1, \dots, \delta_{J-1}]^\top$ , we focus on two main considerations. First, we center the prior on the reference distribution, which means that we center the transformation function on a straight line. Second, note that the number of parameters ( $J - 1$ ) determines the flexibility of the transformation function. Choosing a high value like  $J - 1 = 40$  leads to a very flexible transformation function, but it can also make the model prone to overfitting. Overfitting may show itself in an overly wiggly transformation function that results in a likewise wiggly estimate of the probability density function  $f_Y(y|\mathbf{x})$ . We therefore choose a regularizing prior that moderates the trade-off between flexibility and overfitting.

Both considerations are satisfied with a first-order random walk prior  $\delta_j | \delta_{j-1} \sim \mathcal{N}(\delta_{j-1}, \tau_\delta^2)$  with  $j = 2, \dots, J - 1$  and a constant prior for  $\delta_1$ . Since  $\delta_1, \dots, \delta_{J-1}$  can be thought of as logarithmic differences in B-spline coefficients, this prior effectively penalizes second differences in the transformation function. It resembles the general Bayesian P-spline priors introduced by Lang



& Brezger (2004) and was used in a slightly modified version by Carlan et al. (2023) in the construction of Bayesian conditional transformation models. The variance of the random walk,  $\tau_\delta^2$ , regulates the overall amount of smoothing, with a small variance implying strong smoothing towards a straight line. The joint prior for  $\delta$  is a rank-deficient multivariate normal prior

$$\pi(\delta|\tau_\delta) \propto \left(\frac{1}{\tau_\delta^2}\right)^{\text{rk}(\mathbf{K})/2} \exp\left(-\frac{1}{2\tau_\delta^2}\delta^\top \mathbf{K}\delta\right), \quad (7)$$

with the  $(J-1) \times (J-1)$  penalty matrix  $\mathbf{K} = \mathbf{D}^\top \mathbf{D}$  of rank  $J-2$  constructed from a  $(J-2) \times (J-1)$  first-difference matrix  $\mathbf{D}$  that is zero everywhere except that  $\mathbf{D}_{[d,d+1]} = -\mathbf{D}_{[d,d]} = 1$  for  $d = 1, \dots, J-2$ . In combination with a suitable hyperprior for the variance parameter  $\tau_\delta^2$ , this regularizing prior allows us to equip the model with a generous number of parameters, for example  $J-1 = 30$ , and let the inference algorithm arrive at a sensible amount of smoothness.

The rank-deficient prior (7) does not penalize additive constants in the vector  $\delta$ . For the core transformation function (4), this means that  $\delta$  implicitly includes an unpenalized constant scaling factor that is cancelled out. To see this, let  $\xi = \frac{1}{J-1} \sum_{j=1}^{J-1} \delta_j$  denote the mean of  $\delta$ , and let  $\tilde{\delta}_j = \delta_j - \xi$  denote the deviations from the mean. Then (4) can be written as

$$\text{spline}(\varepsilon) = \frac{\omega \cdot \exp(\xi)}{\exp(\xi) \cdot s(\tilde{\delta})} \cdot \sum_{j=1}^J B_j(\varepsilon) \left( \sum_{\ell=2}^j \exp(\tilde{\delta}_{\ell-1}) \right).$$

This poses an identification problem. For MCMC sampling, we thus fix  $\exp(\xi) = 1$  by applying a sum-to-zero constraint to  $\delta$ . We implement the constraint via reparameterization as described by Wood (2017) (Section 1.8.1).

**Hyperprior for  $\tau_\delta^2$ .** By controlling the deviation of the transformation function from a straight line, the variance parameter  $\tau_\delta^2$  governs how much the conditional distribution distribution can deviate from the reference distribution. For  $\tau_\delta^2 \rightarrow 0$ , the model reduces to the base model, i.e. a location-scale model for the reference distribution. We set up a penalized complexity prior, following the principles outlined by Simpson et al. (2017): First, the prior should favor the base model unless there is clear information to support the more complex model. Second, additional complexity is measured by the Kullback-Leibler divergence. Third, complexity is penalized at a constant rate, and fourth, the user chooses the specific scaling. As shown in detail by Klein & Kneib (2016), for a prior like (7), this leads to a Weibull prior for  $\tau_\delta^2$  with the shape fixed to 0.5 and scale  $\theta$ . The latter parameter provides the user-defined scaling. We conducted prior predictive simulations to inform our selection of a value for  $\theta$ . Figure 4 shows 100 residual densities implied by hierarchical draws from the priors of  $\tau_\delta^2$  and  $\delta$  using a standard normal reference distribution and  $J-1 = 20$ . As our model setup requires, the densities are brought to mean zero and standard deviation one. Our simulation study in Section 4 includes settings with  $\theta = 0.01$  and  $\theta = 0.05$ , as well as an inverse gamma hyperprior  $\tau^2 \sim \mathcal{IG}(1, 0.01)$ ; it suggests that there is little sensitivity for the choice of hyperprior.

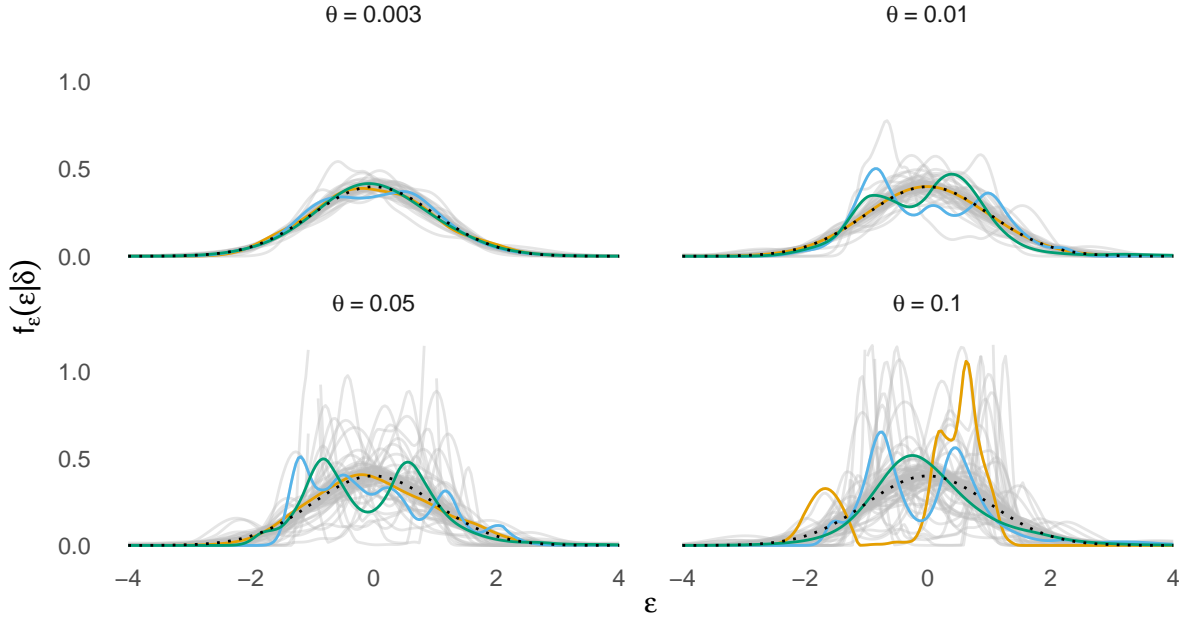


**Figure 4** One hundred residual densities obtained from prior predictive simulations using different scale parameters  $\theta$  in the hyperprior for  $\tau_\delta^2$ . The grey lines are individual samples, the dotted black line is the standard normal distribution for reference. The colored lines are three arbitrarily chosen individual samples for each setting, intended as highlighted examples. Note that we fix the upper limit of the y axis for better general visibility, which causes some clipping for individual samples for  $\theta = 0.05$  and  $\theta = 0.1$ .

### 2.3. Structured additive predictors for location and scale

We use structured additive predictors to model  $\mu(\mathbf{x})$  and  $\sigma(\mathbf{x})$ . Structured additive predictors can represent a wide array of linear, non-linear, random, and spatial functions in a unified framework using basis expansions. Specifically, we define  $\mu(\mathbf{x}) = \beta_0 + \sum_{\ell=1}^L f_\ell(\mathbf{x})$ , where  $\beta_0$  is an intercept and each  $f_\ell(\mathbf{x})$  is given by  $f_\ell(\mathbf{x}) = \sum_{d=1}^D A_{d,\ell}(\mathbf{x})\beta_{d,\ell} = \mathbf{a}_\ell^\top \boldsymbol{\beta}_\ell$ . Here,  $A_{1,\ell}(\mathbf{x}), \dots, A_{D,\ell}(\mathbf{x})$  are the evaluations of basis functions of possibly different types, chosen based on which kind of function should be represented by  $f_\ell(\mathbf{x})$ . The coefficient vectors  $\boldsymbol{\beta}_1, \dots, \boldsymbol{\beta}_L$  are each equipped with a suitable smoothness prior, which is a potentially rank-deficient multivariate normal prior of the form

$$\pi(\boldsymbol{\beta}_\ell | \tau_\ell^2) \propto \left(\frac{1}{\tau_\ell^2}\right)^{\text{rk}(\mathbf{K}_\ell)/2} \exp\left(-\frac{1}{2\tau_\ell^2} \boldsymbol{\beta}_\ell^\top \mathbf{K}_\ell \boldsymbol{\beta}_\ell\right), \quad (8)$$

where  $\ell = 1, \dots, L$  indicates the function,  $\mathbf{K}_\ell$  denotes a  $D \times D$  penalty matrix for a function represented by  $D$  bases and  $\tau_\ell^2$  denotes an inverse smoothing parameter. Collecting  $\mathbf{a} = [\mathbf{a}_1^\top, \dots, \mathbf{a}_L^\top]^\top$  and  $\boldsymbol{\beta} = [\boldsymbol{\beta}_1^\top, \dots, \boldsymbol{\beta}_L^\top]^\top$ , the predictor can be written as  $\mu(\mathbf{x}) = \beta_0 + \mathbf{a}^\top \boldsymbol{\beta}$ . The predictor  $\sigma(\mathbf{x})$  is defined analogously, with intercept  $\gamma_0$ , basis vector  $\mathbf{b}$  and coefficient vector  $\boldsymbol{\gamma}$ . However, since  $\sigma(\mathbf{x})$  is defined only on the positive real line, we use a log-link, so that we have  $\ln \sigma(\mathbf{x}) = \gamma_0 + \mathbf{b}^\top \boldsymbol{\gamma}$ .

The choice of basis functions  $A_{d,\ell}(\mathbf{x})$  and penalty matrix  $\mathbf{K}_\ell$  jointly determines the form of the individual terms. We refer the reader to Fahrmeir et al. (2013, p. 554) for a comprehensive

overview of specifications. In many cases, the setup is completed with hyperpriors on the inverse smoothing parameters  $\tau^2$ . A common choice is an inverse gamma prior  $\tau^2 \sim \mathcal{IG}(a, b)$  with  $a = 1$  and  $b = 0.01$  for a weakly informative setting, although other priors like a scale-dependent prior (Klein & Kneib, 2016) and half-Cauchy, half-Normal, or uniform priors may be preferable in some cases (Gelman, 2006).

## 2.4. Extensions

**Censored responses.** Censoring of response observations can be taken into account by adjusting (2). The likelihood contributions for right-, left-, and interval-censored continuous or discrete observations are given by

$$\begin{aligned}
 & F_Z \left( h \left( \frac{\bar{y} - \mu(\mathbf{x})}{\sigma(\mathbf{x})} \right) \right) \quad \text{for } y \in (-\infty, \bar{y}) && \text{(left censored)} \\
 & 1 - F_Z \left( h \left( \frac{y - \mu(\mathbf{x})}{\sigma(\mathbf{x})} \right) \right) \quad \text{for } y \in (y, \infty) && \text{(right censored)} \\
 & F_Z \left( h \left( \frac{\bar{y} - \mu(\mathbf{x})}{\sigma(\mathbf{x})} \right) \right) - F_Z \left( h \left( \frac{y - \mu(\mathbf{x})}{\sigma(\mathbf{x})} \right) \right) \quad \text{for } y \in (y, \bar{y}) && \text{(interval censored)}.
 \end{aligned}$$

**Count responses.** PTMs can be applied to count responses, explicitly taking zero-inflation into account with a two-component model. A first component covers the probability of an observation  $y = 0$  as a function of covariates using  $\mathbb{P}(Y = 0|\mathbf{x}) = F_Z(\eta_0(\mathbf{x}))$ , where  $\eta_0(\mathbf{x}) = \alpha_0 + \sum_{k=1}^K f_{0,k}(\mathbf{x})$  is a structured additive predictor. A second component covers the nonzero observations using  $\mathbb{P}(Y \leq y|Y > 0, \mathbf{x}) = F_Z(h(\varepsilon))$ , where  $\varepsilon = (\lfloor y \rfloor - \mu(\mathbf{x}))/\sigma(\mathbf{x})$  and  $\lfloor \cdot \rfloor$  is the floor function. In this case,  $\mu(\mathbf{x})$  and  $\sigma(\mathbf{x})$  represent the location and scale of the nonzero component, respectively. Combining the two parts, a two-component count-PTM can be set up as

$$\mathbb{P}(Y \leq y|\mathbf{x}) = F_Z(\eta_0(\mathbf{x})) + \mathbb{I}_{y>0} [1 - F_Z(\eta_0(\mathbf{x}))] F_Z \left( h \left( \frac{\lfloor y \rfloor - \mu(\mathbf{x})}{\sigma(\mathbf{x})} \right) \right),$$

where the indicator function  $\mathbb{I}_{y>0} = 1$  if the condition  $y > 0$  is true and  $\mathbb{I}_{y>0} = 0$  otherwise. Note that the first component does not require a transformation function.

### 3. Posterior inference

#### 3.1. Posterior sampling

Assuming conditional independence between the model parameters, the joint unnormalized posterior is given by

$$p(\boldsymbol{\beta}, \boldsymbol{\gamma}, \boldsymbol{\delta}, \boldsymbol{\tau}^2, \omega | \mathbf{y}) \propto \prod_{i=1}^N f(y_i | \mathbf{x}_i, \boldsymbol{\beta}, \boldsymbol{\gamma}, \boldsymbol{\delta}, \omega) \left[ \prod_{\ell=1}^L \pi(\boldsymbol{\beta}_\ell | \tau_{\ell, \mu}^2) \pi(\tau_{\ell, \mu}^2) \right] \left[ \prod_{s=1}^S \pi(\boldsymbol{\gamma}_s | \tau_{s, \sigma}^2) \pi(\tau_{s, \sigma}^2) \right] \\ \times \pi(\boldsymbol{\delta} | \tau_\delta^2) \pi(\tau_\delta^2) \pi(\omega).$$

The index  $i = 1, \dots, N$  identifies individual observations. To draw samples from this posterior, we implemented the model in Python, building on the probabilistic programming framework Liesel (Riebl et al., 2023). Liesel provides a general No-U-Turn sampler (NUTS) via BlackJAX (Cabezas et al., 2023), combined with automatic differentiation and just-in-time compilation via JAX (Bradbury et al., 2018). We sample all parameters with NUTS and split up sampling into blocks that reflect the model architecture. Within each parameter block, a new sample is proposed using the block’s full conditional posterior density, fixing the remaining parameters at their current values. The positive-valued parameters  $\tau^2$  and  $\omega$  are transformed to the real line for sampling using appropriate bijective link functions  $g : \mathbb{R}_{>0} \rightarrow \mathbb{R}$ , since the performance of the NUTS can benefit from working with parameters defined on the whole real line. By default, we use  $g(x) = \ln(\exp(x) + 1)$ , such that the inverse link is the softplus function. The corresponding prior densities are accordingly transformed using the change of variables theorem, i.e.  $\pi(g(x)) = \pi(x) \left| \frac{\partial}{\partial x} g(x) \right|$ .

We find sensible knots for the B-spline in the core transformation function (4) and good starting values for the model parameters by approximating the posterior modes with a stochastic gradient ascent algorithm. As a default, we use the Adam optimizer as implemented in the Python library Optax (DeepMind et al., 2020). In a first step, we focus on  $\boldsymbol{\beta}$  and  $\boldsymbol{\gamma}$ , keeping the shape parameters  $\boldsymbol{\delta}$  fixed at zero. Given  $N$  input observations, this provides us with an initial set of residuals  $\hat{\varepsilon}_1^*, \dots, \hat{\varepsilon}_N^*$ . We define the knots as an equidistant grid based on these residuals, taking their minimum and maximum as the boundary knots  $a$  and  $b$ . If there are outliers among the residuals, it may be more sensible to use the  $p$  and  $1 - p$  quantiles of the initial residuals instead, respectively, with  $p \in [0, 1]$  chosen manually. Next, we run stochastic gradient ascent a second time, this time including the shape parameters  $\boldsymbol{\delta}$  and the hyperparameters. We use the returned approximations to the posterior modes as starting values for the MCMC sampling process. Algorithm 1 gives an overview of the full inference procedure.

---

**Algorithm 1:** Inference for Bayesian penalized transformation models.

---

1. Initialize the parameters in  $\beta$ ,  $\gamma$ , and  $\delta$  to zero, and  $\omega = 1$ . Initialize the hyperparameters in  $\tau^2 = [\tau_\ell^2, \tau_s^2, \tau_\delta^2]^\top$  to one.
2. Find initial approximations to the posterior modes for  $(\beta, \gamma)$  via stochastic gradient ascent while holding the remaining parameters fixed at their initial values, i.e.  
 $(\hat{\beta}_0^*, \hat{\gamma}_0^*) = \arg \max_{(\beta, \gamma)} \ln p(\beta, \gamma | \delta, \tau^2, \omega, \mathbf{y})$ .
3. Compute an initial set of residuals  $\hat{\varepsilon}_1^*, \dots, \hat{\varepsilon}_N^*$  using  $\hat{\beta}_0^*$  and  $\hat{\gamma}_0^*$ , and set the transformation function's boundary knots  $a$  and  $b$  to the minimum and maximum residual, respectively.
4. Find starting values by computing  $\hat{\theta}^* = \arg \max_{\theta} \ln p(\beta, \gamma, \delta, \tau^2, \omega | \mathbf{y})$  via stochastic gradient ascent, where  $\theta = (\beta, \gamma, \delta, \tau^2, \omega)$ .
5. Draw posterior samples via Markov chain Monte Carlo as follows.

**for** MCMC iterations  $t = 1, \dots, T$  **do**

**for** location terms  $\ell = 1, \dots, L$  **do**

$\beta_\ell^{[t]} \leftarrow \text{NUTS}(\cdot)$

$g(\tau_\ell^2)^{[t]} \leftarrow \text{NUTS}(\cdot)$

**for** scale terms  $s = 1, \dots, S$  **do**

$\gamma_s^{[t]} \leftarrow \text{NUTS}(\cdot)$

$g(\tau_s^2)^{[t]} \leftarrow \text{NUTS}(\cdot)$

$\delta^{[t]}, g(\omega)^{[t]} \leftarrow \text{NUTS}(\cdot)$

$g(\tau_\delta^2)^{[t]} \leftarrow \text{NUTS}(\cdot)$

---

### 3.2. Computational aspects

**Constant intercepts.** We treat the intercepts  $\beta_0$ ,  $\gamma_0$  in the covariate models, and  $\alpha$  in the transformation function as constants that are identified by the model assumptions when the remaining parameters are held fixed. We assume  $\mathbb{E}(\varepsilon) = 0$  and  $\text{Var}(\varepsilon) = 1$ . To identify  $\beta_0$  and  $\gamma_0$ , we first write our covariate models for the location and scale without the respective intercept terms, i.e.  $\tilde{\mu}(\mathbf{x}) = \mu(\mathbf{x}) - \beta_0$  and  $\tilde{\sigma}(\mathbf{x}) = \sigma(\mathbf{x}) / \exp(\gamma_0)$ . Now, if we treat  $\beta_0$  and  $\gamma_0$  as constants, we obtain the expressions

$$\beta_0 = \mathbb{E} \left( \frac{1}{\tilde{\sigma}(\mathbf{x})} \right)^{-1} \mathbb{E} \left( \frac{y - \tilde{\mu}(\mathbf{x})}{\tilde{\sigma}(\mathbf{x})} \right) \quad \text{and} \quad \gamma_0 = \ln \left( \sqrt{\text{Var} \left( \frac{y - \beta_0 - \tilde{\mu}(\mathbf{x})}{\tilde{\sigma}(\mathbf{x})} \right)} \right). \quad (9)$$

During MCMC sampling, we replace the expected value and the variance with their respective sample estimators, so that  $\beta_0$  and  $\gamma_0$  are always immediately available as deterministic functions of the data and the remaining model parameters. Consequently,  $\beta_0$  and  $\gamma_0$  are sampled indirectly during MCMC sampling. We use a similar idea to obtain the intercept  $\alpha$  of the transformation function  $h$  in (3), since we assume  $\mathbb{E}(h(\varepsilon)) = 0$ . Specifically, for a given sample of residuals  $\varepsilon_1, \dots, \varepsilon_N$  and  $\omega, \delta$  fixed,  $\alpha$  is computed as the negative mean of an auxiliary sample of trans-

formed residuals that is computed with  $\alpha = 0$ , that is  $\alpha = -\frac{1}{N} \sum_{i=1}^N h(\varepsilon_i | \alpha = 0)$ . Using this procedure, we obtain a sample of  $\alpha$  in every MCMC iteration.

**Basis matrix approximation.** To avoid having to compute the basis function evaluations of the transformation function's spline segment in every MCMC iteration, we use a grid approximation. That is, we obtain one matrix of basis function evaluations on a tight equidistant grid  $\tilde{\varepsilon}_1, \dots, \tilde{\varepsilon}_{1000}$ , with  $\tilde{\varepsilon}_1 = a$  and  $\tilde{\varepsilon}_{1000} = b$  set to the lower and upper boundary knot, respectively. For a basis function evaluation of a specific value  $\varepsilon$ , we then find the greatest  $\tilde{\varepsilon}_{\text{lo}}$  and the smallest  $\tilde{\varepsilon}_{\text{hi}}$  such that  $\varepsilon \in [\tilde{\varepsilon}_{\text{lo}}, \tilde{\varepsilon}_{\text{hi}}]$  and interpolate between the two corresponding elements  $B(\tilde{\varepsilon}_{\text{lo}})$  and  $B(\tilde{\varepsilon}_{\text{hi}})$  of the pre-computed basis matrix:

$$B_j(\varepsilon) \approx \left(1 - \frac{\varepsilon - \tilde{\varepsilon}_{\text{lo}}}{(b - a)/1000}\right) \cdot B(\tilde{\varepsilon}_{\text{lo}}) + \frac{\varepsilon - \tilde{\varepsilon}_{\text{lo}}}{(b - a)/1000} \cdot B(\tilde{\varepsilon}_{\text{hi}}).$$

### 3.3. Posterior estimates

The fully Bayesian inference gives us access not only to the posterior distribution of the directly sampled parameters, but also to derived quantities. Specifically, by propagating the posterior samples through the model, we can obtain posterior predictive distributions of the response's conditional CDF, PDF, and quantiles. This straightforward form of uncertainty quantification is one of the major advantages gained from our fully Bayesian inference.

Specifically, for each posterior sample  $t = 1, \dots, T$ , an estimate of the conditional cumulative distribution given a vector of covariate observations  $\mathbf{x}^*$  can be obtained as

$$\hat{F}_Y^{[t]}(y|\mathbf{x}) = F_Z \left( h \left( \frac{y - \mu(\mathbf{x}^* | \boldsymbol{\beta}^{[t]})}{\sigma(\mathbf{x}^* | \boldsymbol{\gamma}^{[t]})} \middle| \alpha^{[t]}, \omega^{[t]}, \boldsymbol{\delta}^{[t]} \right) \right).$$

These samples  $\hat{F}_Y^{[1]}(y|\mathbf{x}^*), \dots, \hat{F}_Y^{[T]}(y|\mathbf{x}^*)$  can be used to derive summary statistics like posterior quantiles, highest posterior density intervals, or the posterior mean  $\hat{F}_Y(y|\mathbf{x}^*) = \frac{1}{T} \sum_{t=1}^T \hat{F}_Y^{[t]}(y|\mathbf{x}^*)$  as a Bayesian point estimate. Similarly, we can obtain the posterior samples of the predictive conditional density  $\hat{f}_Y^{[1]}(y|\mathbf{x}^*), \dots, \hat{f}_Y^{[T]}(y|\mathbf{x}^*)$ . Conditional quantiles of the response distribution can be obtained by numerical inversion of the transformation function.

## 4. Simulation study

We conducted simulations to evaluate the performance of penalized transformation models (PTMs) in several regards using both normally distributed and non-normally distributed data. First, we focus on the model's ability to recover the conditional response distribution and compare it to a normal location-scale model, as well as to quantile regression and Bayesian

conditional transformation models. Second, we assess the model’s ability to obtain unbiased estimates of linear and nonlinear covariate effects on both the location and scale of the response. Third, we compare different prior and hyperprior specifications and vary some implementation details.

#### 4.1. Simulation design

**Data generation.** We generate both conditionally normal and conditionally non-normal data from the model

$$y_i = \mu(\mathbf{x}_i) + \sigma(\mathbf{x}_i)\varepsilon_i$$

for  $i = 1, \dots, N_{\text{obs}}$ . The covariate effects are defined as

$$\begin{aligned} \mu(\mathbf{x}) &= s_1(x_1) + s_2(x_2) + s_3(x_3) + s_4(x_4), \text{ and} \\ \sigma(\mathbf{x}) &= \exp\left(0.2s_1(x_1) + 0.1s_2(x_2) + 0.1s_3(x_3) + 0.1s_4(x_4)\right). \end{aligned}$$

All covariates are generated as i.i.d realizations from  $\mathcal{U}(-2, 2)$  and standardized to mean zero and scale one. The four test functions consist of a linear function  $s_1(x) = x$ , a u-shaped function with a linear trend  $s_2(x) = x + \frac{(2x)^2}{5.5}$ , an oscillating function with a negative trend  $s_3(x) = -x + \pi \sin(\pi x)$ , and a bell-shaped function with a small positive trend  $s_4(x) = 0.5x + 15\phi(2(x - 0.2)) - \phi(x + 0.4)$ .

We control the (non-)normality through the generation of the residuals  $\varepsilon_i$ . For the conditionally normal data, we draw  $\varepsilon_i \stackrel{i.i.d.}{\sim} \mathcal{N}(0, 1)$ . For the conditionally non-normal data, we generate  $\varepsilon_i$  as follows. We first obtain a random sample  $z_i \sim \mathcal{N}(0, 1)$  from a standard normal distribution and a random sample of  $\boldsymbol{\delta}$  from its random walk prior under a sum-to-zero constraint, using  $J - 1 = 10$  and  $\tau_\delta = 0.5$ . The residuals are then obtained as  $\varepsilon_i = h^{-1}(z_i | \boldsymbol{\delta})$  by numerically inverting the transformation function (3), with  $\omega = 1$  and the shift term  $\alpha$  chosen to ensure a mean of zero for the sample of residuals. The details of this procedure are described in Section C.1 of the supplemental materials, including plots of all generated densities. A new sample of  $\boldsymbol{\delta}$  is used in every simulation iteration, such that each iteration uses a different true density. This allows us to investigate the model’s performance for a wide range of non-normal residual densities.

**Tested models.** We fit the simulated data using models of four different families. Below, we lay out on the general model specifications. Table 1 gives an overview of all models including a number of PTMs with slight variations in specification details or hyperprior setup.

1. Bayesian penalized transformation models (PTMs) with a standard normal reference distribution and a dimension of  $J - 1 = 30$  for the vector of shape parameters  $\boldsymbol{\delta}$ . The models can be written as

$$\mathbb{P}(Y \leq y_i) = \Phi\left(h\left(\frac{y_i - \mu(\mathbf{x}_i)}{\sigma(\mathbf{x}_i)}\right)\right),$$

where  $\mathbf{x}_i = [x_{i1}, x_{i2}, x_{i3}, x_{i4}]^\top$ . The location model part is specified as

$$\mu(\mathbf{x}_i) = \beta_0 + s_1(x_{i1}) + s_2(x_{i2}) + s_3(x_{i3}) + s_4(x_{i4}),$$

where each  $s_1, \dots, s_4$  is a 20-parameter Bayesian P-spline. The inverse smoothing parameters of these P-splines receive inverse gamma hyperpriors with concentration 1 and scale 0.01. The scale model part is specified analogously, additionally using a logarithmic link function.

2. Normal location-scale models, which can be written in analogy to PTMs as

$$\mathbb{P}(Y \leq y_i) = \Phi\left(\frac{y_i - \mu(\mathbf{x}_i)}{\sigma(\mathbf{x}_i)}\right)$$

by letting the transformation function  $h$  equal the identity function. The covariate models  $\mu(\mathbf{x}_i)$  and  $\sigma(\mathbf{x}_i)$  are specified exactly as in the PTMs.

3. Bayesian conditional transformation models (BCTM, [Carlan et al., 2023](#)) with standard normal reference distribution. The BCTMs use the form

$$\mathbb{P}(Y \leq y_i) = \Phi(\gamma_0 + h_1(y_i|x_{i1}) + h_2(y_i|x_{i2}) + h_3(y_i|x_{i3}) + h_4(y_i|x_{i4})),$$

where

$$h_j(y_i|x_{ij}) = (\mathbf{a}(y_i)^\top \otimes \mathbf{b}_j(x_{ij})^\top)^\top \boldsymbol{\gamma}_j, \quad j = 1, \dots, 4,$$

are the BCTM's partial transformation functions, with  $\otimes$  denoting the Kronecker product. The bases  $\mathbf{a}$  and  $\mathbf{b}$  are chosen as B-spline bases. The BCTM uses inverse gamma hyperpriors with concentration 1 and scale 0.01 for all inverse smoothing parameters of the tensor product terms.

4. Bayesian quantile regression (QGAM, [Fasiolo et al., 2021b](#)). The models are of the form

$$Q_Y(\alpha|\mathbf{x}_i) = \beta_0 + s_{\alpha,1}(x_{i1}) + s_{\alpha,2}(x_{i2}) + s_{\alpha,3}(x_{i3}) + s_{\alpha,4}(x_{i4}),$$

where each  $s_{\alpha,1}, \dots, s_{\alpha,4}$  is a 20-parameter P-spline and  $Q_Y(\alpha|\mathbf{x}_i)$  is the conditional  $\alpha$ -quantile of the response  $Y$ .

**Replications and sampling.** We used  $N_{\text{sim}} = 100$  replications for all models. For the main comparisons, we used sample sizes  $N_{\text{obs}} \in \{500, 1000, 2000\}$ , representing a challenging, an informative setting, and a highly informative setting. For secondary comparisons, we generally limited the study to  $N_{\text{obs}} = 1000$ . An exhaustive overview of conditions is included in [Table A1](#) in the supplemental materials. Inference for the PTM and the normal location-scale model was conducted via MCMC using the Python library `liesel_ptm` ([Brachem et al., 2024](#)). Inference for the BCTM was conducted using the Python library `liesel_bctm` ([Brachem et al., 2023](#)). Both libraries build on the probabilistic programming framework `Liesel` ([Riebl et al., 2023](#)). We used a warmup duration of 1500 samples and drew 5000 posterior samples from each of



**Table 1** Overview of the models fitted in the simulation studies. The table is divided into three sections, separated by horizontal lines. The first section contains the models used in the main comparisons. The second section contains some variations in the specification of PTMs. The third sections contains additional comparison models.

Model	Description
normal	Fully specified normal location-scale model.
ptm	Fully specified PTM with a Weibull hyperprior for $\tau_\delta^2$ using a scale of 0.05, such that $\tau_\delta^2 \sim \text{Weibull}(0.5, 0.05)$ . The scalar $\omega$ has a truncated normal prior with location 1, scale 0.1, and lower bound 0.01, which induces $\omega \in [0.01, \infty)$ . We use softplus as the inverse link function, such that $\omega = \ln(1 + \exp(\nu))$ , and sample $\nu$ via NUTS.
bctm-10	BCTM with 10-parameter bases in all tensor products, resulting in a total of 400 parameters.
qgam	Fully specified Bayesian quantile regression model, using 20-parameter P-splines for all covariates. Fitted for a grid of 25 probability levels, evenly spaced between 0.005 and 0.995.
ptm-wb01	Like ptm, but with the scale of the Weibull hyperprior for $\tau_\delta^2$ set to 0.01.
ptm-ig	Like ptm, but with an inverse gamma hyperprior for $\tau_\delta^2$ with concentration $a = 1$ and scale $b = 0.01$ .
ptm-ridge	Like ptm, but with an i.i.d. ridge prior on $\delta$ instead of a random walk prior. That is, $\delta \sim \mathcal{N}(\mathbf{0}, \tau_\delta^2 \mathbf{I})$ and $\tau^2 \sim \text{Weibull}(0.5, 0.05)$ . This model does not include an additional sum-to-zero constraint on the elements of $\delta$ .
ptm-bounded	Like ptm, but the scalar $\omega$ is given by $\omega = 1 + 0.3(1 - 2\nu)$ , where $\nu$ has a beta prior $\mathcal{B}(15, 15)$ and $\text{logit}(\nu)$ is sampled via NUTS. This induces $\omega \in [0.7, 1.3]$ , with expectation one and a moderate concentration of prior probability mass close to the expectation.
ptm-const	Like ptm, but in $\omega = \ln(1 + \exp(\nu))$ , we use a constant prior for $\nu$ .
ptm-fixed	Like ptm, but with $\omega = 1$ fixed.
ptm-std	Like ptm, but $\omega = 1$ is fixed and for a given sample of transformed residuals $\{h(\varepsilon_i)^{[t]}\}_{i=1}^n$ in MCMC iteration $t$ , the sample is brought to standard deviation one by dividing by its sample standard deviation.
bctm-15	BCTM with 15-parameter bases in tensor products, resulting in a total of 900 parameters.
qgam-big	Like qgam, but including a model $\kappa(\mathbf{x})$ for the variance of the preliminary location-scale GAM fit used in the qgam inference algorithm. The term $\kappa(\mathbf{x})$ includes 7-parameter P-splines for all covariates.

four chains. The QGAM models were fitted using the R package `qgam` (Fasiolo et al., 2021a). Overall, the simulation study follows a  $(2 \times 3)$  design with the factors *data generation* (normal / non-normal) and *sample size* (500 / 1000 / 2000), such that we arrive at 600 simulation runs for each model.

## 4.2. Conditional response distribution

**Performance measures.** To evaluate the performance of the model in recovering the conditional response distribution on a quantitative level, we created a test dataset of size  $N_{\text{test}} = 500$  in each replication, using the true shape parameters  $\delta$ . We use four performance measures to assess how well the models recover the conditional response distribution:

1. The widely-applicable information criterion (WAIC) can be viewed as an estimator for the expected log pointwise predictive density (Vehtari et al., 2017; Watanabe, 2010). It thus measures predictive performance. On the deviance scale, the WAIC is given by  $\text{WAIC} = -2(\text{lppd} - p_{\text{WAIC}})$ , where the log pointwise predictive density (lppd) is

$$\text{lppd} = \sum_{i=1}^N \ln \left( \frac{1}{T} \sum_{t=1}^T \hat{f}_Y^{[t]}(y_i | \mathbf{x}_i) \right)$$

and the effective number of parameters is given by

$$p_{\text{WAIC}} = \sum_{i=1}^N \widehat{\text{Var}}_{t=1}^T (\ln \hat{f}_Y^{[t]}(y_i | \mathbf{x}_i)).$$

The WAIC is a fully Bayesian model choice criterion and can be applied without knowledge of the true distribution. On the deviance scale, a smaller WAIC indicates a better predictive performance.

2. The mean absolute difference (MAD) between the true cumulative density function (CDF) evaluations of the test data and the estimated CDF for the test data, given by

$$\text{MAD}^{[t]} = \frac{1}{N_{\text{test}}} \sum_{i=1}^{N_{\text{test}}} \left| F_{\text{true}}(y_i | \mathbf{x}_i) - \hat{F}^{[t]}(y_i | \mathbf{x}_i) \right|.$$

3. The Kullback-Leibler divergence (KLD) is a common measure to assess the statistical distance between two distributions. We estimate the KLD as

$$\widehat{\text{KLD}}^{[t]} = \frac{1}{N_{\text{test}}} \sum_{i=1}^{N_{\text{test}}} (\ln f_{\text{true}}(y_i | \mathbf{x}_i) - \ln \hat{f}^{[t]}(y_i | \mathbf{x}_i)).$$

4. The continuous ranked probability score (CRPS) is given by

$$\text{CRPS} = \int_0^1 \text{QS}_\alpha(\hat{F}, y) \, d\alpha, \quad (10)$$

see Gneiting & Raftery (2007) and Gneiting (2011). We compute quantile score  $\text{QS}_\alpha$  for a probability level  $\alpha$  for a test observation  $y_i$  as

$$\text{QS}_\alpha(\hat{F}, y_i) = \frac{2}{T} \sum_{t=1}^T \left( (\mathbb{I}_{y_i < F^{-1, [t]}(\alpha)} - \alpha) \cdot (F^{-1, [t]}(\alpha) - y_i) \right),$$

where  $\mathbb{I}_{(\cdot)}$  is the indicator function for the condition  $(\cdot)$ . We evaluate the quantile score for a grid of 25 probability levels  $\alpha$ , evenly spaced between 0.005 and 0.995, and evaluate the integral in (10) numerically using the trapezoid rule.

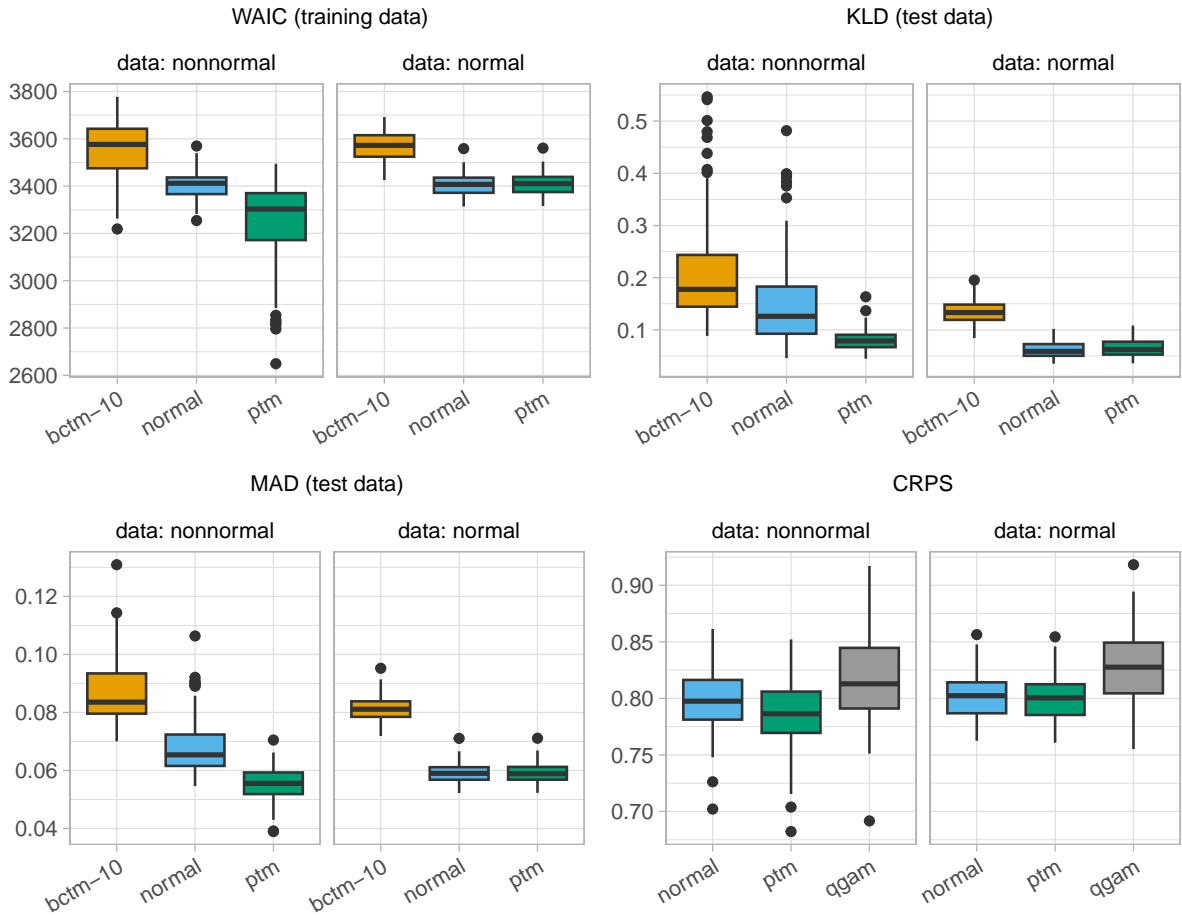


**Figure 5** Performance criteria for the conditional response density estimation. The plots depict results for  $N_{\text{obs}} = 1000$ . MAD, KLD, and CRPS are averaged over all  $T = 20,000$  samples for each seed.

We apply the MAD, KLD, and CRPS only to the test data, and the WAIC to the data used for model fitting. The MAD, KLD, and WAIC are used to compare the models `ptm`, `normal`, and `bctm-10`. The CRPS is used to compare the models `ptm`, `normal`, and `qgam`.

**Results.** Figure 5 shows the performance criteria for the comparison of PTMs with the evaluated competing models. The plots depict the results for  $N_{\text{obs}} = 1000$ . In all measures, the PTM shows a better performance than the comparisons for non-normal data, and equal performance to the normal model for normal data. This indicates that the PTM successfully recovers more information about the conditional response distribution than the compared models in the non-normal scenario, while reducing to the base model in the normal scenario as intended, without excessive overfitting.

Notably, both the BCTM and the quantile regression fall short even of the performance of the gaussian location-scale model. Model diagnostics for the BCTM showed a lack of convergence and suggest identification problems, most likely due to the inclusion of multiple tensor product terms. In previous applications, BCTMs and CTMs have typically been limited to a single tensor product. Multiple tensor products in BCTMs may cause identification issues, since a “main”

effect for the response  $y$  is included in each of the tensor product terms. Somewhat similarly, the data-generating process used here may be challenging for quantile regression, since the covariate effects on the response’s scale are accounted for only implicitly through the different fits for different quantiles, whereas the gaussian model and the penalized transformation model both allow for explicit covariate models for the scale. However, the differences between the models in terms of CRPS seem to be less pronounced than in the other measures.

**Additional comparisons.** In the following, we summarize the findings about additional models and sample sizes included in the simulation study. More extensive reports are included in Section E of the supplemental materials.

- The pattern described above holds for all three considered sample sizes  $N_{\text{obs}} \in \{500, 1000, 2000\}$ .
- `ptm-fixed` and `ptm-bounded` perform virtually identical to `ptm`.
- Differences between `ptm` and `ptm-ridge` are small or not discernible with respect to the WAIC (applied to both test and training data), the MAD, and the CRPS. When considering the KLD, we observe a clearly higher distance to the true distribution under `ptm-ridge`. Figure 6 provides two representative examples for a visual inspection of posterior estimates of the conditional densities. The estimates tend to be less wiggly under the random walk prior employed in `ptm`, just as intended. Similar plots for all seeds of the simulation study are included in Section E.6 of the supplemental materials.
- `ptm-const` and `ptm-std` both tend to generate extreme outliers in terms of WAIC and KLD when applied to test data. The reason is that these models can produce edge cases with extreme slopes of the transformation function due to insufficient regularization.
- There is no meaningful difference between the models `ptm-ig`, `ptm-wb01`, and `ptm`, indicating little sensitivity to the choice of hyperprior.
- Regarding the BCTMs, the results do not change when increasing the sample size to  $N_{\text{obs}} = 2000$ : all models achieve a better fit, but BCTMs still fare worse than the compared models. The `bctm-15` model shows the same patterns as `bctm-10`.
- There is no meaningful difference between the models `qgam` and `qgam-big` in terms of CRPS.

### 4.3. Covariate effects

We measure the performance of the covariate effect estimators using the mean squared error,

$$\text{MSE}(\hat{s}^{[t]}) = \frac{1}{N} \sum_{i=1}^N (s_{\text{true}}(x_i) - \hat{s}^{[t]}(x_i))^2,$$

averaged over all  $T = 20,000$  samples. The results are depicted on an aggregated level in Figure 7, additionally averaged over all four covariate effects in each seed for  $N_{\text{obs}} = 1000$ . A

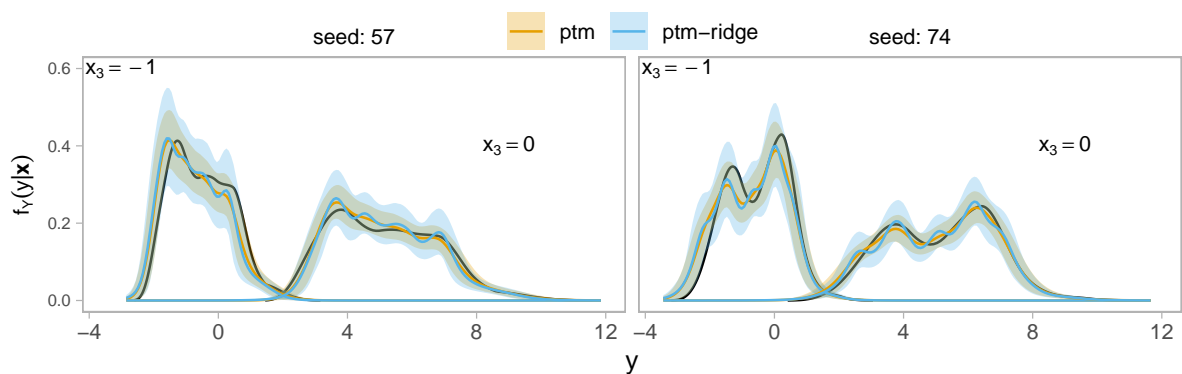


**Figure 6** Representative examples of average posterior conditional densities obtained with the penalized transformation model (PTM) with random walk prior (`ptm`) and ridge prior (`ptm-ridge`) for  $\delta$ . The plot shows two example densities for  $N_{\text{obs}} = 1000$ , each for two different covariate values  $x_3 = -1$  (left),  $x_3 = 0$  (right), while  $x_1 = x_2 = x_4 = 0$ . The true conditional densities are included as black lines and the shaded areas mark the .1 and .9 posterior quantiles.

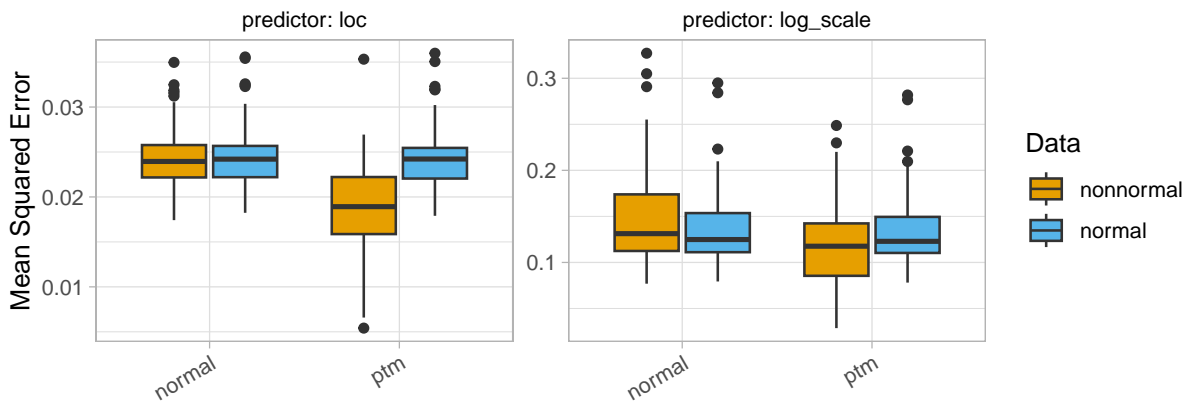


**Figure 7** Aggregated mean squared errors for covariate effect estimates obtained with `ptm` and the normal baseline.

more detailed breakdown, including separate plots for bias and posterior standard deviation for each covariate effect, is included in Section E.1 of the supplemental material. The results indicate that the estimation of covariate effects using the PTMs leads to a slightly lower MSE for non-normal data compared to the normal location-scale model. As the detailed inspection in the supplemental materials shows, this is driven by a lower variance in the covariate effects estimated with the PTM. Both models achieve practically unbiased estimates. The results confirm the viability of PTMs for the estimation of interpretable covariate effects in the vein of generalized additive models for location and scale.

## 5. Applications

In both applications reported here, we use a Weibull hyperprior with scale 0.05 for the random walk variance parameter  $\tau_\delta^2$ . Also, we use a truncated normal prior on the scalar  $\omega$  in both applications, just as described in the condition `ptm` in Table 1.

### 5.1. Fourth Dutch Growth Study

For an illustration of the use of PTMs and a contrast to quantile regression, we use a dataset consisting of cross-sectional measurements of the body mass index (BMI) and age of dutch boys between the ages 0 and 21 years. The data originates from the Fourth Dutch Growth Study (Fredriks, van Buuren, Wit, et al., 2000; Fredriks, van Buuren, Burgmeijer, et al., 2000). We use a subset of 7294 observations provided in the R package `gamlss.data` (Stasinopoulos et al., 2021). We set up three models:

1. A location-scale penalized transformation model (PTM)

$$\text{bmi}_i = \mu(\text{age}_i) + \sigma(\text{age}_i)\varepsilon_i, \quad (11)$$

where  $i = 1, \dots, 7294$ . We use a standard normal reference distribution, such that  $h(\varepsilon_i|\boldsymbol{\delta}) \stackrel{\text{i.i.d.}}{\sim} \mathcal{N}(0, 1)$ , and  $J - 1 = 30$  shape-parameters  $\delta_1, \dots, \delta_{J-1}$ . The location and scale functions  $\mu(\text{age}_i)$  and  $\sigma(\text{age}_i)$  are modelled using Bayesian P-splines with 20 parameters each. For  $\sigma(\text{age}_i)$ , we use a logarithmic link function to ensure positivity.

2. A normal location-scale model of the same form as (11), but using  $\varepsilon_i \stackrel{\text{i.i.d.}}{\sim} \mathcal{N}(0, 1)$ , such that  $\text{bmi}_i \sim \mathcal{N}(\mu(\text{age}_i), \sigma(\text{age}_i)^2)$ . Implementation-wise, we set up this model by simply fixing  $\boldsymbol{\delta} = \mathbf{0}$  in the PTM from point one.
3. A set of quantile regression models  $Q_\alpha(\text{bmi}_i|\text{age}_i) = s_\alpha(\text{age}_i)$  for probability levels  $\alpha \in \{0.01, 0.1, 0.25, 0.5, 0.75, 0.9, 0.99\}$ . We use the Bayesian quantile regression model introduced by Fasiolo et al. (2021b) and provided in the R package `qgam` (Fasiolo et al., 2021a). The functions  $s_\alpha(\text{age}_i)$  are again modeled through P-splines with 20 parameters.

The results are summarized in Figure 8. The top row shows the quantile curves obtained from quantile regression and the corresponding derived quantile curves from the normal model and the PTM. The derived quantiles from the normal model appear to underestimate both the  $\alpha = 0.01$  quantile and the  $\alpha = 0.99$  quantile, while quantile regression, as is well-known, gives better estimates. The derived quantiles from the PTM appear to be clear improvements over the normal model, too.

Looking closely at the  $\alpha = 0.99$  quantile, we can nicely observe a difference between the effects estimated with quantile regression and the PTM. Because it uses a global location effect, the PTM captures the peak in the effect of the age on bmi at an early age not only for lower quantiles,

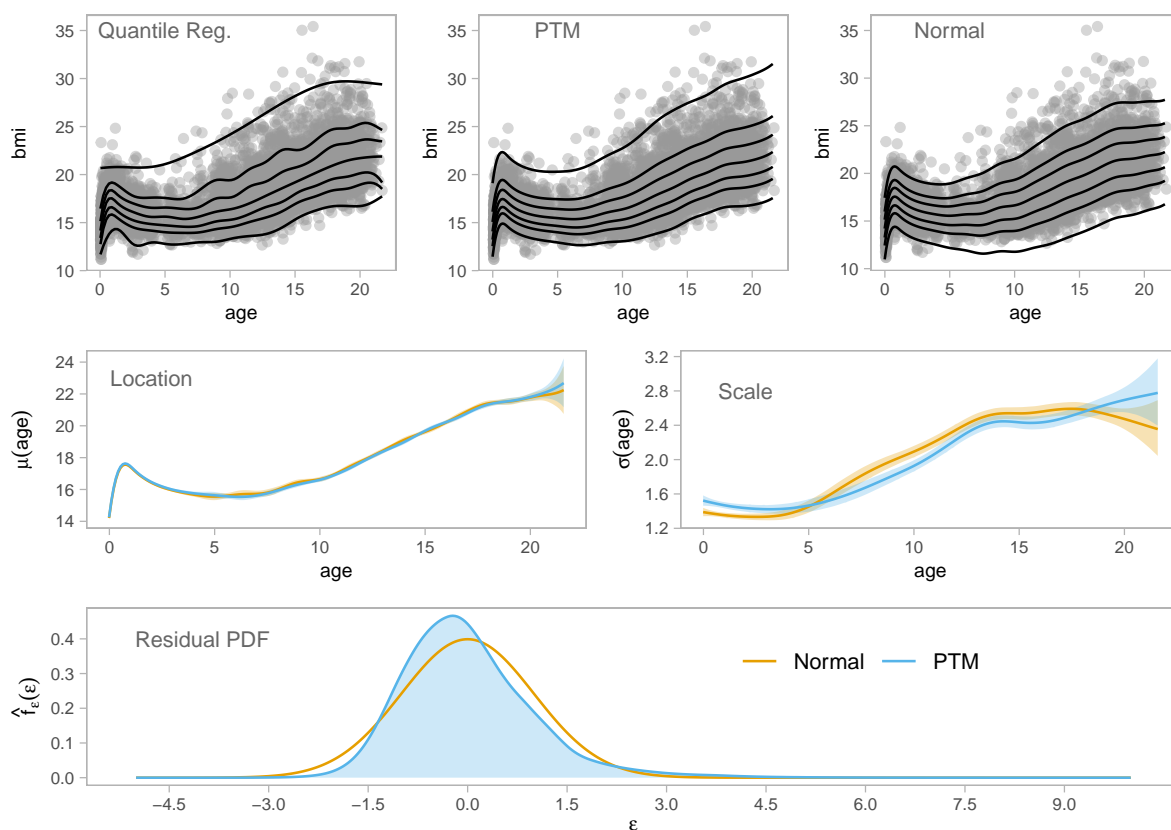


**Figure 8** These plots summarize the modelling of the dutch boys dataset with a penalized transformation model and provide comparisons of the results to quantile regression and normal location-scale regression. The top row shows quantile curves for the probability levels 0.01, 0.1, 0.25, 0.5, 0.75, 0.9, and 0.99. The middle row shows the posterior mean of the location and scale functions using PTMs (blue) and normal location-scale regression (yellow), as well as the .1 and .9 posterior quantiles (shaded area). The bottom row shows the estimated conditional probability density function given a fixed value of age = 12.5 implied by the PTM and the normal model.

but also for  $\alpha = 0.99$ . This peak is not included in the quantile curve obtained with the quantile regression model. Judging from the visual assessment, the PTM thus seems to capture the pattern present in the data better than the quantile regression model.

The middle row of Figure 8 shows the location and scale effects as functions of the age for both the normal model and the PTM. Since there are no such global functions for the quantile regression model, quantile regression is not represented in these plots. The location functions are visually almost indistinguishable. The scale functions are very similar, but do show some differences. Notably, the PTM results in a slightly higher scale estimate at the margins of the range of observed ages and lower scale estimate, approximately between the ages of 5 and 18. Most importantly, there is no direct equivalent to the scale function in quantile regression. Being able to assess this function makes it easier to summarize and understand patterns in the data in PTMs compared to quantile regression.

The bottom row of Figure 8 shows the residual density. Again, quantile regression is not included in this subplot, because it does not yield a corresponding estimate. Note that, in the normal model, this residual density is implied by the assumption of a normal distribution. In the PTM, the shape of the conditional density is estimated directly from the data, in addition to relating its location and scale to covariates. Here, this estimation results in a right-skewed conditional distribution, which in turn gives improved estimates of the quantile curves. The normal distribution is symmetric around the mean, and this appears to be what causes the underestimation of both the  $\alpha = 0.01$  and  $\alpha = 0.99$  derived quantile curves in the normal model. Being able to estimate and visualize the conditional distribution like this provides another way in which the PTM aids interpretation compared to quantile regression, while capturing more information from the data than a model assuming a fully parametric conditional distribution.

By providing a single coherent model, PTMs also fully prevent quantile crossing. Quantile crossing is the observation that two quantile curves obtained with quantile regression can cross, implying that there are covariate values for which the predicted quantile at a probability level  $\alpha_1$  can be greater than the predicted quantile at a higher probability level  $\alpha_2 > \alpha_1$ . This is a logical inconsistency that can arise due to the fact that, typically, quantile regression models are fitted independently of each other for different probability levels. While solutions to this problem exist (see, for instance, [Schnabel & Eilers, 2013](#)), we view it as an advantage of PTMs that the problem never even arises.

## 5.2. Framingham Heart Study

We now turn to the Framingham Heart Study data ([Zhang & Davidian, 2001](#)) for a slightly more complex model including a random intercept and a contrast of PTMs to the related Bayesian conditional transformation models (BCTMs). The Framingham data comprises a total of 1044 cholesterol level measurements taken of 200 study participants over the course of up to ten years. For 133 participants, there are six data points, while for the remaining 67 participants we have between one and five observations each. The data further contains participants' *sex* (binary, with 0 = female and 1 = male), their *age* in years at study onset and the *years* between the start of the study and the current measurement. For model fitting, we standardize the cholesterol levels and age by subtracting their respective mean and dividing by their standard deviation, and we center the covariate year by subtracting the median. We fit four penalized transformation models (PTMs) as variants of the model

$$\text{cholst}_{ij} = \mu_{ij} + \sigma_{ij}\varepsilon_{ij},$$

where the index  $i = 1, \dots, 200$  identifies the participant and  $j = 1, \dots, n_i$  indicates the individual observations available for participant  $i$ . All models use a standard normal reference distribution, such that  $\mathbb{P}(\varepsilon \leq \varepsilon_{ij}) = \Phi(h(\varepsilon_{ij}|\delta))$ . The vector of shape parameters  $\delta$  has length 30 in all models.



We use identical covariate models for the location  $\mu_{ij}$  and the natural logarithm of the scale  $\sigma_{ij}$ :

$$\begin{aligned}\mu_{ij} &= \beta_0 + \beta_1 \text{age}_{ij} + \beta_2 \text{year}_{ij} + \beta_3 \text{sex}_{ij} \\ \ln \sigma_{ij} &= \gamma_0 + \gamma_1 \text{age}_{ij} + \gamma_2 \text{year}_{ij} + \gamma_3 \text{sex}_{ij}.\end{aligned}$$

We vary the model by employing a 20-parameter P-spline for the effect of age and by adding a participant-specific i.i.d. random intercept to the location part of both models. For baseline comparisons, we also fit normal location-scale versions of all four PTMs. Additionally, we include a Bayesian conditional transformation model (BCTM) of the form

$$\mathbb{P}(\text{cholst} \leq \text{cholst}_{ij}) = \Phi\left(\gamma_0 + (\mathbf{a}(\text{cholst}_{ij})^\top \otimes \mathbf{b}(\text{age}_{ij})^\top)^\top \boldsymbol{\gamma}_1 + \gamma_2 \text{year}_{ij} + \gamma_3 \text{sex}_{ij}\right),$$

where  $\otimes$  denotes the Kronecker product. The bases  $\mathbf{a}(y_{ij})^\top$  and  $\mathbf{b}(\text{age}_{ij})^\top$  are 10-dimensional B-spline bases. In the random walk prior for the BCTM's tensor product term, we use an inverse gamma hyperprior with concentration  $a = 1$  and scale  $b = 0.01$  for the random walk variance parameter  $\tau^2$ . The coefficients  $\gamma_2$  and  $\gamma_3$  receive constant priors. See Carlan et al. (2023) for more on BCTMs. Like the PTMs, the BCTM is additionally fit with an i.i.d. random intercept.

**Predictive performance.** Table 2 shows how the models compare to each other in terms of the widely-applicable information criterion (WAIC). Among the models without random intercept, the nonlinear penalized transformation model yields the best (i.e. lowest) score. Notably, even the linear PTM yields a notably lower score than the nonlinear normal model. For the random-intercept models, we report both the conditional and the marginal WAIC (Merkle et al., 2019). The conditional WAIC assumes that we wish to predict the response in a known cluster that was contained in the original data. The marginal WAIC assumes that the cluster is unknown; it can be thought of as measuring predictive performance for the purpose of generalizing beyond the set of study participants. We include details about the computation of the conditional and marginal WAIC in Section G.2 of the supplemental materials. Among the models with random intercept, the BCTM yields the best conditional WAIC, while the linear PTM yields the best marginal WAIC. This suggests that the predictive performance of the BCTM is better for study participants, while the PTM is more effective at generalizing predictions beyond the set of study participants. A striking observation from Table 2 is the fact that for the BCTM, the drop in predictive performance between the conditional WAIC and the marginal WAIC is much more pronounced than for the normal models or the PTMs. This is partly due to the much lower decrease in the number of effective parameters observed for the BCTM. It seems that the BCTM is heavily overfitting to the set of study participants in the random intercept model.

**Model interpretation.** Penalized transformation models can be summarized by interpreting the covariate effects just like they would be interpreted in a normal location-scale model, and additionally plotting the residual distribution. Panel a) of Figure 9 displays the residual distribution for both PTMs without random intercept. Both models yield right-skewed residual distributions. The plot additionally displays a kernel density estimation of the posterior distribution of the

**Table 2** Observed widely applicable information criterion (WAIC) values for different models fitted to the Framingham heart study dataset. The columns  $p_{\text{WAIC}}$  indicate the effective sample size. The columns cWAIC and mWAIC give the conditional and marginal WAIC for the models with random intercepts. The lowest WAIC value in each column is marked by bold print.

Family	Model	WAIC	$p_{\text{WAIC}}$	Random intercept models			
				cWAIC	$p_{\text{cWAIC}}$	mWAIC	$p_{\text{mWAIC}}$
Normal	Linear	2822	7	1611	170	1757	10
Normal	Nonlinear	2775	22	1613	175	1760	18
PTM	Linear	2736	14	1608	207	<b>1747</b>	16
PTM	Nonlinear	<b>2699</b>	25	1610	211	1751	23
BCTM		2718	19	<b>1575</b>	176	2290	156

person-specific random intercept in the linear normal model. Note how closely the posterior distribution of the random intercept resembles the PTMs' residual distributions: both show the same right-skew. It seems that the PTMs implicitly capture the variability induced by individual-specific factors through the residual distribution, which means the residual distribution recovers the same information as the random intercept. As we can see, the PTM does not require explicit information about cluster membership for this. Additionally, a PTM will natively incorporate the full information in its predictive distribution, while predictions based on a random intercept model typically involve integrating over the random effect's gaussian prior, updated only with its posterior variance. It should be noted however that a PTM does not protect against distortions caused by highly *imbalanced* unobserved cluster memberships.

Panel b) of Figure 9 shows how the mean and standard deviation relate to participants' age in the nonlinear PTM without random intercept. For both parameters, we can observe a positive association: a higher age is associated with higher average cholesterol levels and higher average standard deviations. However, at an age of about 55 years, the average cholesterol level drops, stabilizing again at an age of about 60 years. It should be noted that the data contain only 16 individuals with an age above 55 years, so estimation in this age category has high uncertainty. Panel c) of Figure 9 compares three conditional density estimations obtained using the nonlinear PTM and the BCTM without random intercept. The other covariate effects are set to zero in both models. For the ages of 35 and 45, both models yield very similar results; the right-skewed distribution observed in Panel a). For an age of 55 however, there is a notable difference. In both models, the scale is higher at an age of 55 compared to the two lower ages on display, but the BCTM yields a rather symmetrical bell-shaped conditional distribution, while the PTM still predicts a right-skewed shape. In Section G.3 of the supplemental materials, we include and comment on parameter estimates for the linear regression coefficients.

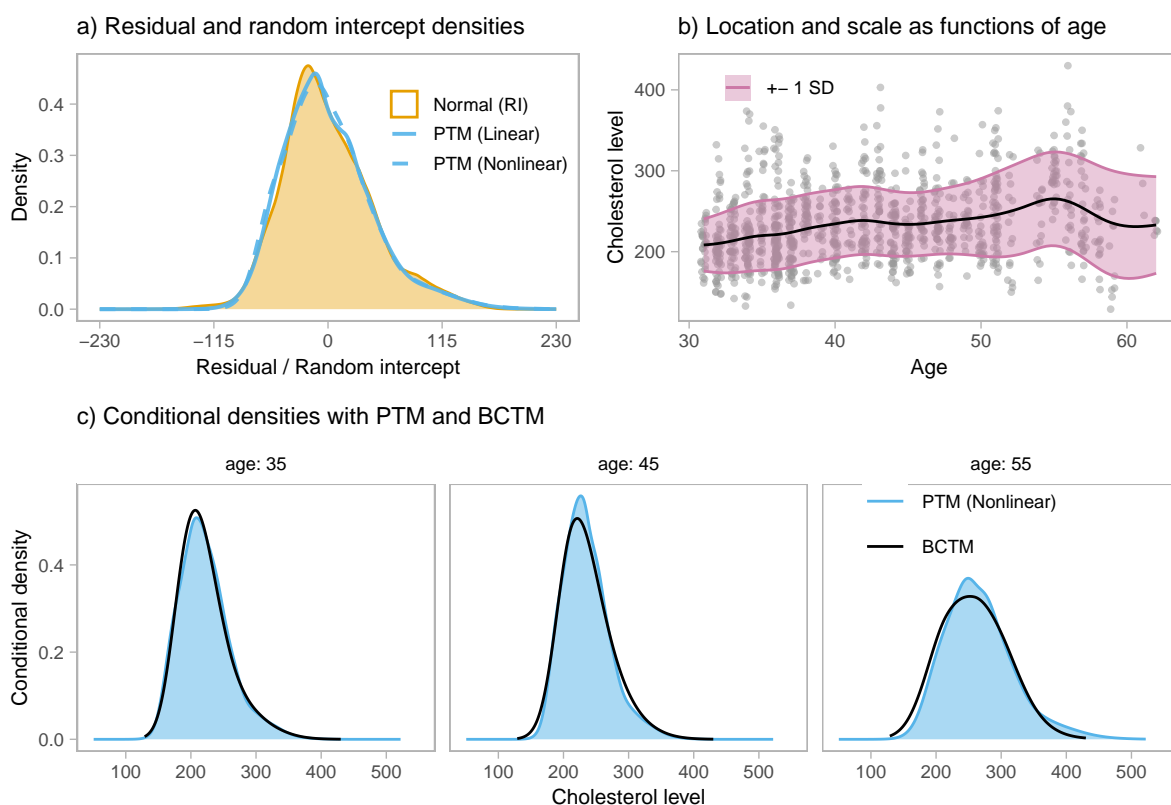


**Figure 9** a) Comparison of posterior density estimate of the random intercept obtained in the linear normal location-scale model with residual densities obtained in the linear and nonlinear PTMs without random intercepts. b) Posterior mean effect of age in the nonlinear PTM without random intercept, fixing the other covariates to zero. The shaded area shows  $\pm 1$  of the posterior mean scale as a function of age. c) Comparison of conditional densities at three different ages obtained using the Bayesian CTM and the nonlinear PTM, both without random intercepts.

## 6. Outlook and conclusion

With penalized transformation models, we contribute a well-interpretable model for the location and scale of arbitrary distributions. Thanks to the transformation model at the core of the distribution estimation, we obtain a proper density that can be used to investigate conditional quantiles of the response distribution. The model can be conveniently summarized by plotting the estimated residual density alongside the location and scale effects. The Bayesian approach to PTMs is especially attractive due to its straightforward quantification of uncertainty about the complex derived estimates for the conditional distribution and conditional quantiles. Through the random walk prior on the shape parameters  $\delta$ , the Bayesian view also provides a natural interpretation of regularization: it moderates the trade-off between a more complex model and the base model defined by the reference distribution. Our simulation studies and application examples underline how PTMs can be used as drop-in replacements for gaussian location-scale regression models. The simulations show how the PTM can even lead to markedly improved results in scenarios in which conditional transformation models and quantile regression actually fare worse than gaussian location-scale regression.

PTMs provide a fruitful basis for future developments. On one hand, an attractive road for development lies in tailoring PTMs to specific applications like count data, censored data, or heavy-tailed data. On the other hand, we can envision general extensions like introducing a binary switch between the base model and the more general model through the use of spike and slab priors and extensions to modelling higher moments of the response distribution. We elaborate on the extensions below.

- Count data PTMs as briefly outlined in Section 2.4 natively handle zero-inflation and offer a similarly nice setup and interpretation of covariate effects as continuous PTMs through their location and scale model parts. The latter also directly solves the problem of overdispersion. Count data PTMs relate to conditional transformation models (CTMs) for count data (Carlan & Kneib, 2022; Siegfried & Hothorn, 2020) in a similar way as continuous PTMs relate to continuous CTMs and transformation additive models (Hothorn et al., 2018; Siegfried et al., 2023): the location and scale parameters of count PTMs act directly on the probability mass function at the response level. This means, changes to these parameters can be thought of as horizontally moving the probability mass to the left or right, and lowering or heightening its variance, respectively. Count CTMs, on the other hand, involve either tensor product terms that potentially affect all moments of the distribution, or location shift terms that act on the latent level and are hence harder to interpret.
- For censored data, take a survival time response as the most common case. A PTM applied to a log-transformed survival time response can be regarded as an accelerated failure time model with a nonparametrically baseline hazard function estimated directly from the data. Similar models have been developed (for example Burke et al., 2020), but different from PTMs they typically do not yield a fully specified distribution, and inference is challenging.
- For extending PTMs to model heavy-tailed responses, recall first that, due to the linear extrapolation of the transformation function, the PTM implies a location-scale model for the reference distribution for the tails of the distribution. Heavy tails could consequently be incorporated by assumption through the choice of reference distribution. But if data on outliers is available, an extended PTM could even include the estimation of (some of) the reference distribution's parameters - for example the degrees of freedom in a  $t$ -distribution. This would be a new development for transformation models, since the reference distribution is typically assumed to be fully specified without unknown parameters.
- Spike and slab priors as described by Klein et al. (2021) can be placed on the shape parameter's random walk variance  $\tau_\delta^2$  to introduce a dichotomous switch between a model for the reference distribution and a model that allows divergence from the reference distribution.

- In order to capture covariate effects on higher moments of the conditional response distribution, structured additive predictors could be placed on the shape parameters  $\delta$ . This idea has a close connection to the work of Sick et al. (2021), who used Bernstein polynomials for the transformation function in a model  $F_Y(y) = F_Z(h(y|\vartheta(\mathbf{x})))$  and related the function's parameters  $\vartheta(\mathbf{x})$  to covariates with deep neural networks. This approach, however, has the drawback of sacrificing interpretability for flexibility, since the location and scale model parts cannot be easily disentangled from the shape of the distribution anymore.

On a final note, the model construction allows not only for the fully Bayesian approach developed here, but also for maximum-likelihood inference. In this case, the random walk variance parameter  $\tau_\delta^2$  is instead interpreted as an inverse smoothing parameter and can be optimized, for example, using cross validation (Eilers & Marx, 1996).

In conclusion, we view PTMs as a highly promising option in statistician's toolkit with a wealth of applications and extensions on the horizon due to its combination of flexibility and interpretability.

## References

- Betancourt, M. (2018). *A conceptual introduction to hamiltonian monte carlo*. arXiv. <http://arxiv.org/abs/1701.02434>
- Brachem, J., Wiemann, P., & Kneib, T. (2023). *Liesel-bctm: Bayesian conditional transformation models in Liesel [Python library]* (Version 0.2.0). <https://github.com/liesel-devs/liesel-bctm>
- Brachem, J., Wiemann, P., & Kneib, T. (2024). *Liesel-ptm: Penalized transformation models in Liesel [Python library]* (Version 0.1.0). <https://github.com/liesel-devs/liesel-ptm>
- Bradbury, J., Frostig, R., Hawkins, P., Johnson, M. J., Leary, C., Maclaurin, D., Necula, G., Paszke, A., VanderPlas, J., Wanderman-Milne, S., & Zhang, Q. (2018). *JAX: Composable transformations of Python+NumPy programs [Python library]* (Version 0.4.20). <http://github.com/google/jax>
- Burke, K., Eriksson, F., & Pipper, C. B. (2020). Semiparametric multiparameter regression survival modeling. *Scandinavian Journal of Statistics*, 47(2), 555–571. <https://doi.org/10.1111/sjos.12416>
- Cabezas, Alberto, J., Lao, & Louf, R. (2023). *Blackjax: A sampling library for JAX [Python library]* (Version 1.0.0). <http://github.com/blackjax-devs/blackjax>
- Carlan, M., & Kneib, T. (2022). Bayesian discrete conditional transformation models. *Statistical Modelling*. <https://doi.org/10.1177/1471082X221114177>
- Carlan, M., Kneib, T., & Klein, N. (2023). Bayesian conditional transformation models. *Journal of the American Statistical Association*, 79(388), 1–24. <https://doi.org/10.1080/01621459.2023.2191820>
- DeepMind, Babuschkin, I., Baumli, K., Bell, A., Bhupatiraju, S., Bruce, J., Buchlovsky, P., Budden, D., Cai, T., Clark, A., Danihelka, I., Dedieu, A., Fantacci, C., Godwin, J., Jones, C., Hemsley,

- R., Hennigan, T., Hessel, M., Hou, S., . . . Viola, F. (2020). *The DeepMind JAX Ecosystem [Python libraries]*. <https://github.com/google-deeppmind>
- Eilers, P. H. C., & Marx, B. D. (1996). Flexible smoothing with B-splines and penalties. *Statistical Science*, 11(2), 89–121. <https://doi.org/10.1214/ss/1038425655>
- Eilers, P. H. C., & Marx, B. D. (2021). *Practical smoothing: The joys of P-splines* (1st ed.). Cambridge University Press. <https://doi.org/10.1017/9781108610247>
- Fahrmeir, L., Kneib, T., Lang, S., & Marx, B. (2013). *Regression - models, methods and applications*. Springer Berlin Heidelberg. <https://doi.org/10.1007/978-3-642-34333-9>
- Fasiolo, M., Wood, S. N., Zaffran, M., Nedellec, R., & Goude, Y. (2021a). Qgam: Bayesian nonparametric quantile regression modeling in r. *Journal of Statistical Software*, 100(9). <https://doi.org/10.18637/jss.v100.i09>
- Fasiolo, M., Wood, S. N., Zaffran, M., Nedellec, R., & Goude, Y. (2021b). Fast calibrated additive quantile regression. *Journal of the American Statistical Association*, 116(535), 1402–1412. <https://doi.org/10.1080/01621459.2020.1725521>
- Fredriks, A. M., van Buuren, S., Burgmeijer, R. J., Meulmeester, J. F., Beuker, R. J., Brugman, E., Roede, M. J., Verloove-Vanhorick, S. P., & Wit, J. M. (2000). Continuing positive secular growth change in The Netherlands 1955-1997. *Pediatric Research*, 47(3), 316–323. <https://doi.org/10.1203/00006450-200003000-00006>
- Fredriks, A. M., van Buuren, S., Wit, J. M., & Verloove-Vanhorick, S. P. (2000). Body index measurements in 1996-7 compared with 1980. *Archives of Disease in Childhood*, 82(2), 107–112. <https://doi.org/10.1136/adc.82.2.107>
- Gelman, A. (2006). Prior distributions for variance parameters in hierarchical models (comment on article by Browne and Draper). *Bayesian Analysis*, 1(3). <https://doi.org/10.1214/06-BA117A>
- Gneiting, T. (2011). Quantiles as optimal point forecasts. *International Journal of Forecasting*, 27(2), 197–207. <https://doi.org/10.1016/j.ijforecast.2009.12.015>
- Gneiting, T., & Raftery, A. E. (2007). Strictly proper scoring rules, prediction, and estimation. *Journal of the American Statistical Association*, 102(477), 359–378. <https://doi.org/10.1198/016214506000001437>
- Hanson, T., & Johnson, W. O. (2002). Modeling regression error with a mixture of polya trees. *Journal of the American Statistical Association*, 97(460), 1020–1033. <https://doi.org/10.1198/016214502388618843>
- Hoffman, M. D., & Gelman, A. (2014). The No-U-Turn sampler: Adaptively setting path lengths in hamiltonian monte carlo. *Journal of Machine Learning Research*, 15(1), 1593–1623.
- Hothorn, T., Kneib, T., & Bühlmann, P. (2014). Conditional transformation models. *Journal of the Royal Statistical Society: Series B (Statistical Methodology)*, 76(1), 3–27. <https://doi.org/10.1111/rssb.12017>
- Hothorn, T., Möst, L., & Bühlmann, P. (2018). Most likely transformations. *Scandinavian Journal of Statistics*, 45(1), 110–134. <https://doi.org/10.1111/sjos.12291>

- Klein, N., Carlan, M., Kneib, T., Lang, S., & Wagner, H. (2021). Bayesian effect selection in structured additive distributional regression models. *Bayesian Analysis*, 16(2), 545–573. <https://doi.org/10.1214/20-BA1214>
- Klein, N., & Kneib, T. (2016). Scale-dependent priors for variance parameters in structured additive distributional regression. *Bayesian Analysis*, 11(4), 1071–1106. <https://doi.org/10.1214/15-BA983>
- Lang, S., & Brezger, A. (2004). Bayesian P-splines. *Journal of Computational and Graphical Statistics*, 13(1), 183–212. <https://doi.org/10.1198/1061860043010>
- Leslie, D. S., Kohn, R., & Nott, D. J. (2007). A general approach to heteroscedastic linear regression. *Statistics and Computing*, 17(2), 131–146. <https://doi.org/10.1007/s11222-006-9013-8>
- Merkle, E. C., Furr, D., & Rabe-Hesketh, S. (2019). Bayesian comparison of latent variable models: Conditional versus marginal likelihoods. *Psychometrika*, 84(3), 802–829. <https://doi.org/10.1007/s11336-019-09679-0>
- Pya, N., & Wood, S. N. (2015). Shape constrained additive models. *Statistics and Computing*, 25(3), 543–559. <https://doi.org/10.1007/s11222-013-9448-7>
- Riebl, H., Wiemann, P. F. V., & Kneib, T. (2023). *Liesel: A probabilistic programming framework for developing semi-parametric regression models and custom bayesian inference algorithms*. <http://arxiv.org/abs/2209.10975>
- Rigby, R. A., & Stasinopoulos, D. M. (2005). Generalized additive models for location, scale and shape. *Journal of the Royal Statistical Society: Series C (Applied Statistics)*, 54(3), 507–554. <https://doi.org/10.1111/j.1467-9876.2005.00510.x>
- Schnabel, S. K., & Eilers, P. H. C. (2013). Simultaneous estimation of quantile curves using quantile sheets. *AStA Advances in Statistical Analysis*, 97(1), 77–87. <https://doi.org/10.1007/s10182-012-0198-1>
- Sick, B., Hothorn, T., & Dürr, O. (2021). Deep transformation models: Tackling complex regression problems with neural network based transformation models. *25th International Conference on Pattern Recognition (ICPR)*, 2476–2481. <https://doi.org/10.1109/ICPR48806.2021.9413177>
- Siegfried, S., & Hothorn, T. (2020). Count transformation models. *Methods in Ecology and Evolution*, 11(7), 818–827. <https://doi.org/10.1111/2041-210X.13383>
- Siegfried, S., Kook, L., & Hothorn, T. (2023). Distribution-free location-scale regression. *The American Statistician*, 77(4), 345–356. <https://doi.org/10.1080/00031305.2023.2203177>
- Simpson, D., Rue, H., Riebler, A., Martins, T. G., & Sørbye, S. H. (2017). Penalising model component complexity: A principled, practical approach to constructing priors. *Statistical Science*, 32(1). <https://doi.org/10.1214/16-STS576>
- Stasinopoulos, M., Rigby, B., & De Bastiani, F. (2021). *Gamlss.data: Data for generalised additive models for location scale and shape [R package]* (Version 6.0-2). <https://CRAN.R-project.org/package=gamlss.data>

- Umlauf, N., Klein, N., & Zeileis, A. (2018). Bamlss: Bayesian additive models for location, scale, and shape (and beyond). *Journal of Computational and Graphical Statistics*, 27(3), 612–627. <https://doi.org/10.1080/10618600.2017.1407325>
- Vehtari, A., Gelman, A., & Gabry, J. (2017). Practical Bayesian model evaluation using leave-one-out cross-validation and WAIC. *Statistics and Computing*, 27(5), 1413–1432. <https://doi.org/10.1007/s11222-016-9696-4>
- Watanabe, S. (2010). Asymptotic equivalence of bayes cross validation and widely applicable information criterion in singular learning theory. *Journal of Machine Learning Research*, 11, 3571–3594.
- Wood, S. N. (2017). *Generalized additive models* (2nd ed.). Chapman & Hall/CRC.
- Zhang, D., & Davidian, M. (2001). Linear mixed models with flexible distributions of random effects for longitudinal data. *Biometrics*, 57(3), 795–802. <https://doi.org/10.1111/j.0006-341X.2001.00795.x>



## A. Contrast to Transformation Additive Models

Siegfried et al. (2023) proposed transformation additive models (TAMLS), which are closely related to penalized transformation models. However, there is a key difference that we briefly lay out here. They parameterize the response CDF as

$$F_Y(y) = F_Z\left(\frac{h(y)}{\sigma(\mathbf{x})} - \mu(\mathbf{x})\right).$$

Thus, the terms  $\mu(\mathbf{x})$  and  $\sigma(\mathbf{x})$  model location and scale of the *transformed* response, respectively. The model can also be written as

$$z = \frac{h(y)}{\sigma(\mathbf{x})} - \mu(\mathbf{x}) \sim F_Z$$

and slightly rearranged to

$$h(y) = \frac{\mu(\mathbf{x})}{\sigma(\mathbf{x})} + \sigma(\mathbf{x})z, \quad z \sim F_Z,$$

to reveal a form that is reminiscent of a generalized additive model (GAM) for location and scale with link function  $h$ . Thus, the approach developed by Siegfried et al. (2023) can be seen as a GAM with a nonparametric link function that is inferred from the data. Siegfried et al. (2023) show how, through careful specification of the reference distribution and covariate effects, this general form comprises several well-established models like, for example, the proportional hazards model and proportional odds model. These models also offer interpretability on a general level in the sense that the response's location and scale are monotonic functions of  $\mu(\mathbf{x})$  and  $\sigma(\mathbf{x})$ , respectively. However, care should be taken with these interpretations, because  $\mu(\mathbf{x})$  and  $\sigma(\mathbf{x})$  in TAMLS do not satisfy the definitions of location and scale parameters. Figure A1 illustrates that, when location shifts are applied to the transformed response  $h_Y(y)$ , they can affect the shape of the implied conditional distribution in significant and difficult-to-predict ways. Note that, in panel (a) of Figure A1, the location shift on the transformed level can turn a unimodal and roughly symmetrical density ( $\mu(\mathbf{x}) = 0$ ) into a bimodal density ( $\mu(\mathbf{x}) = -2$ ) or left-skewed ( $\mu(\mathbf{x}) = 2$ ) density. Similar patterns apply for scale effects on the transformed level. Since PTMs model the location and scale on the response level prior to transformation to the residual distribution, they fully retain the interpretation as the response distribution's location and scale.

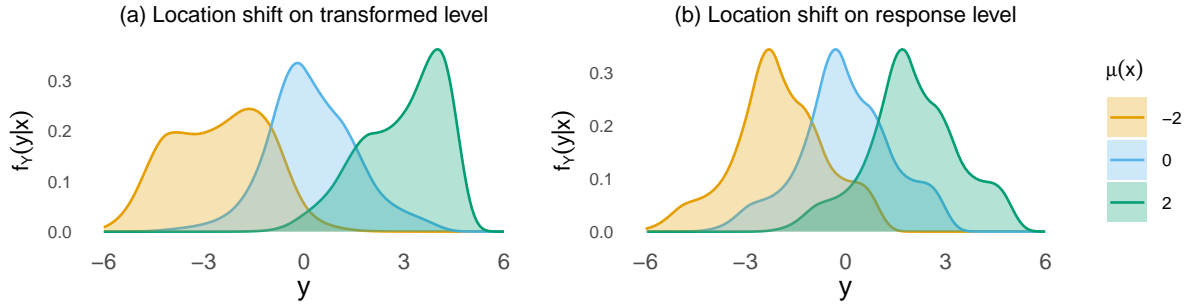


**Figure A1** Conditional response densities resulting from location shifts on the level of the transformation (a) and the level of the response (b). Panel (a) reflects a transformation function of the form  $h(y|\mathbf{x}) = h_Y(y) - \mu(\mathbf{x})$ , while panel (b) reflects a transformation function of the form  $h(y|\mathbf{x}) = h(y - \mu(\mathbf{x}))$ .

## B. Proofs

### B.1. Proof of Proposition 2.1

We lay out the notation and some basic results in Definition B.1, Lemma B.1 and Lemma B.2. The largest part of the work is done in Lemma B.3, before bringing all parts together in Proposition B.1.

**Definition B.1** (Monotonically increasing B-spline). Let  $f : \mathbb{R} \rightarrow \mathbb{R}$  be given by

$$f(\varepsilon) = \sum_{j=1}^J B_j^{(3)}(\varepsilon) \left( \alpha + \sum_{\ell=2}^j \exp(\delta_{\ell-1}) \right), \quad (12)$$

with parameters  $\alpha, \delta_1, \delta_2, \dots, \delta_{J-1} \in \mathbb{R}$  and B-spline bases  $B_j^{(3)}$  of order 3 using an equidistant knot base  $k_{-2} < k_{-1} < k_0 < \dots < k_J < k_{J+1}$ . Then we call (12) a monotonically increasing B-spline.

We use the recursive definition of a B-spline basis as given by Fahrmeir et al. (2013):

$$B_j^{(m)}(\varepsilon) = \frac{\varepsilon - k_{j-m}}{k_j - k_{j-m}} B_{j-1}^{(m-1)}(\varepsilon) + \frac{k_{j+1} - \varepsilon}{k_{j+1} - k_{j+1-m}} B_j^{(m-1)}(\varepsilon). \quad (13)$$

The order of the basis is given by  $m$ , with  $m = 3$  for cubic splines. The basis of order  $m = 0$  is given by

$$B_j^{(0)}(\varepsilon) = I(k_j \leq \varepsilon < k_{j+1}), \quad j = 1, \dots, J-1,$$

where  $I(\cdot)$  is the indicator function for the enclosed condition. For equidistant knots  $k_{j+1} - k_j = d$ , the basis (13) simplifies to

$$B_j^{(m)}(\varepsilon) = \frac{\varepsilon - k_{j-m}}{md} B_{j-1}^{(m-1)}(\varepsilon) + \frac{k_{j+1} - \varepsilon}{md} B_j^{(m-1)}(\varepsilon). \quad (14)$$

**Lemma B.1** (Derivative of a monotonically increasing B-spline). *Let  $f : \mathbb{R} \rightarrow \mathbb{R}$  be a monotonically increasing B-spline as given in Definition B.1. Then the derivative of  $f$  is*

$$\frac{\partial}{\partial \varepsilon} f(\varepsilon) = \sum_{j=2}^J B_j^{(2)}(\varepsilon) \frac{\exp(\delta_{j-1})}{d}. \quad (15)$$

*Proof.* This result is little more but a restatement of a well-known result about the derivatives of B-splines: the derivative of an  $m^{\text{th}}$ -order B-spline is an  $(m-1)^{\text{th}}$ -order B-spline whose coefficients are first differences in the original coefficients, scaled by the distance between the corresponding knots. See for example Eilers & Marx (2021), p. 20. Here, we treat  $\gamma_j = \left( \alpha + \sum_{\ell=2}^j \exp(\delta_{\ell-1}) \right)$ ,  $j = 1, \dots, J$  as the coefficients of the original B-spline, such that  $\exp(\delta_1)/d, \dots, \exp(\delta_{J-1})/d$  become the coefficients of the first derivative. □

**Lemma B.2** (Derivative in a segment). *Let  $f : \mathbb{R} \rightarrow \mathbb{R}$  be a monotonically increasing B-spline as given in Definition B.1. If  $\varepsilon \in [k_j, k_{j+1}]$ , where  $1 \leq j \leq J-3$ , then we know that the first derivative of  $f$  evaluated at  $\varepsilon$  is*

$$\frac{\partial}{\partial \varepsilon} f(\varepsilon) = \sum_{j'=j}^{j+2} B_{j'}^{(2)}(\varepsilon) \frac{\exp(\delta_{j'})}{d}. \quad (16)$$

*Proof.* A well-known property of B-splines of order  $m$  is the fact that at any point  $\varepsilon \in [k_1, k_{J-2}]$ , we have  $m+1$  positive basis functions, while the remaining basis functions evaluate to zero (see p. 429, Fahrmeir et al., 2013). Since the derivative of the monotonically increasing B-spline uses bases of order  $m=2$ , that means at any point  $\varepsilon \in [k_1, k_{J-2}]$ , we have 3 positive basis functions. If we know that  $\varepsilon \in [k_j, k_{j+1}]$ , it follows from (14) that the positive basis functions are  $B_j, B_{j+1}$ , and  $B_{j+2}$ , which directly lets (15) simplify to (16). □

**Lemma B.3** (Average derivative in a segment). *Let  $f : \mathbb{R} \rightarrow \mathbb{R}$  be a monotonically increasing B-spline as given in Definition B.1. If  $\varepsilon \in [k_j, k_{j+1}]$ , the average derivative of  $f$  in the corresponding function segment is given by*

$$\frac{1}{d} \int_{k_j}^{k_{j+1}} \left( \frac{\partial}{\partial \varepsilon} f(\varepsilon) \right) d\varepsilon = \frac{1}{d} \left( \frac{1}{6} \exp(\delta_j) + \frac{2}{3} \exp(\delta_{j+1}) + \frac{1}{6} \exp(\delta_{j+2}) \right). \quad (17)$$

*Proof.* First, note that since  $\varepsilon \in [k_j, k_{j+1}]$ , we can apply Lemma B.2 to write

$$\begin{aligned} \frac{1}{d} \int_{k_j}^{k_{j+1}} \left( \frac{\partial}{\partial \varepsilon} f(\varepsilon) \right) d\varepsilon = & \frac{1}{d} \left( \frac{\exp(\delta_j)}{d} \int_{k_j}^{k_{j+1}} B_j^{(2)}(\varepsilon) d\varepsilon \right. \\ & \left. + \frac{\exp(\delta_{j+1})}{d} \int_{k_j}^{k_{j+1}} B_{j+1}^{(2)}(\varepsilon) d\varepsilon + \frac{\exp(\delta_{j+2})}{d} \int_{k_j}^{k_{j+1}} B_{j+2}^{(2)}(\varepsilon) d\varepsilon \right). \end{aligned}$$

A sufficient condition for this expression to simplify to (17) is given by the following three statements:

$$\int_{k_j}^{k_{j+1}} B_j^{(2)}(\varepsilon) d\varepsilon \stackrel{!}{=} \frac{d}{6}, \quad (\text{s1})$$

$$\int_{k_j}^{k_{j+1}} B_{j+1}^2(\varepsilon) d\varepsilon \stackrel{!}{=} \frac{2d}{3}, \quad \text{and} \quad (\text{s2})$$

$$\int_{k_j}^{k_{j+1}} B_{j+2}^2(\varepsilon) d\varepsilon \stackrel{!}{=} \frac{d}{6}. \quad (\text{s3})$$

In the following we show first that s1 and s3 hold, before showing that s2 holds.

1. To show that s1 holds, we substitute the definition of a B-spline basis (14) and simplify, such that we obtain

$$\int_{k_j}^{k_{j+1}} B_j^{(2)}(\varepsilon) d\varepsilon = \frac{1}{2d^2} \int_{k_j}^{k_{j+1}} (k_{j+1} - \varepsilon)^2 d\varepsilon.$$

The integral is readily solved using  $u$ -substitution with  $u = k_{j+1} - \varepsilon$ . Inserting the integral limits, we get

$$\frac{1}{2d^2} \int_{k_j}^{k_{j+1}} (k_{i+1} - \varepsilon)^2 d\varepsilon = \frac{1}{2d^2} \frac{(k_{j+1} - k_j)^3}{3} = \frac{d^3}{6d^2} = \frac{d}{6},$$

confirming that s1 is true. The solution for s3 works in complete analogy.

2. Substituting the definition of a B-spline basis into s2, we obtain

$$\int_{k_j}^{k_{j+1}} B_{j+1}^2(\varepsilon) d\varepsilon = \frac{1}{2d^2} \left( - \int_{k_j}^{k_{j+1}} (\varepsilon - k_{j-1})(\varepsilon - k_{j+1}) d\varepsilon - \int_{k_j}^{k_{j+1}} (\varepsilon - k_j)(\varepsilon - k_{j+2}) d\varepsilon \right). \quad (18)$$

The two integrals in (18) can be solved analogously. Considering the left-hand term, we have

$$- \int_{k_j}^{k_{j+1}} (\varepsilon - k_{j-1})(\varepsilon - k_{j+1}) d\varepsilon = - \left[ \left( \frac{2k_{j+1}^3 - 6k_{j+1}^2 d}{6} \right) - \left( \frac{-4k_j^3 + 6k_j k_{j-1} k_{j+1}}{6} \right) \right].$$

Next, we substitute  $k_j = k_{j+1} - d$  and  $k_{j-1} = k_{j+1} - 2d$  and simplify further, which results in

$$- \int_{k_j}^{k_{j+1}} (\varepsilon - k_{i-1})(\varepsilon - k_{i+1}) d\varepsilon = \frac{2d^3}{3}.$$

Applying the analogous procedure to the right-hand term in (18), we get

$$\frac{1}{2d^2} \int_{k_j}^{k_{j+1}} (k_{i+1} - \varepsilon)^2 d\varepsilon = \frac{1}{2d^2} \left( \frac{2d^3}{3} + \frac{2d^3}{3} \right) = \frac{2d}{3},$$

concluding the proof of s2.

Since we have shown that the sufficient conditions s1, s2, and s3 are met, this concludes the proof. □

**Proposition B.1** (Average slope of a monotonically increasing B-spline). *Let  $f : \mathbb{R} \rightarrow \mathbb{R}$  be a monotonically increasing B-spline  $f(\varepsilon) = \sum_{j=1}^J B_j(\varepsilon) \left( \sum_{\ell=2}^j \exp(\delta_{\ell-1}) \right)$  with bases of order 3, on an equidistant knot base  $k_{-2} < k_{-1} < k_0 < \dots < k_J < k_{J+1}$ , and with parameters  $\delta \in \mathbb{R}^{J-1}$ . Let  $a = k_1$  and  $b = k_{J-2}$  denote the boundary knots. Then the average slope of  $f$  over the interval  $[a, b]$  is given by*

$$\begin{aligned} s(\delta) &= \frac{1}{b-a} \int_a^b \frac{\partial}{\partial \varepsilon} f(\varepsilon) d\varepsilon \\ &= \frac{1}{b-a} \sum_{j=1}^{J-3} \left( \frac{\exp(\delta_j) + \exp(\delta_{j+2})}{6} + \frac{2 \exp(\delta_{j+1})}{3} \right), \end{aligned} \tag{19}$$

*Proof.* The integral can be additively decomposed using the interior knots as the bounds of integration, such that we can write

$$\frac{1}{b-a} \int_a^b \frac{\partial}{\partial \varepsilon} f(\varepsilon) d\varepsilon = \frac{1}{b-a} \sum_{j=1}^{J-3} \left( \int_{k_j}^{k_{j+1}} \frac{\partial}{\partial \varepsilon} f(\varepsilon) d\varepsilon \right).$$

By Lemma B.3, the individual integrals in the right-hand-side sum can be written in terms of the parameters  $\delta_j$ ,  $\delta_{j+1}$ , and  $\delta_{j+2}$ , such that we can write

$$\frac{1}{b-a} \int_a^b \frac{\partial}{\partial \varepsilon} f(\varepsilon) d\varepsilon = \frac{1}{b-a} \sum_{j=1}^{J-3} \left( \frac{1}{6} \exp(\delta_j) + \frac{2}{3} \exp(\delta_{j+1}) + \frac{1}{6} \exp(\delta_{j+2}) \right),$$

which directly simplifies to (5). □

## B.2. Proof of Theorem 2.1

**Theorem B.1** (Monotonicity of the transformation function). *Let the function  $h : \mathbb{R} \rightarrow \mathbb{R}$  and the core segment spline( $\varepsilon$ ) be given as defined in Section 2.1 of the main text. Then  $h$  is strictly monotonically increasing in  $\varepsilon$ ; that is, for all  $\varepsilon_1, \varepsilon_2 \in \mathbb{R}$  with  $\varepsilon_1 < \varepsilon_2$ , we have  $h(\varepsilon_1) < h(\varepsilon_2)$ .*

*Proof.* We prove the theorem by showing that  $\frac{\partial}{\partial \varepsilon} h(\varepsilon) > 0$  for all  $\varepsilon \in \mathbb{R}$ , which is equivalent to monotonicity. We proceed by cases.

1. *Case 1: Linear segments.* Note that in the linear function segments, when  $\varepsilon \in (-\infty, a - \lambda) \cup (b + \lambda, \infty)$ , we have  $\frac{\partial}{\partial \varepsilon} h(\varepsilon) = 1$ , which is strictly greater than zero. Thus, in the linear segments,  $h$  is strictly monotonically increasing.
2. *Case 2: Core segment.* The derivative of the core segment, when  $\varepsilon \in [a, b]$ , is given by

$$\frac{\partial}{\partial \varepsilon} \text{spline}(\varepsilon) = \frac{\omega}{s(\boldsymbol{\delta}) \cdot d} \sum_{j=2}^J B_j^{(2)}(\varepsilon) \exp(\delta_{j-1}).$$

Note that, by definition, any basis function evaluation  $B_j^{(2)}(\varepsilon)$  is nonnegative, and for any given  $\varepsilon \in [a, b]$ , three basis function evaluations are positive. Note also that  $\omega > 0$  by definition, the distance between adjacent knots  $d = k_{j+1} - k_j > 0$  by construction, and  $s(\boldsymbol{\delta}) > 0$ . Finally, observe that  $\exp(\delta) > 0$  for all  $\delta \in \mathbb{R}$ . As a result,  $\frac{\partial}{\partial \varepsilon} \text{spline}(\varepsilon) > 0$  for all  $\varepsilon \in [a, b]$ .

3. *Case 3: Transition segments.* We start with the left transition segment, when  $\varepsilon \in [a - \lambda, a)$ . Let

$$t_a(\varepsilon) = \frac{\varepsilon}{\lambda} \left[ a - \frac{\varepsilon}{2} + \left( \lambda - a + \frac{\varepsilon}{2} \right) \cdot \frac{\partial}{\partial a} \text{spline}(a) \right] + A$$

denote the left transition segment. Then the derivative of this segment is given by

$$\frac{\partial}{\partial \varepsilon} t_a(\varepsilon) = \left( 1 - \frac{a - \varepsilon}{\lambda} \right) \cdot \frac{\partial}{\partial a} \text{spline}(a) + \frac{a - \varepsilon}{\lambda}$$

Observe that  $a - \lambda \leq \varepsilon < a$  and  $\lambda > 0$ , such that  $\frac{a-\varepsilon}{\lambda} \in (0, 1]$ . Thus,

$$\min \left( \frac{\partial}{\partial \varepsilon} t_a(\varepsilon) \right) = \min \left\{ \frac{\partial}{\partial a} \text{spline}(a), 1 \right\}.$$

Since we know that  $\frac{\partial}{\partial \varepsilon} \text{spline}(\varepsilon) > 0$  for all  $\varepsilon \in [a, b]$  from Case 2, this means that  $\frac{\partial}{\partial \varepsilon} t_a(\varepsilon) > 0$  for all  $\varepsilon \in [a - \lambda, a]$ . The proof for the right transition, when  $\varepsilon \in (b, b + \lambda]$ , works analogously.

We have shown that  $\frac{\partial}{\partial \varepsilon} h(\varepsilon) > 0$  if  $\varepsilon \in (-\infty, a - \lambda) \cup (b + \lambda, \infty)$  (Case 1), if  $\varepsilon \in [a - \lambda, a)$  or  $\varepsilon \in (b, b + \lambda]$  (Case 3), and if  $\varepsilon \in [a, b]$  (Case 2). Observe that

$$\mathbb{R} = (-\infty, a - \lambda) \cup [a - \lambda, a) \cup [a, b] \cup (b, b + \lambda] \cup (b + \lambda, \infty).$$

Thus, we conclude that  $\frac{\partial}{\partial \varepsilon} h(\varepsilon) > 0$  for all  $\varepsilon \in \mathbb{R}$ , which is equivalent to saying that  $h$  is strictly monotonically increasing in  $\varepsilon$  for all  $\varepsilon \in \mathbb{R}$ . □

### B.3. Software implementation

We provide a feature-rich open source implementation in the Python library `liesel-ptm`. The library is hosted on GitHub (<https://github.com/liesel-devs/liesel-ptm>) and can be installed directly from the repository. Documentation is available from <https://liesel-devs.github.io/liesel-ptm/>. The library supports the whole process of setting up a penalized transformation model and drawing samples from its posterior distribution. The following is a non-exhaustive list of steps that users can perform:

1. Set up penalized transformation models using the class `PTMLocScale`. Users can choose from several options for priors on  $\tau_\delta^2$  and  $\omega$ , or supply their own choices by providing `liesel.model.Var` objects.
2. Define the terms of structured additive predictors in the location and scale models using the class `StructuredAdditiveTerm`. This class is a highly generalized interface that allows users to provide an adequate basis function, penalty matrix, and variance parameter. The library also provides shortcuts for defining linear effects (`LinearTerm`), Bayesian P-splines (`PSpline`), and random intercepts (`RandomIntercept`).
3. Run stochastic gradient descent as a pre-optimization step for identifying suitable knots and providing a “warm start” for the MCMC algorithm. The functionality is provided in the methods `PTMLocScale.optimize_knots` and `PTMLocScale.build_graph`.
4. Set up a `liesel.goose.EngineBuilder` object implementing the sampling scheme described in Step 5 of Algorithm 1, and use it to conduct MCMC sampling. The functionality is provided in the method `PTMLocScale.setup_engine_builder`.

5. Compute the widely applicable information criterion (WAIC) for model choice using the method `PTMLocScale.waic`.
6. Given a set of posterior samples, compute posterior predictions using the class `PTMLocScalePredictions`. This class provides methods for the computation of the posterior distribution of the response's conditional CDF and PDF as well as conditional quantiles. Posterior predictions for individual covariate terms can be obtained with the `.predict` methods of the respective classes.
7. Generate random samples from a PTM using the class `PTMLocScaleDataGen` with the procedure used for data generation in our simulation study. Non-normal example data for testing out the library can quickly be generated using the function `example_data`.

## C. Simulation study design

### C.1. Data generation details

In sum, the data generation has four steps:

1. Sample  $\boldsymbol{\delta} \in \mathbb{R}^{(J-1) \times 1}$ .
2. Prepare for sampling residuals.
3. Sample residuals.
4. Sample observations.

Intricacies are present mainly in Step 2. In Steps 2 and 3, we assume a standard normal reference distribution, although the process could be generalized with few modifications. We provide details on all four steps below.

1. Sample  $\boldsymbol{\delta} \in \mathbb{R}^{(J-1) \times 1}$ .
  - a) Sample  $\boldsymbol{\delta}_z \sim \mathcal{N}(\mathbf{0}, \mathbf{I})$ , where  $\boldsymbol{\delta}_z$  has dimension  $(J-2) \times 1$  and  $\mathbf{0}$  and  $\mathbf{I}$  have appropriate dimensions.
  - b) Compute  $\boldsymbol{\delta} = \tau_\delta \mathbf{Z} \mathbf{L}^{-\top} \boldsymbol{\delta}_z$ , where  $\tau_\delta \in (0, \infty)$  and the matrices  $\mathbf{Z} \in \mathbb{R}^{(J-1) \times (J-2)}$  and  $\mathbf{L} \in \mathbb{R}^{(J-2) \times (J-2)}$  are found as follows.
  - c) Let  $\mathbf{K} = \mathbf{D}^\top \mathbf{D}$  of dimension  $(J-1) \times (J-1)$  be a penalty matrix based on a first-difference matrix of dimension  $(J-2) \times (J-1)$  as described earlier.
  - d) Let  $\mathbf{QR} = \mathbf{K}$  be the QR decomposition of  $\mathbf{K}$ , where  $\mathbf{Q}$  is an  $(J-1) \times (J-1)$  orthogonal matrix. Discarding the first column of  $\mathbf{Q}$  yields  $\mathbf{Z}$ , which has dimensions  $(J-1) \times (J-2)$ .
  - e) Then  $\mathbf{L}^\top \mathbf{L} = \mathbf{Z}^\top \mathbf{K} \mathbf{Z}$  is the Cholesky decomposition of  $\mathbf{Z}^\top \mathbf{K} \mathbf{Z}$ .
2. Prepare for sampling residuals. We want to obtain a sample of residuals  $\varepsilon_1, \dots, \varepsilon_{N_{\text{obs}}}$  with expectation zero and variance one. However, given a specific observation of  $\boldsymbol{\delta}$ , the



transformation function must be scaled and shifted to achieve this goal. The goal of this pre-processing step is to estimate the amount of this scaling and shifting.

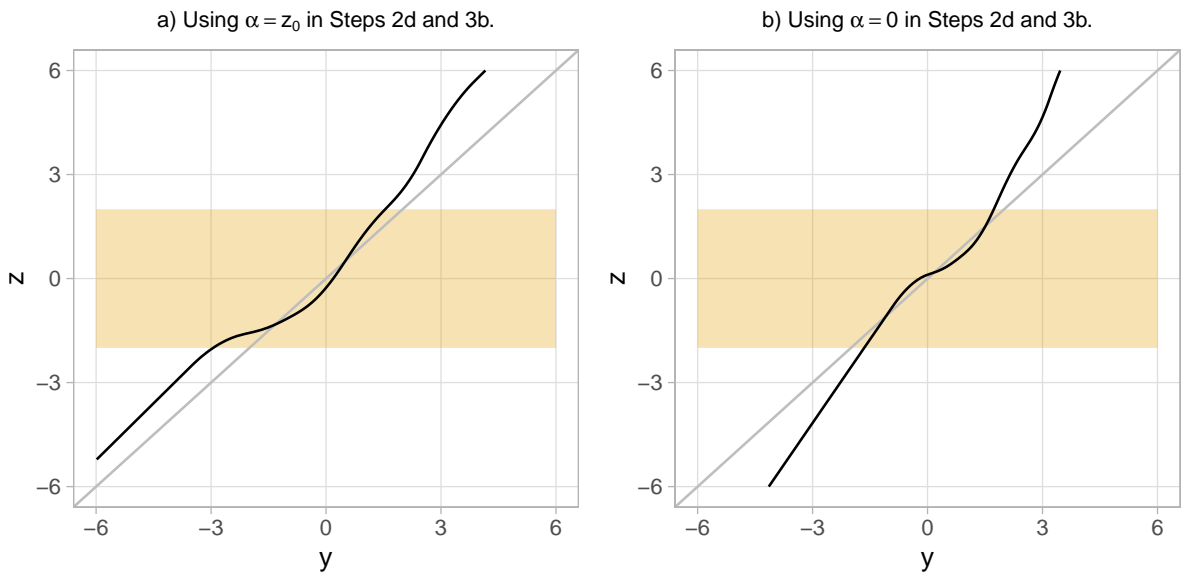
- a) Define a knot base for the evaluation of the transformation function  $h$ . We use evenly spaced knots  $k_1 < k_2 < \dots < k_{J+3} < k_{J+4}$ , setting the boundary knots  $k_4 = -2.5$  and  $k_{J+1} = 2.5$ .
- b) Compute  $q_i$  for  $i = 1, \dots, N_{\text{grid}}$ , where  $q_i = \Phi^{-1}(p_i)$  and  $p_1, \dots, p_{N_{\text{grid}}}$  is a grid of evenly spaced probability levels between  $p_1 = 0.0001$  and  $p_{N_{\text{grid}}} = 0.9999$ . We obtain a representative grid of normal quantiles. We use a grid of size  $N_{\text{grid}} = 1000$ .
- c) Compute  $z_0 = h(0|\alpha = 0, \omega = 1, \delta)$ . This is the value of the transformation function at the mean residual value of zero.
- d) Compute  $e_i = h^{-1}(q_i|\alpha = z_0, \omega = 1, \delta)$  for  $i = 1, \dots, N_{\text{grid}}$  by numerical inversion. Here, we obtain a representative, finite sample of unstandardized residuals  $e_1, \dots, e_{N_{\text{grid}}}$ . We use  $\alpha = z_0$  for an initial shift of the transformation function. This makes sure that the range of the transformation function's core segment has a large overlap with the interval  $[-2, 2]$ , which means that we have nonlinearity of the transformation function inverse for values with a high probability of being sampled from a standard normal distribution. Figure A2 illustrates this point.
- e) Compute the sample mean and standard deviation  $m = \text{mean}_{i=1}^{N_{\text{grid}}}(e_i)$  and  $s = \sqrt{\text{Var}_{i=1}^{N_{\text{grid}}}(e_i)}$ .

### 3. Sample residuals.

- a) Sample  $z_i \stackrel{i.i.d.}{\sim} \mathcal{N}(0, 1)$  for  $i = 1, \dots, N_{\text{obs}}$ . This is a random sample of normal quantiles of size  $N_{\text{obs}}$ .
- b) Compute  $\tilde{e}_i = h^{-1}(z_i|\alpha = z_0, \omega = 1, \delta)$  by numerical inversion for  $i = 1, \dots, N_{\text{obs}}$ . This is an unstandardized random sample of residuals.
- c) Compute  $\varepsilon_i = (\tilde{e}_i - m)/s$  for  $i = 1, \dots, N_{\text{obs}}$ . This is a standardized random sample of residuals.

### 4. Sample observations.

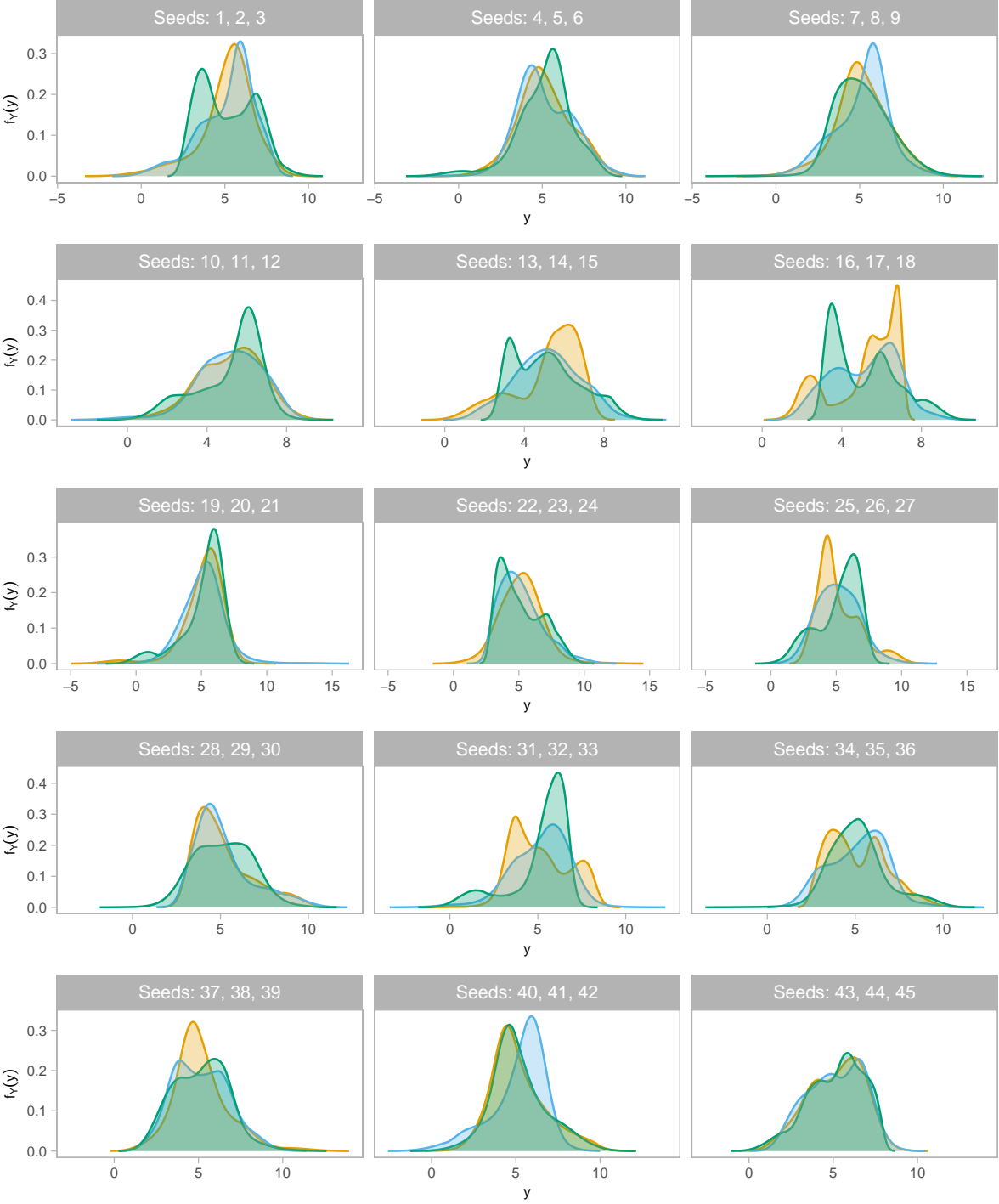
- a) Sample  $\tilde{x}_{ij} \sim \mathcal{U}(-2, 2)$  for  $i = 1, \dots, N_{\text{obs}}$  and  $j = 1, 2, 3, 4$ .
- b) Standardize all covariates to mean zero and scale one,  
i.e.  $x_{ij} = (\tilde{x}_{ij} - \text{mean}_{i=1}^{N_{\text{obs}}}(\tilde{x}_{ij}))/\sqrt{\text{Var}_{i=1}^{N_{\text{obs}}}(\tilde{x}_{ij})}$ .
- c) Compute  $\mu(\mathbf{x}_i)$  and  $\sigma(\mathbf{x}_i)$  for  $i = 1, \dots, N_{\text{obs}}$ , where the functions are given as described in the main text and  $\mathbf{x}_i = [x_{i1}, x_{i2}, x_{i3}, x_{i4}]^T$ .
- d) Compute  $y_i = \mu(\mathbf{x}_i) + \sigma(\mathbf{x}_i)\varepsilon_i$  for  $i = 1, \dots, N_{\text{obs}}$ . With the values  $y_1, \dots, y_{N_{\text{obs}}}$ , we have obtained our random sample.

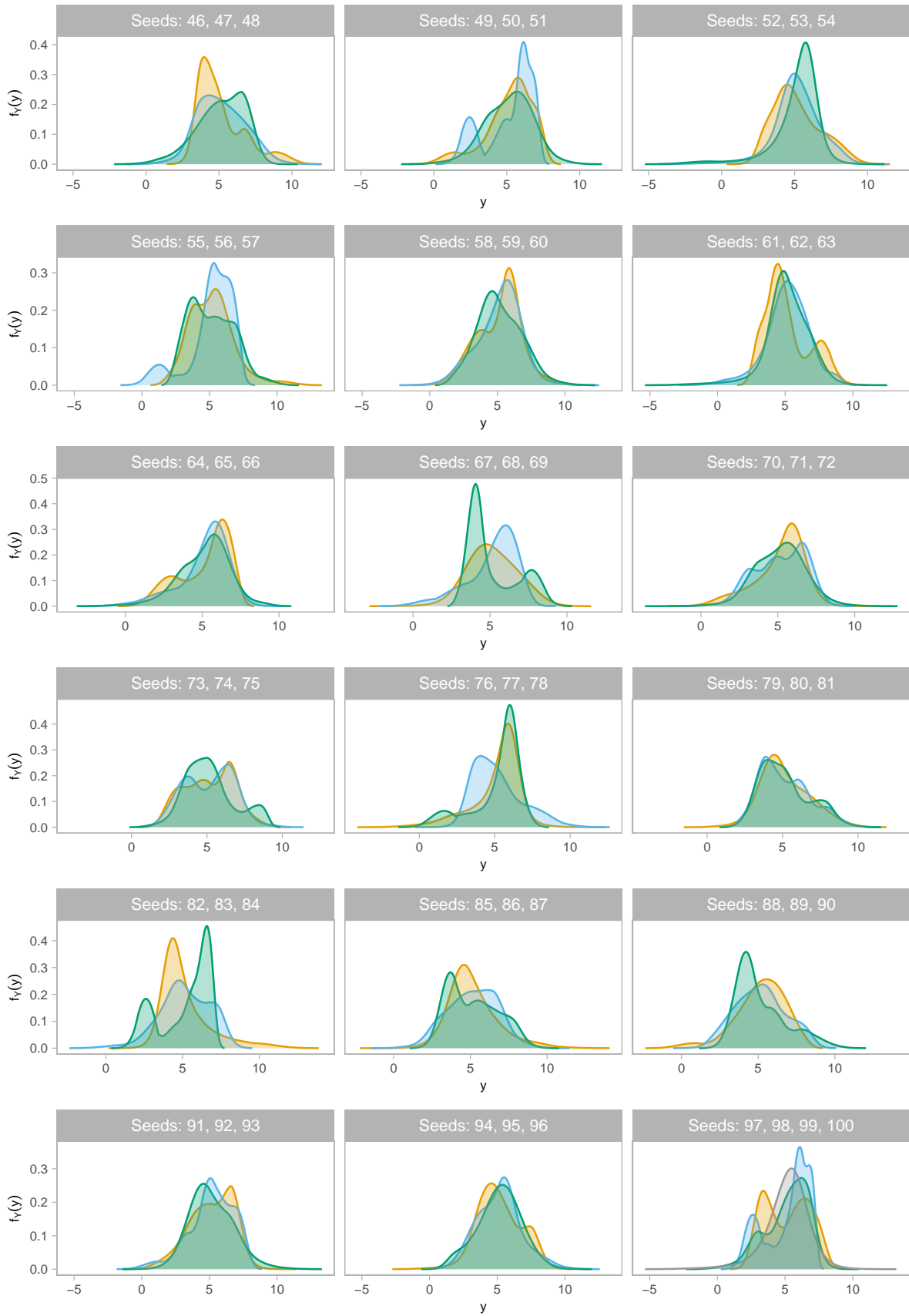


**Figure A2** Illustration of the initial shift of the transformation function conducted in Steps 2d and 3b of the data generation process. Both transformation functions use the same  $\delta$  parameters, generated via Step 1. The shaded area marks  $z \in [-2, 2]$ . The grey line is the identity function, plotted for reference.

### C.2. Generated densities

The plots below show all conditional densities generated for the simulation study. All of these plots depict the conditional response density for covariate observations  $x_1 = x_2 = x_3 = x_4 = 0$ . Each panel shows the densities of three seeds merely in order to achieve a compact representation.





### C.3. Detailed overview of conditions

**Table A1** Overview of simulation study conditions. Main models are marked with (\*).

No.	Model	Data	$N_{obs}$	$N_{sim}$
1	* bctm-10	nonnormal	500	100
2	* bctm-10	nonnormal	1000	100
3	* bctm-10	nonnormal	2000	100
4	* bctm-10	normal	500	100
5	* bctm-10	normal	1000	100
6	* bctm-10	normal	2000	100
7	bctm-15	nonnormal	500	100
8	bctm-15	nonnormal	1000	100
9	bctm-15	nonnormal	2000	100
10	bctm-15	normal	500	100
11	bctm-15	normal	1000	100
12	* normal	nonnormal	500	100
13	* normal	nonnormal	1000	100
14	* normal	nonnormal	2000	100
15	* normal	normal	500	100
16	* normal	normal	1000	100
17	* normal	normal	2000	100
18	* ptm	nonnormal	500	100
19	* ptm	nonnormal	1000	100
20	* ptm	nonnormal	2000	100
21	* ptm	normal	500	100
22	* ptm	normal	1000	100
23	* ptm	normal	2000	100
24	ptm-bounded	nonnormal	1000	100
25	ptm-bounded	normal	1000	100
26	ptm-const	nonnormal	1000	100
27	ptm-const	normal	1000	100
28	ptm-fixed	nonnormal	1000	100
29	ptm-fixed	normal	1000	100
30	ptm-ig	nonnormal	1000	100
31	ptm-ig	normal	1000	100
32	ptm-ridge	nonnormal	1000	100
33	ptm-ridge	normal	1000	100
34	ptm-std	nonnormal	1000	100
35	ptm-std	normal	1000	100
36	ptm-wb01	nonnormal	1000	100
37	ptm-wb01	normal	1000	100
38	* qgam	nonnormal	500	100
39	* qgam	nonnormal	1000	100
40	* qgam	nonnormal	2000	100
41	* qgam	normal	500	100
42	* qgam	normal	1000	100
43	* qgam	normal	2000	100
44	qgam-big	nonnormal	1000	100
45	qgam-big	normal	1000	100

### C.4. Details on the used covariate effects

Figure A3 displays the used covariate effects.

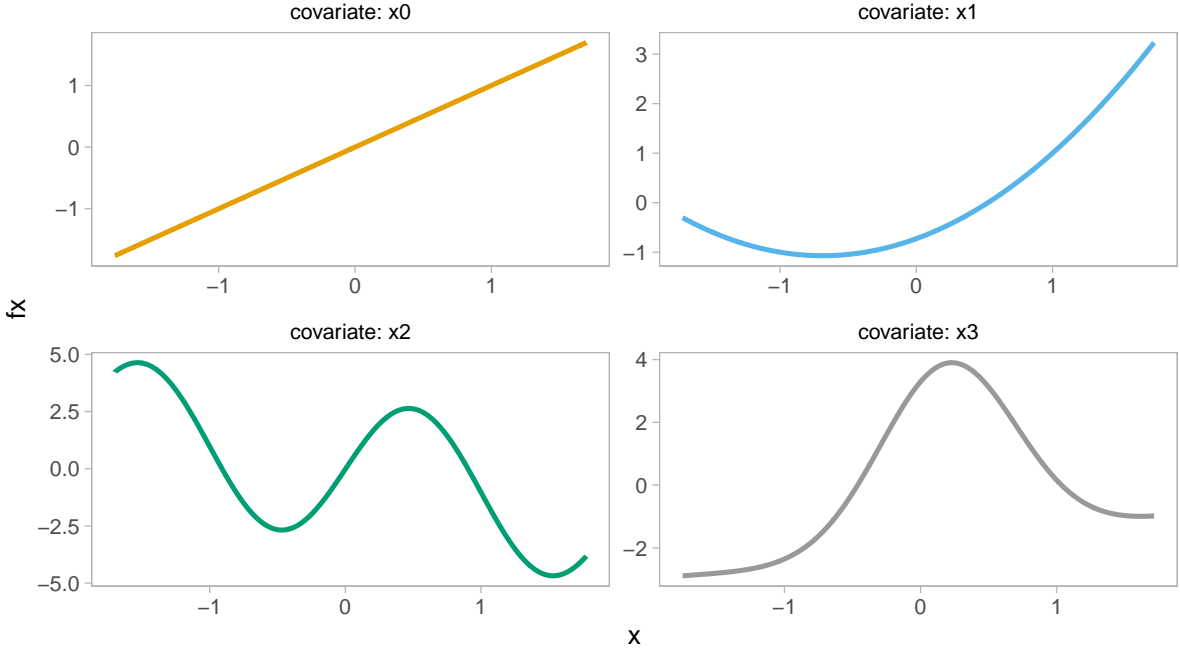
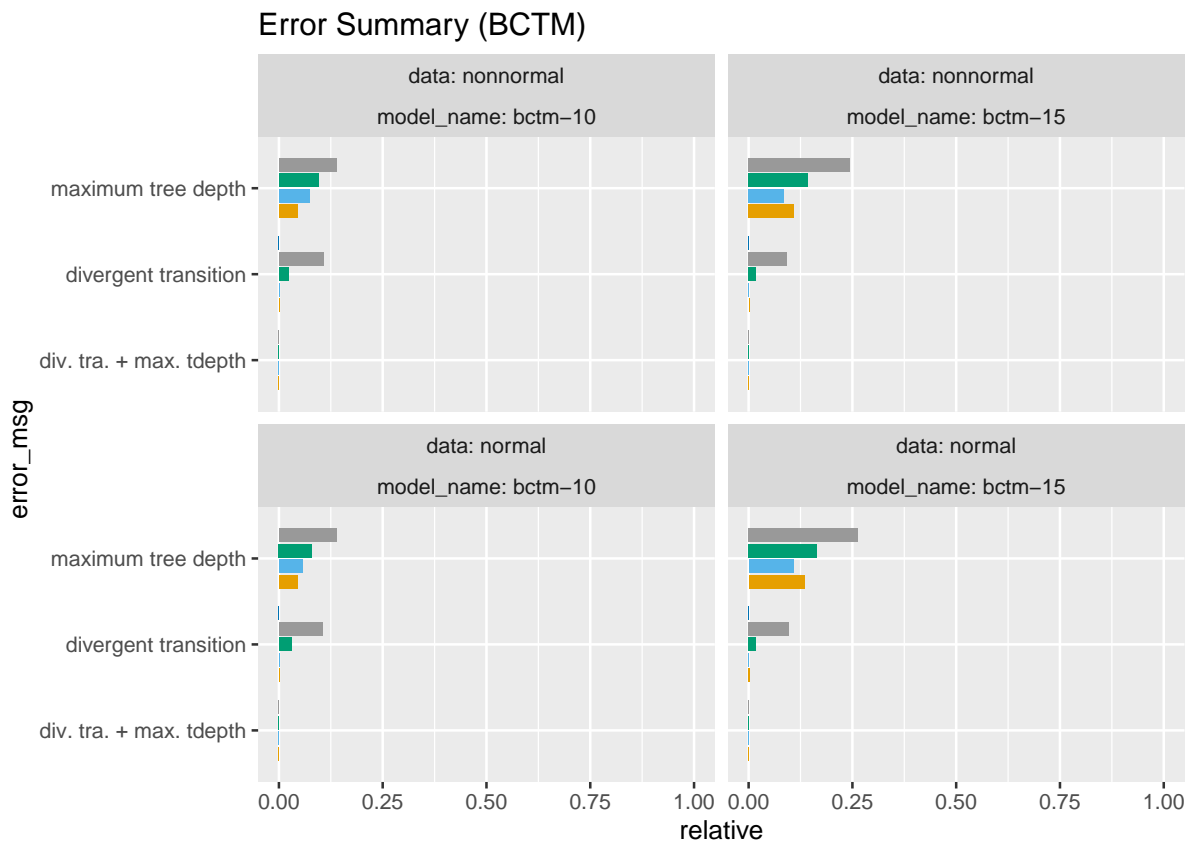


**Figure A3** Covariate functions used in the simulation study. The plotted effects are the location effects, but note that the scale effects have the same form.

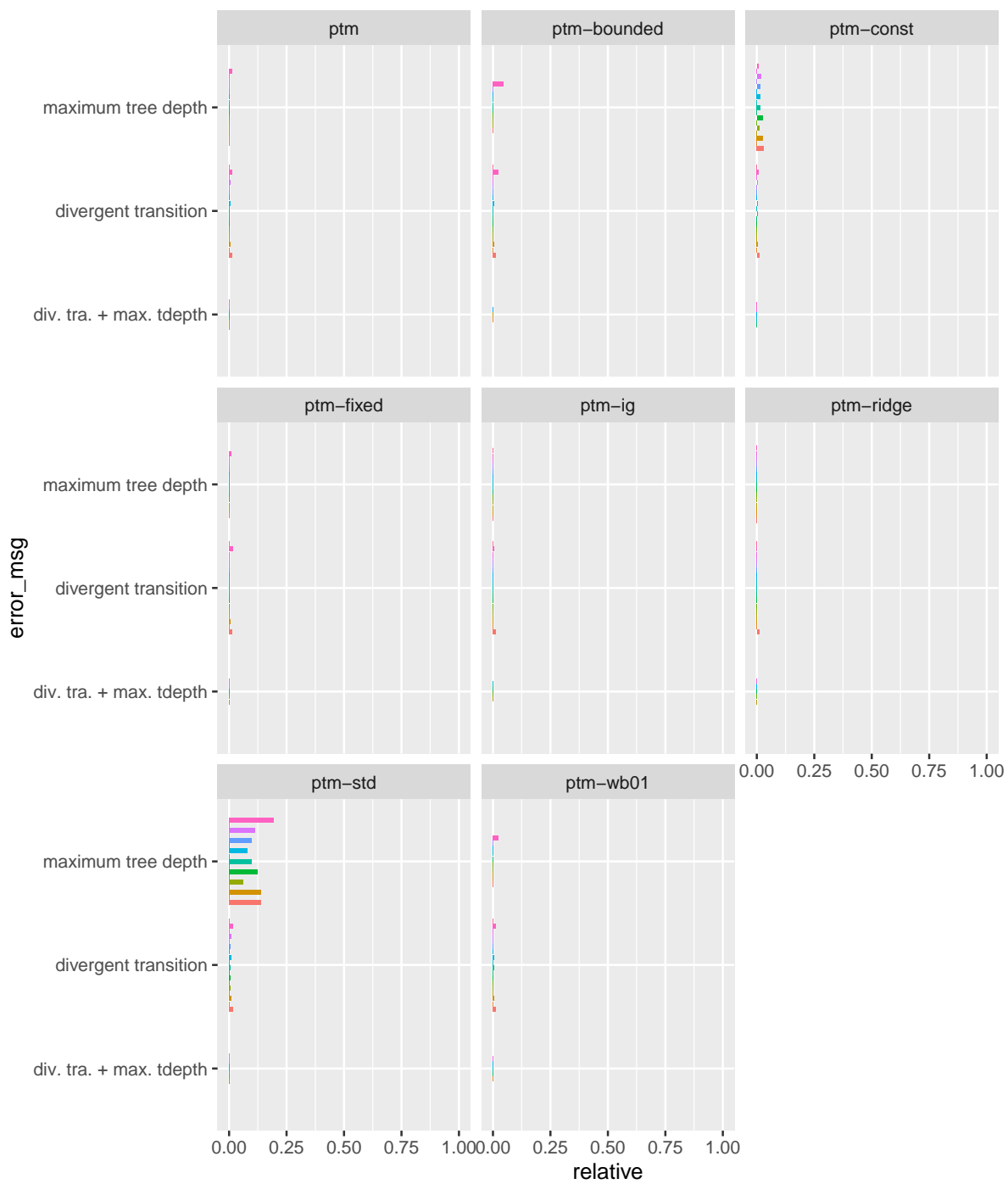
## D. Simulation study diagnostics

### D.1. MCMC errors

We look at the errors on an aggregated level. For each simulation run, we obtain the relative error frequency, a number between 0 and 1, for each MCMC kernel. We average this relative frequency over the sample size and the simulation seeds. We end up with an average error frequency per MCMC kernel. We do not look specifically at which MCMC kernel gives many errors, rather we focus on the general patterns.

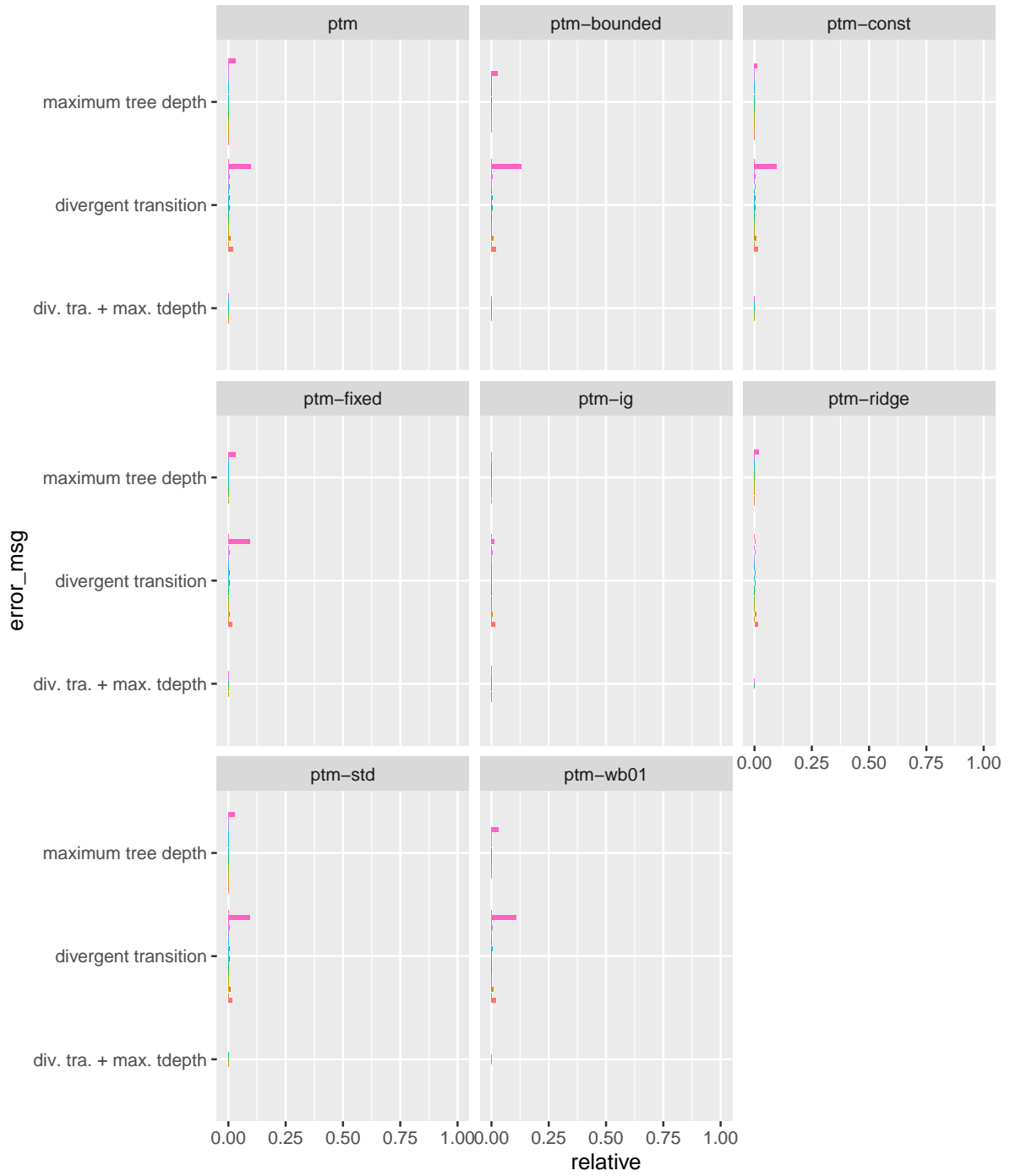


### Error Summary (PTM, nonnormal data)

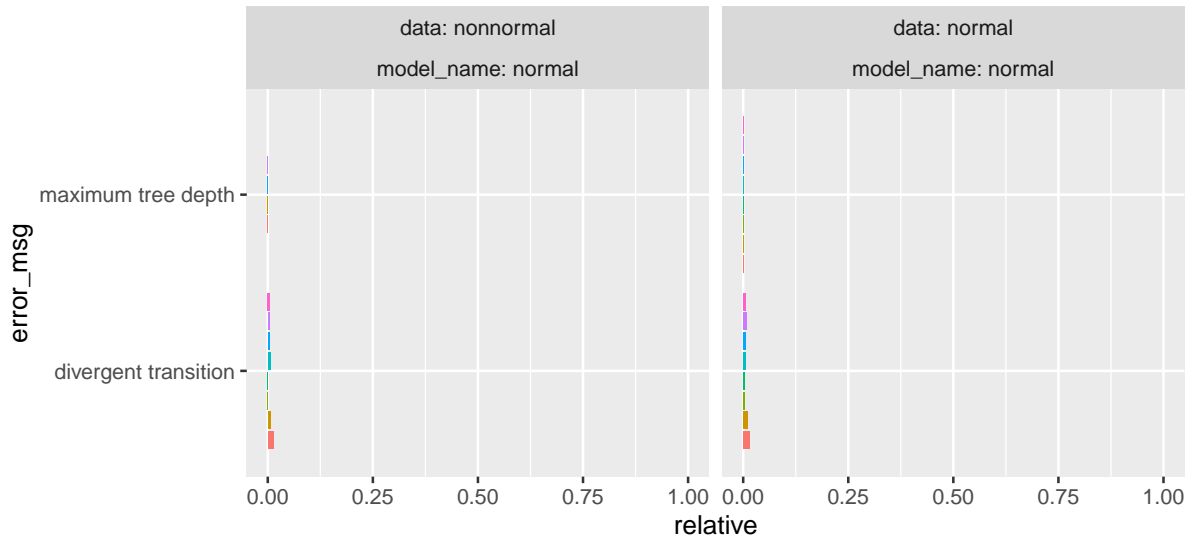




### Error Summary (PTM, normal data)

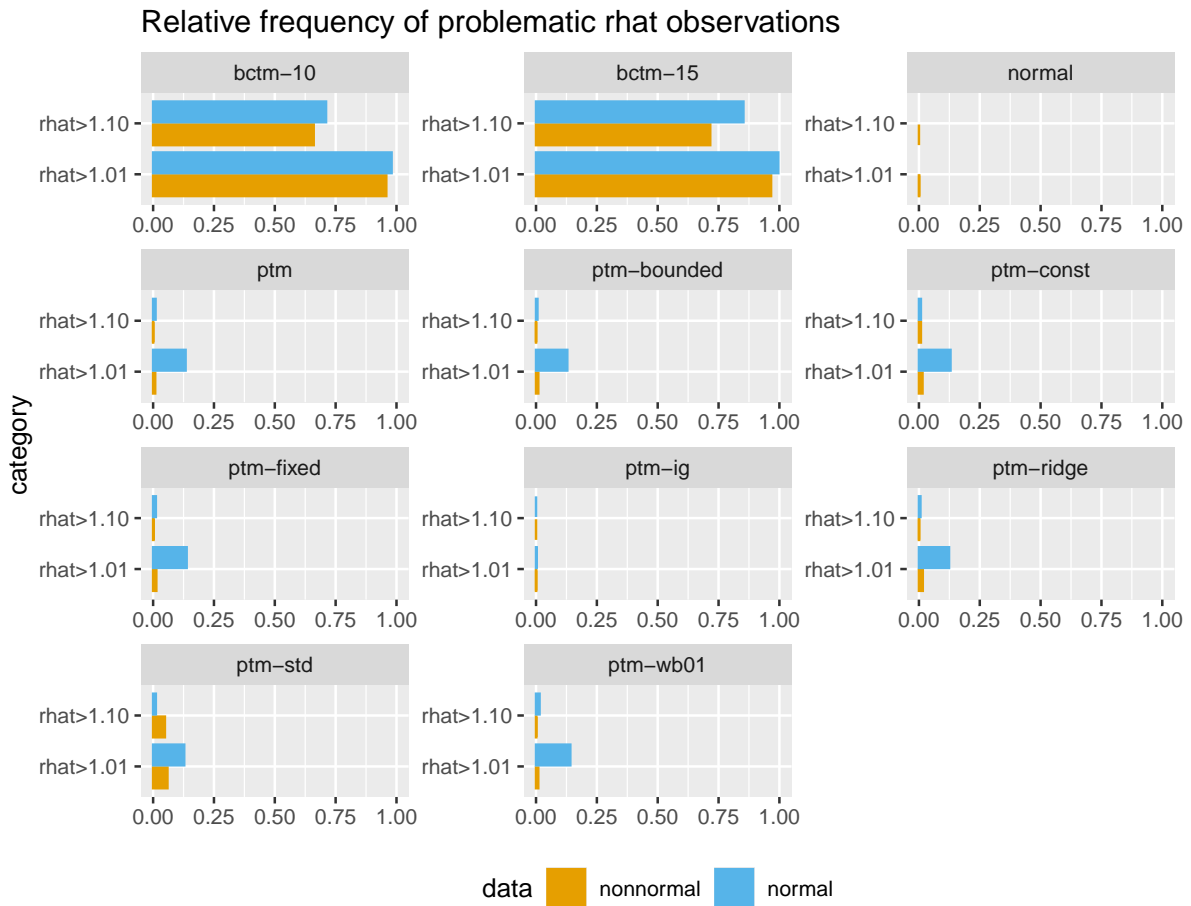


### Error Summary (Normal model)



## D.2. Rhat convergence measure

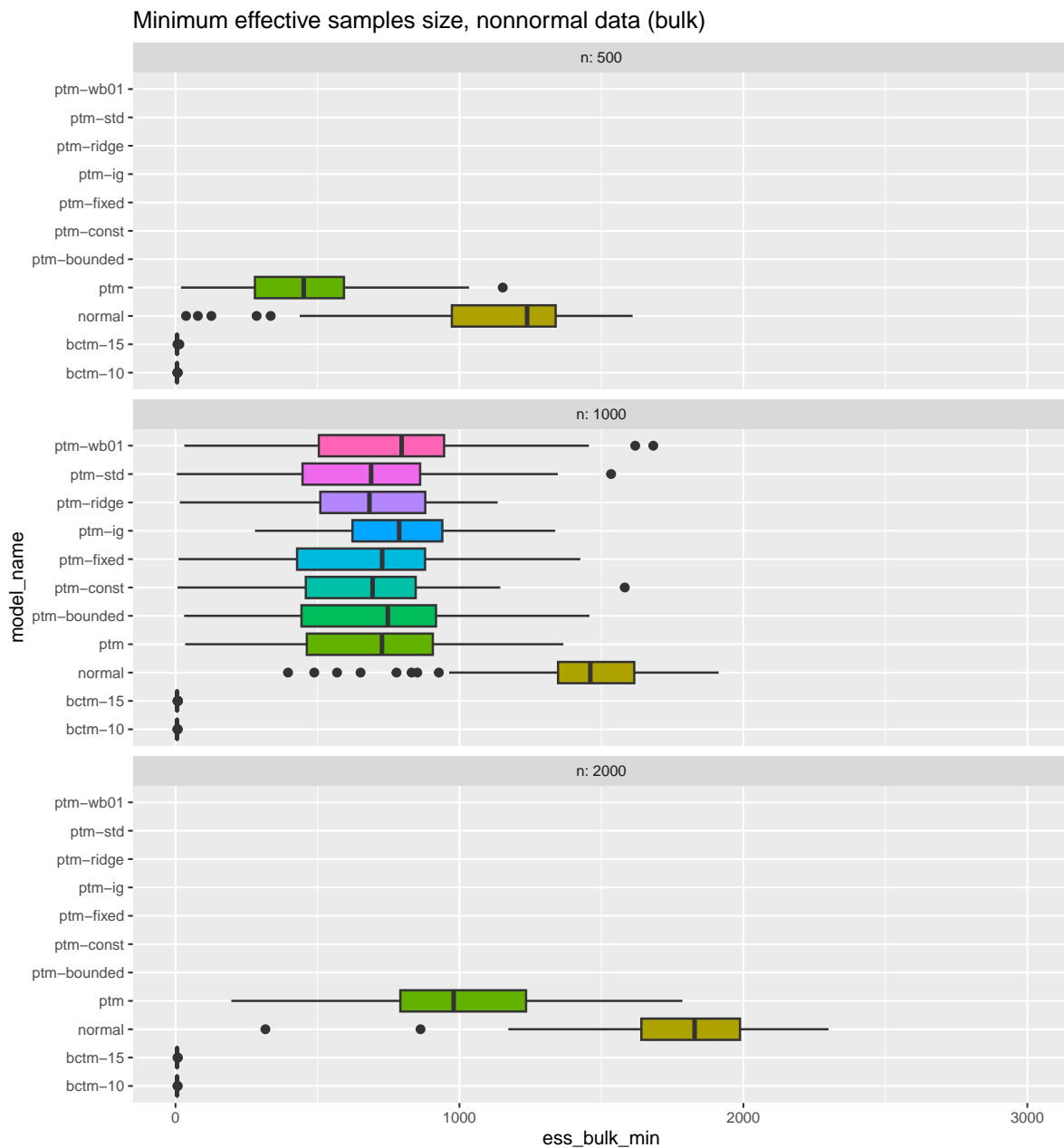
For each model and dataset, we identify the relative frequency of observing a Gelman-Rubin  $\hat{r}$  statistic larger than 1.1 and larger than 1.01, which are suggested thresholds for poor convergence. The displayed results are aggregated over all kernels and sample sizes. The results for the PTMs and the normal model indicate good overall converge, while the results for the BCTMs indicate severe convergence issues.



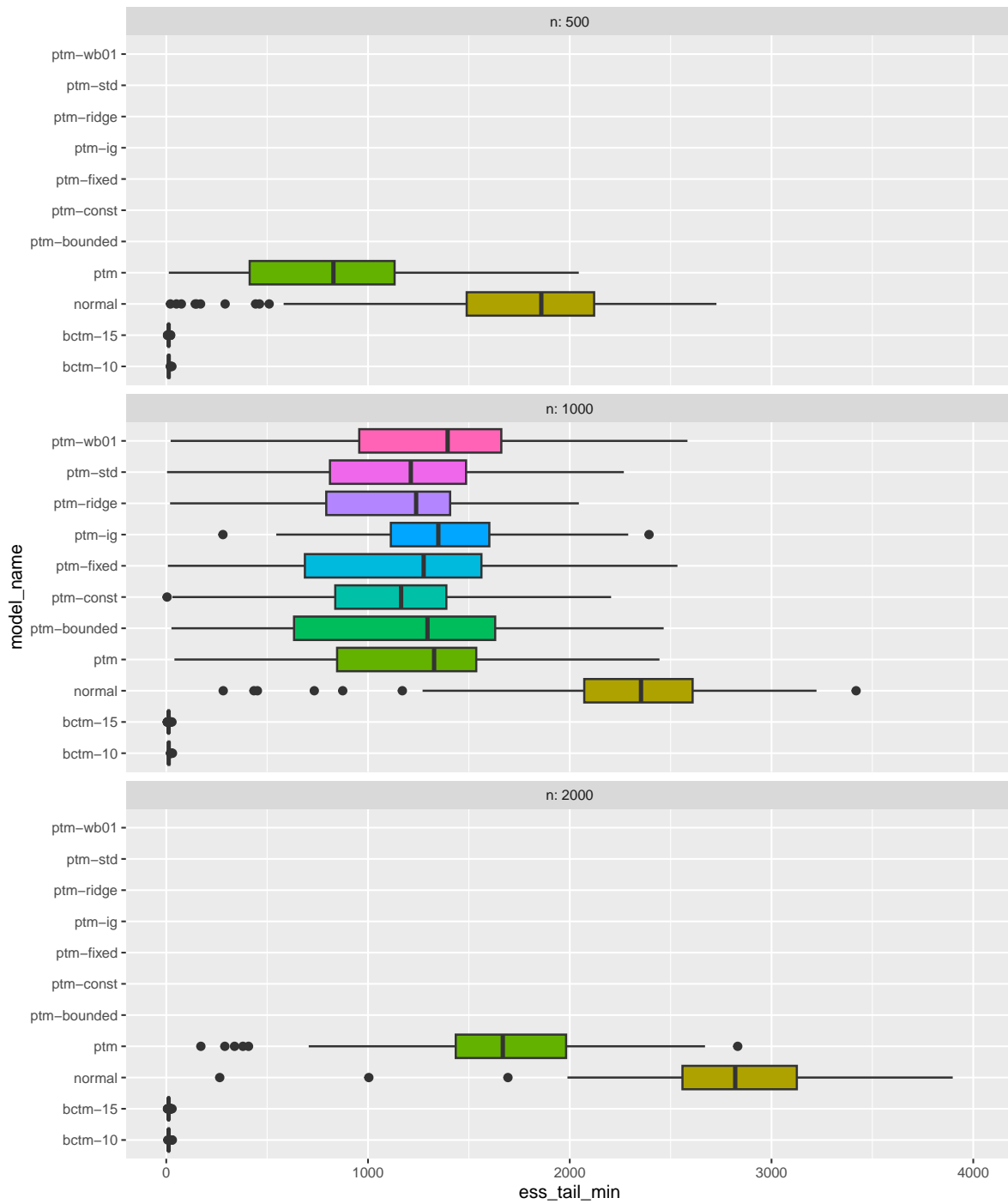
### D.3. Effective sample size

The following plots summarise the effective sample sizes. The plots are split by data and sample size. The boxplot of effective sample sizes within each model and subplot is created using the effective sample sizes of all parameters in the respective model. Main observations:

- The BCTMs have very low effective sample sizes.
- The normal models tend to have slightly higher effective sample sizes than the PTMs
- The `ptm-ridge` tends to have slightly lower effective sample sizes than the other PTMs.
- Generally, the PTMs seem to do well in terms of effective sample size.



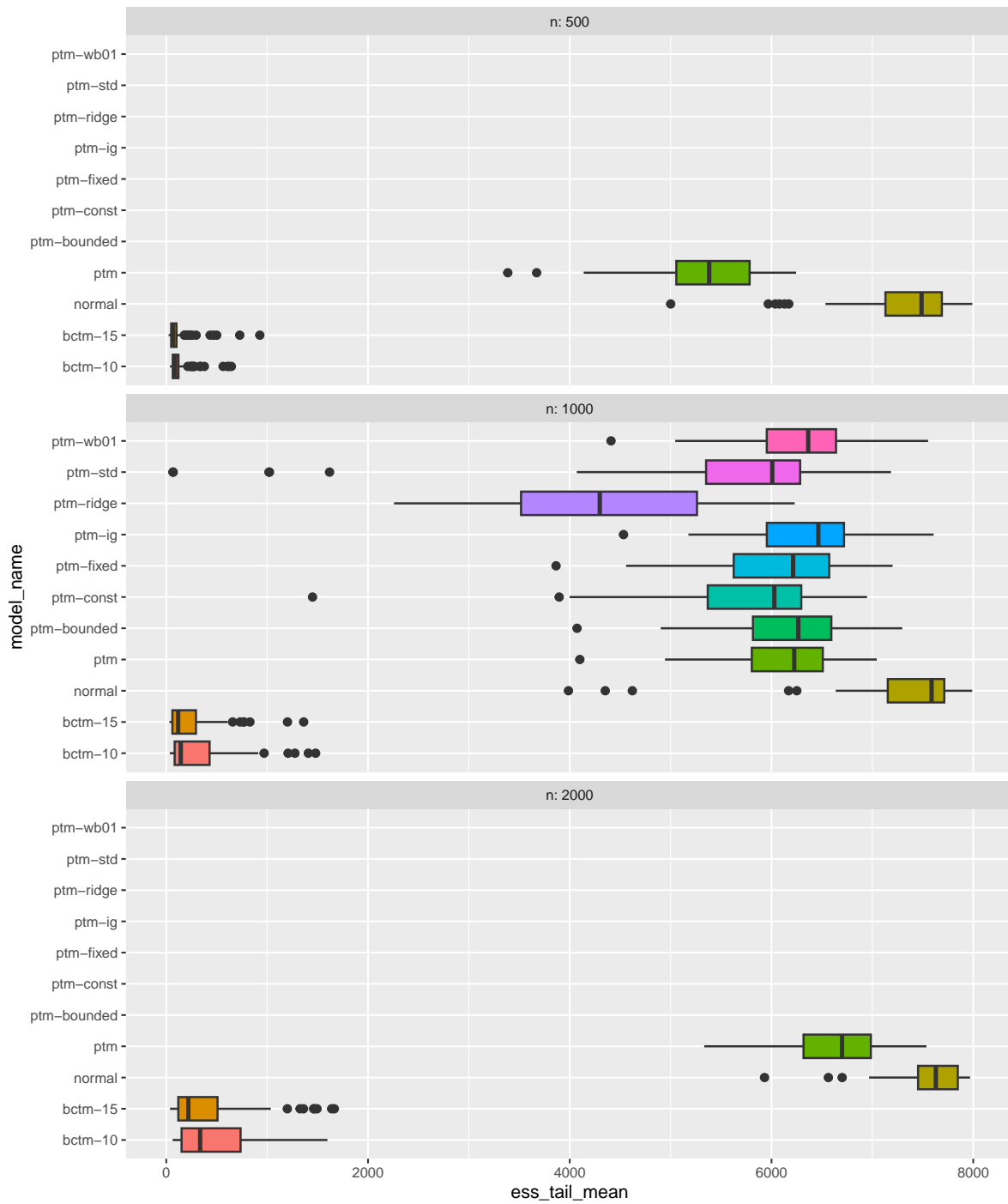
### Minimum effective samples size, nonnormal data (tail)



### Mean effective samples size, nonnormal data (bulk)



### Mean effective samples size, nonnormal data (tail)



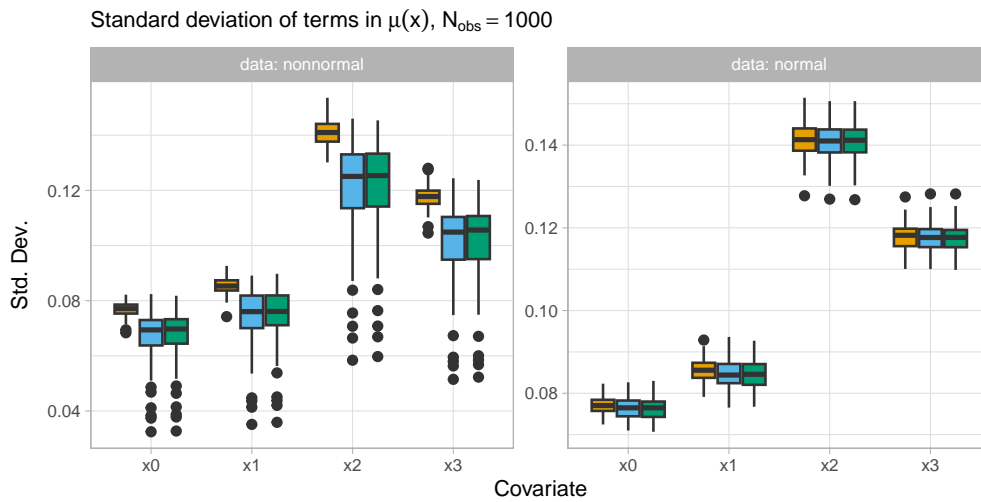
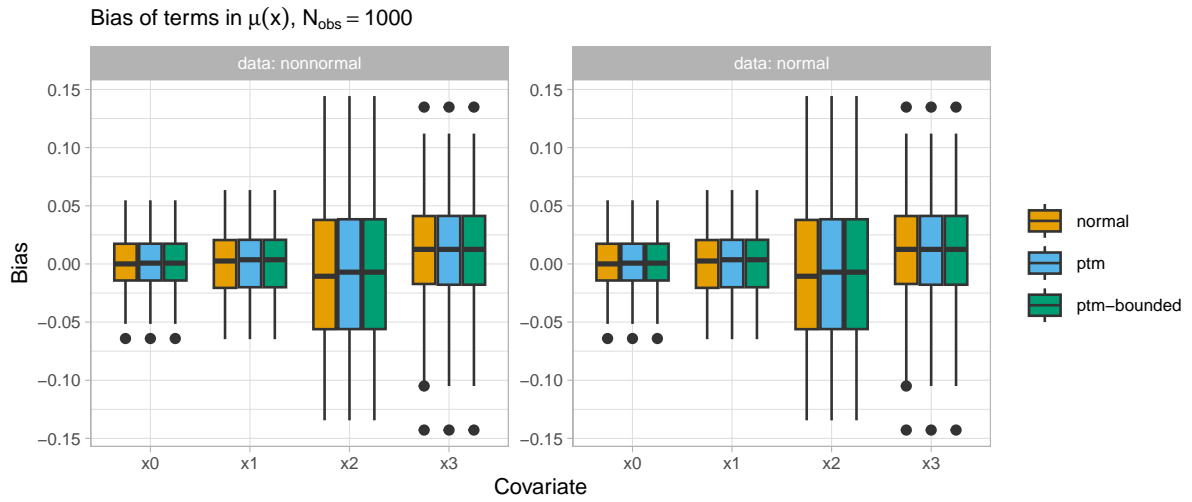
## E. Simulations study results

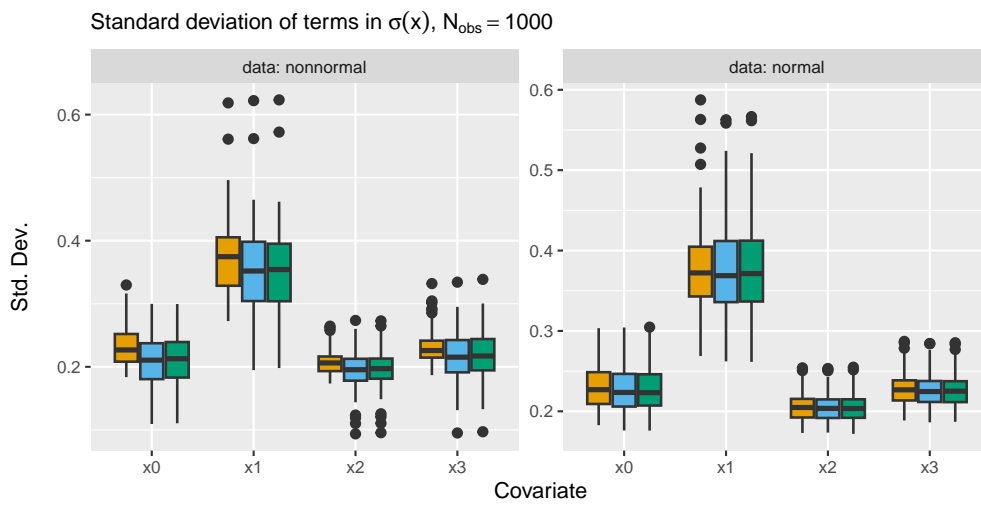
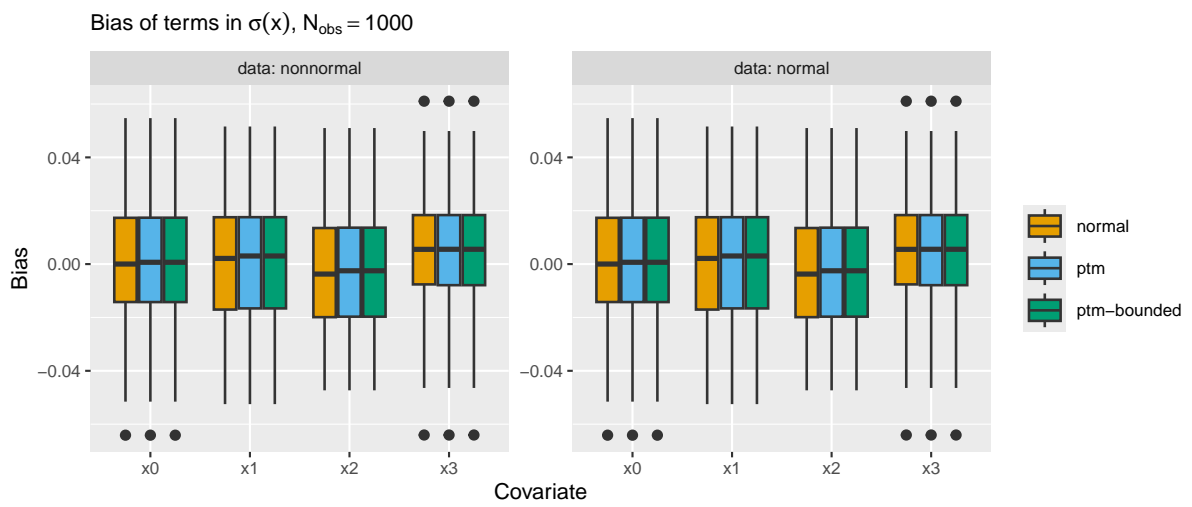
Main observations:

- All covariate effect estimates are essentially unbiased, and the PTMs and the normal model are practically indistinguishable in terms of their bias. However, the PTMs yield a lower posterior standard deviation for all location covariate effects with non-normal data.
- The BCTM variants do not substantially differ.
- The QGAM variants do not substantially differ.
- All PTM variants do fairly equal in terms of WAIC (training data) and MAD (test data).
- When looking at WAIC (test data) and KLD (test data), we observe the following:
  - `ptm-const` produces at least one extreme outlier
  - `ptm-std` produces at least two extreme outliers
  - `ptm-ridge` yields slightly higher WAIC and a higher KLD than the other models.
- Looking at the quantile score, we observe:
  - `ptm-const` produces outliers
  - `ptm` shows a weaker performance than the remaining models, except for `ptm-const`.
- The results indicate the same patterns for all sample sizes.



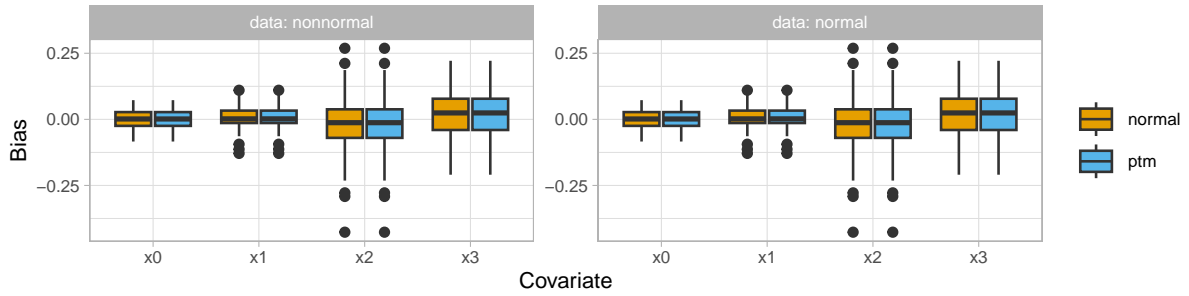
## E.1. Details on covariate effects results





Bias and standard deviation of terms in  $\mu(x)$ ,  $N_{obs} = 500$

a) Bias



b) Standard deviation

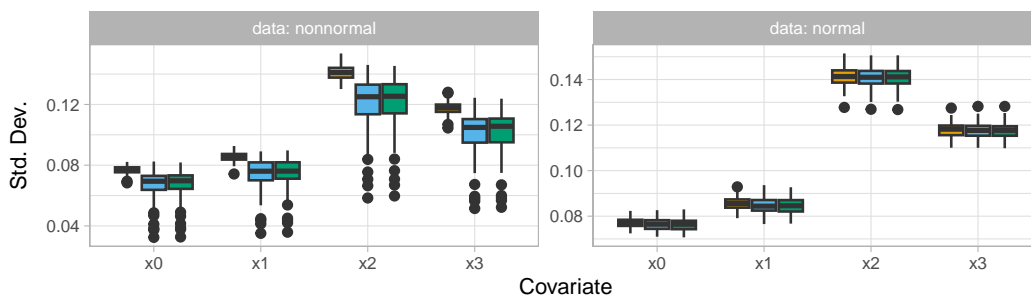
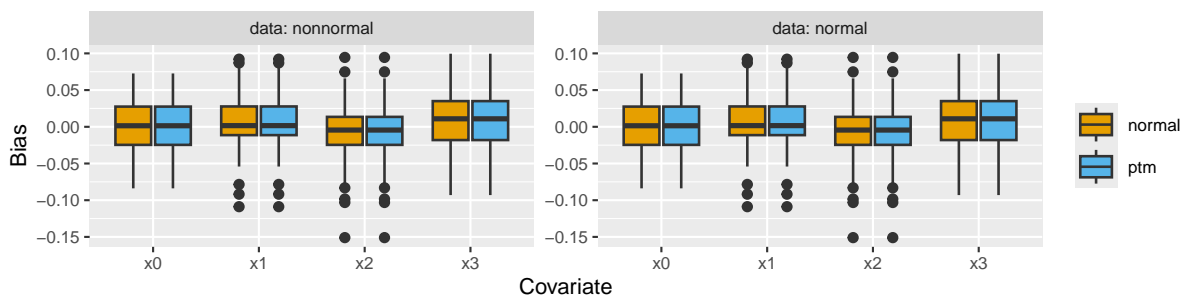


**Figure A4** Bias and variance of location covariate effects with  $N_{obs} = 500$ .

Bias and standard deviation of terms in  $\sigma(x)$ ,  $N_{obs} = 500$

a) Bias



b) Standard deviation

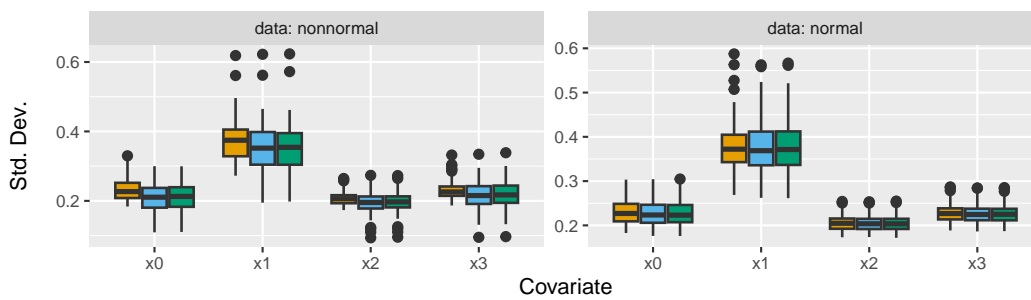
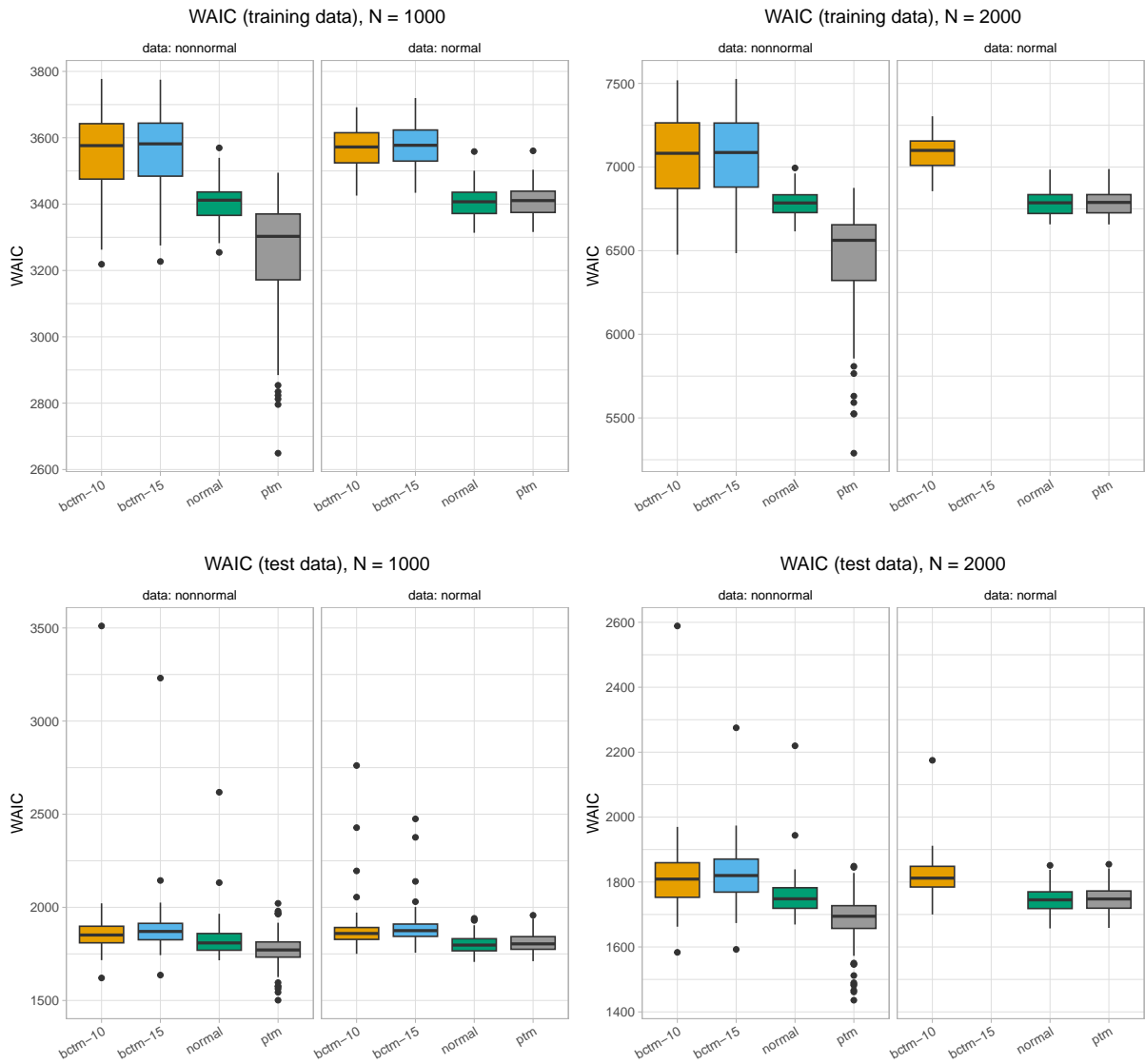
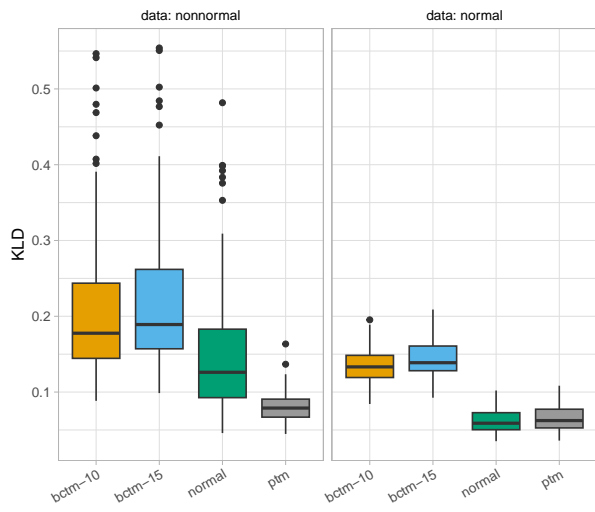


**Figure A5** Bias and variance of location covariate effects with  $N_{obs} = 500$ .

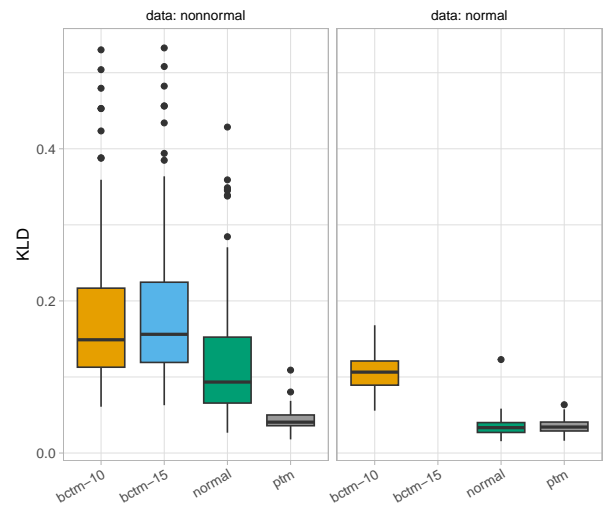
## E.2. BCTM variants



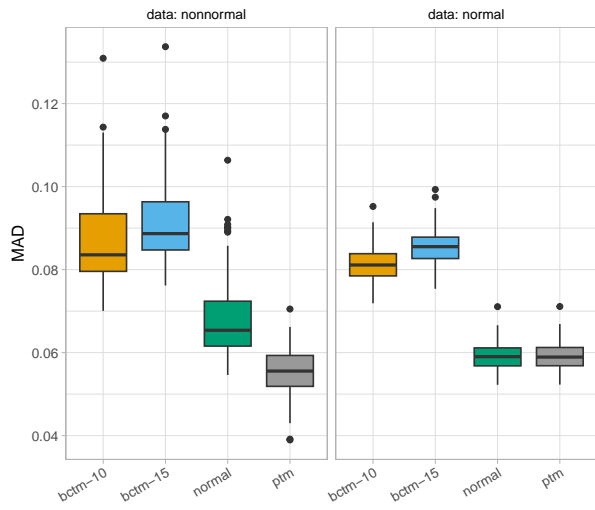
KLD (test data), N = 1000



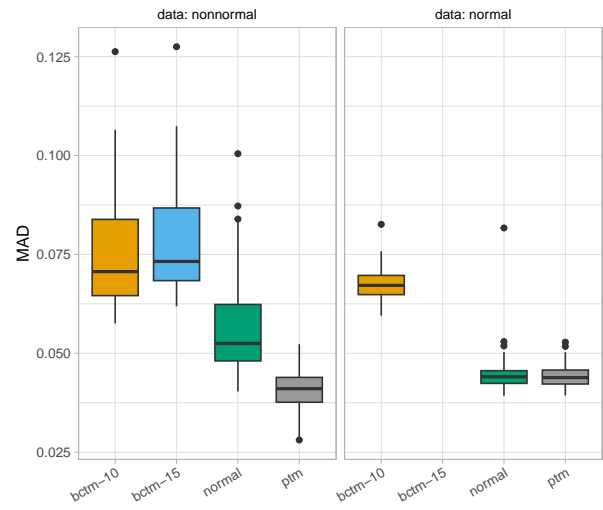
KLD (test data), N = 2000



MAD (test data), N = 1000

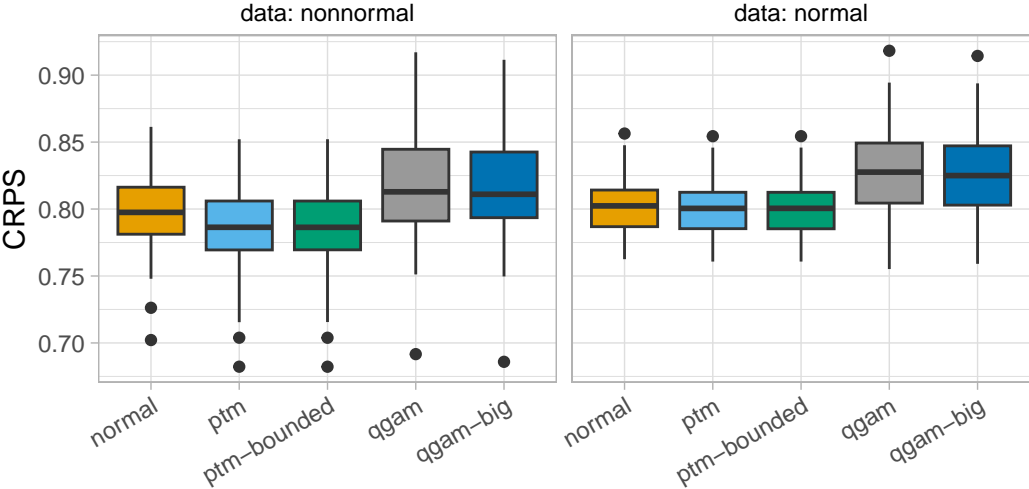


MAD (test data), N = 2000

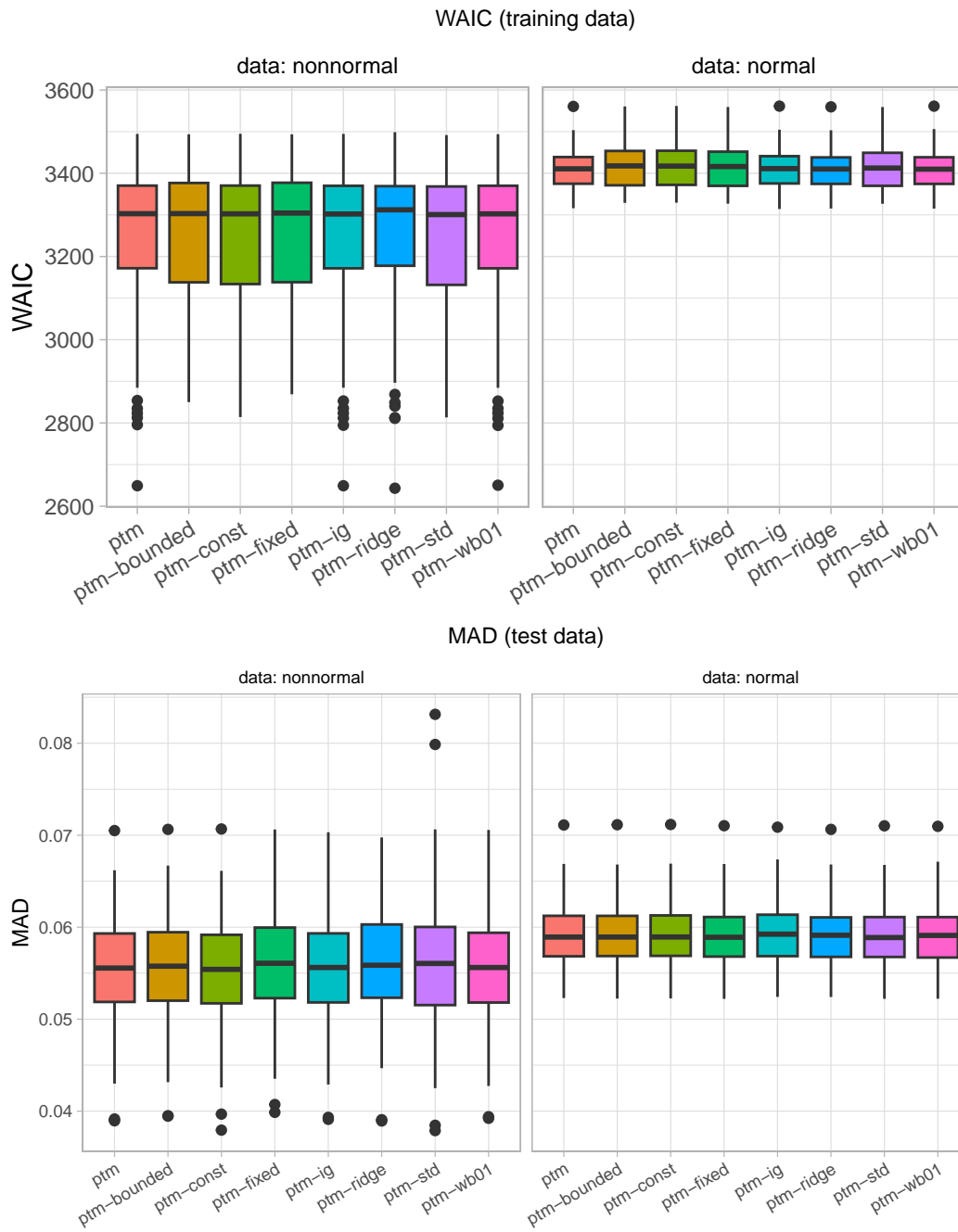


### E.3. QGAM variants

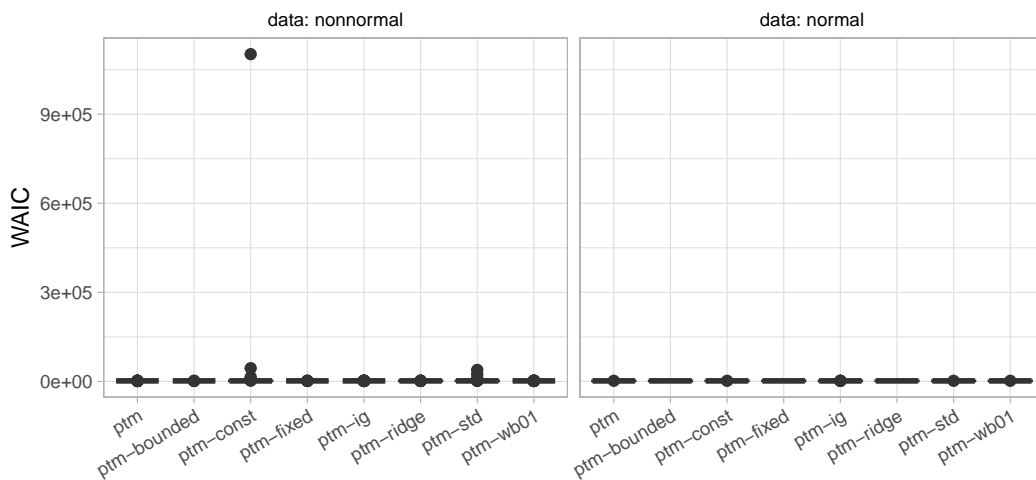
#### CRPS



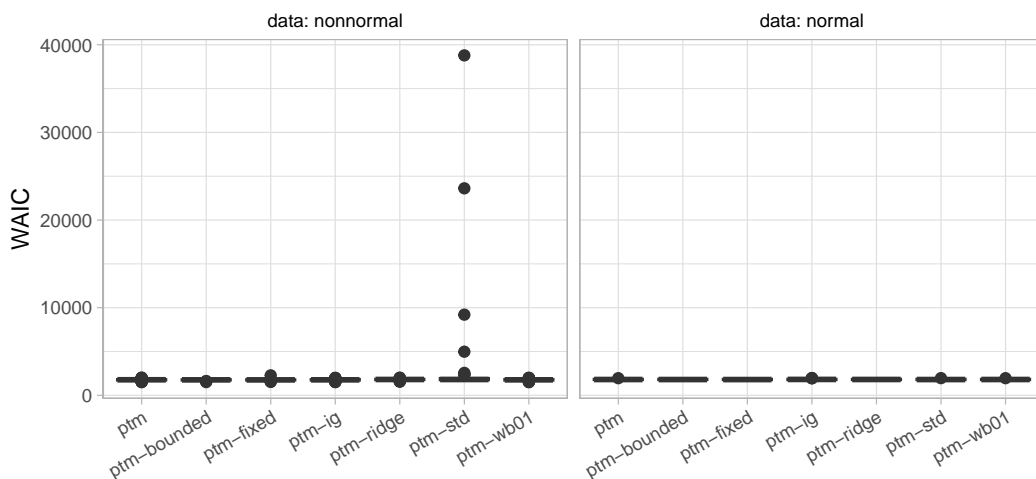
## E.4. PTM variants



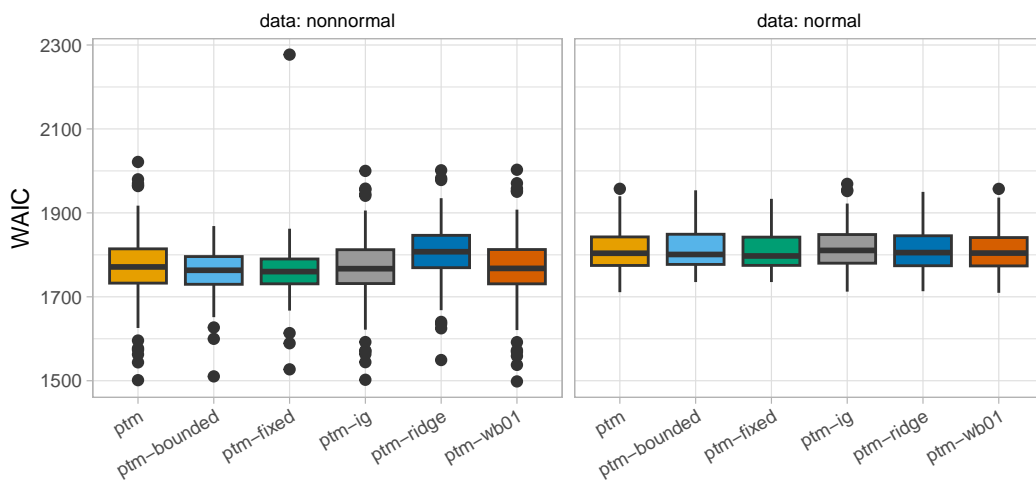
WAIC (test data)



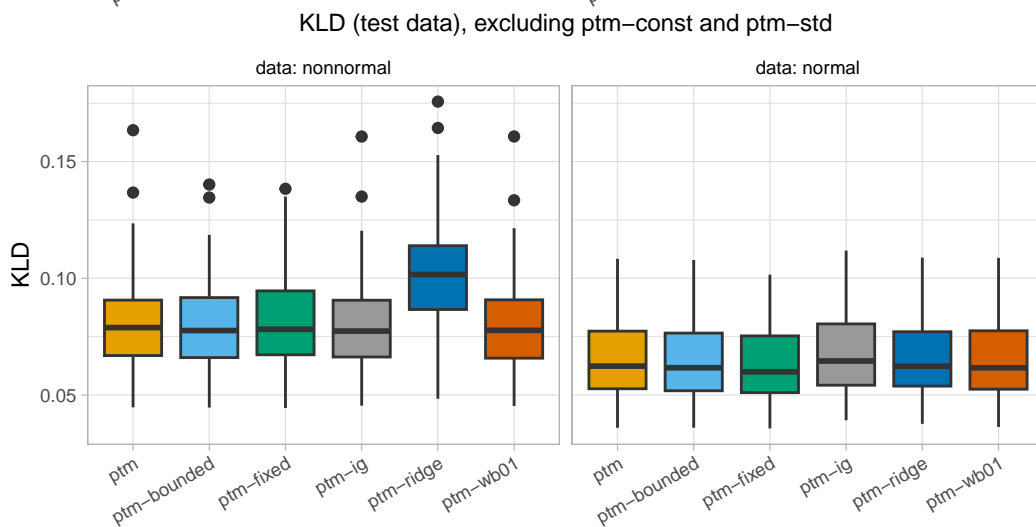
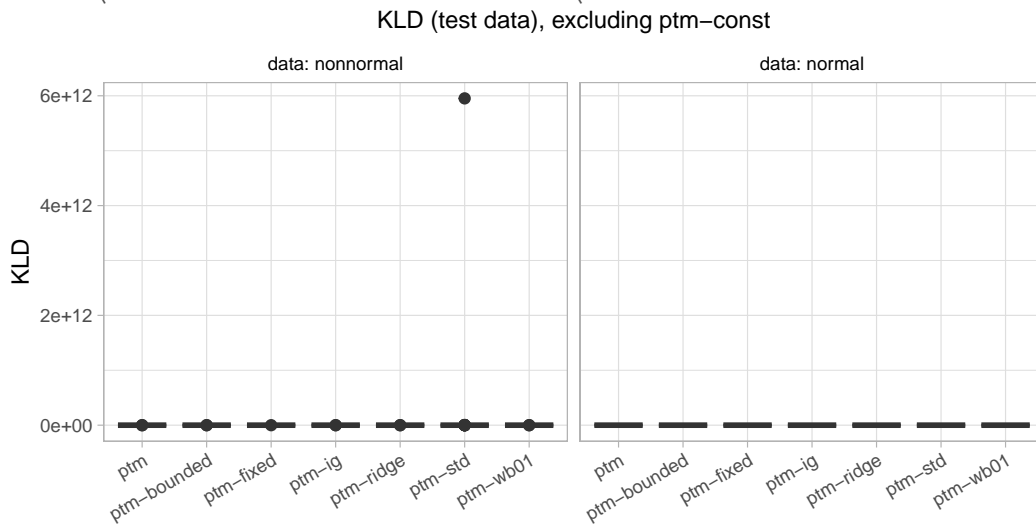
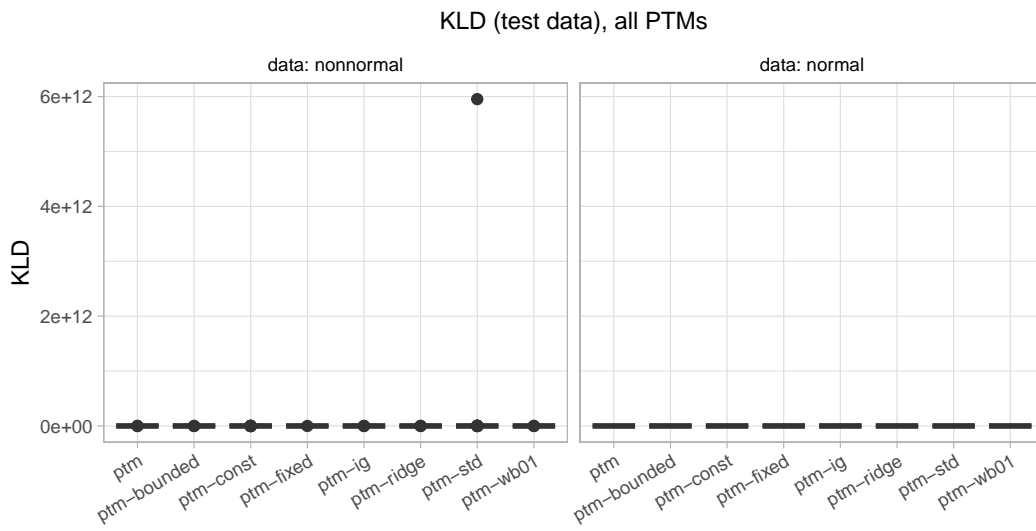
WAIC (test data)



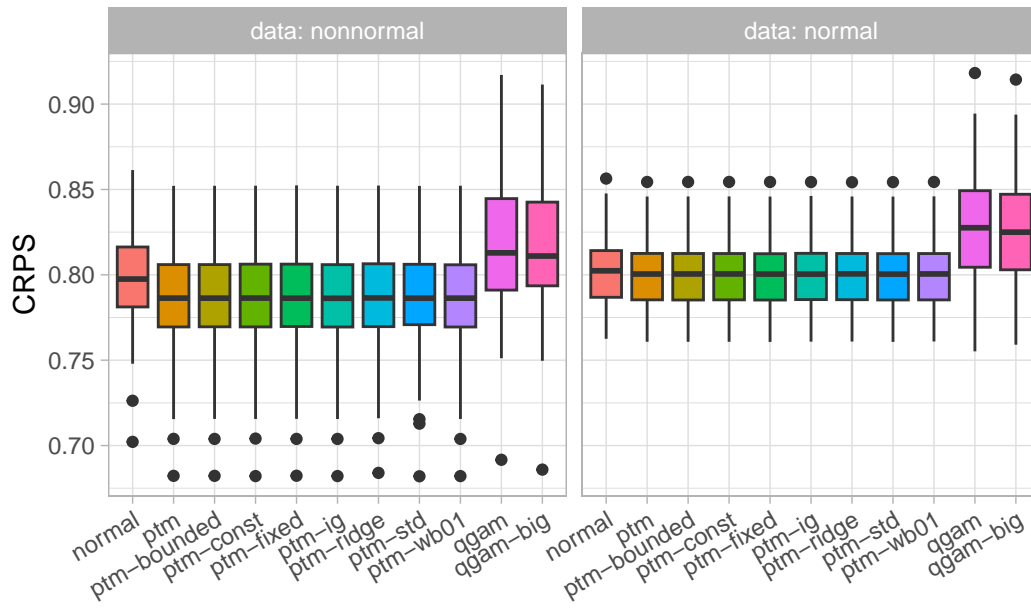
WAIC (test data)







# CRPS



## E.5. Different sample sizes

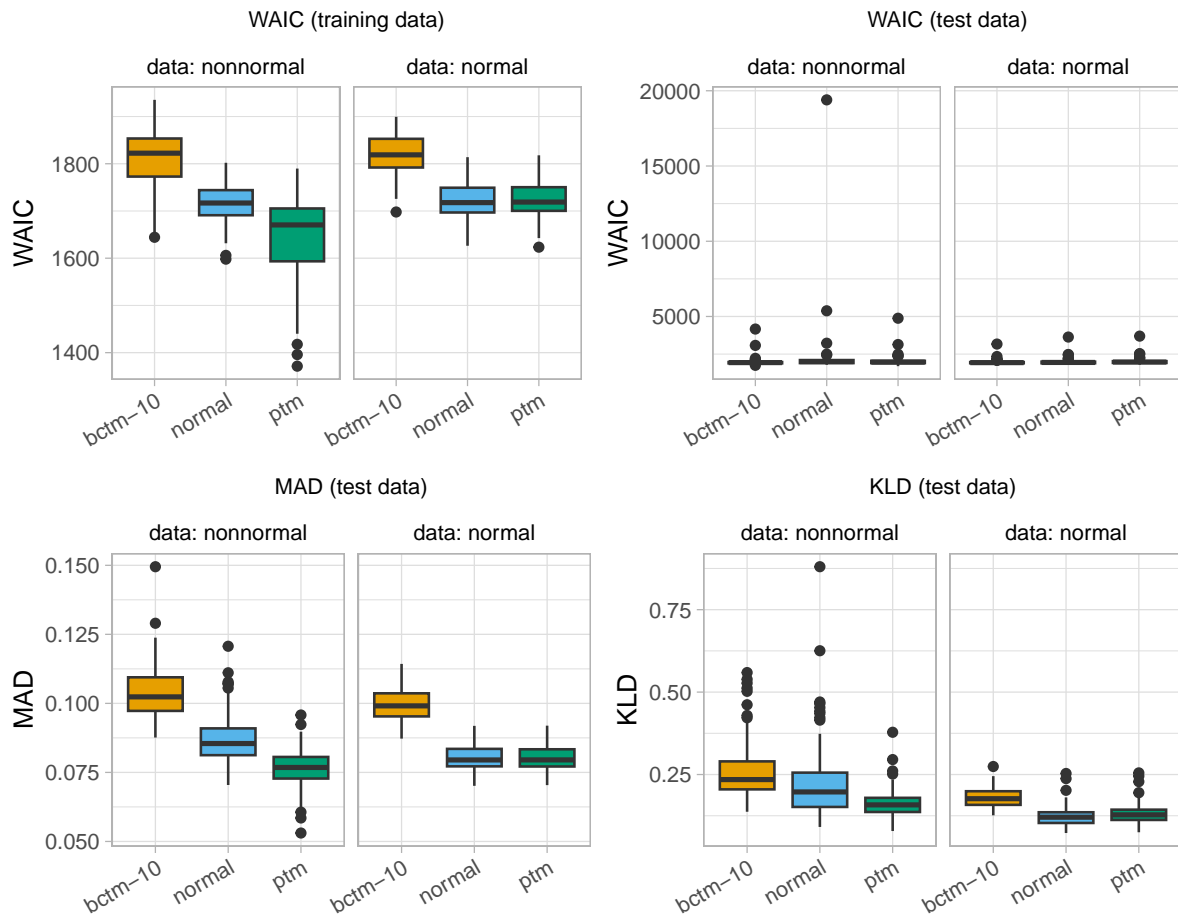


**Figure A6** Performance criteria for comparison of PTMs with the normal location-scale model and the BCTM. The plots depict results for  $N_{\text{obs}} = 500$ . MAD and KLD are averaged over all  $T = 20,000$  samples for each seed.

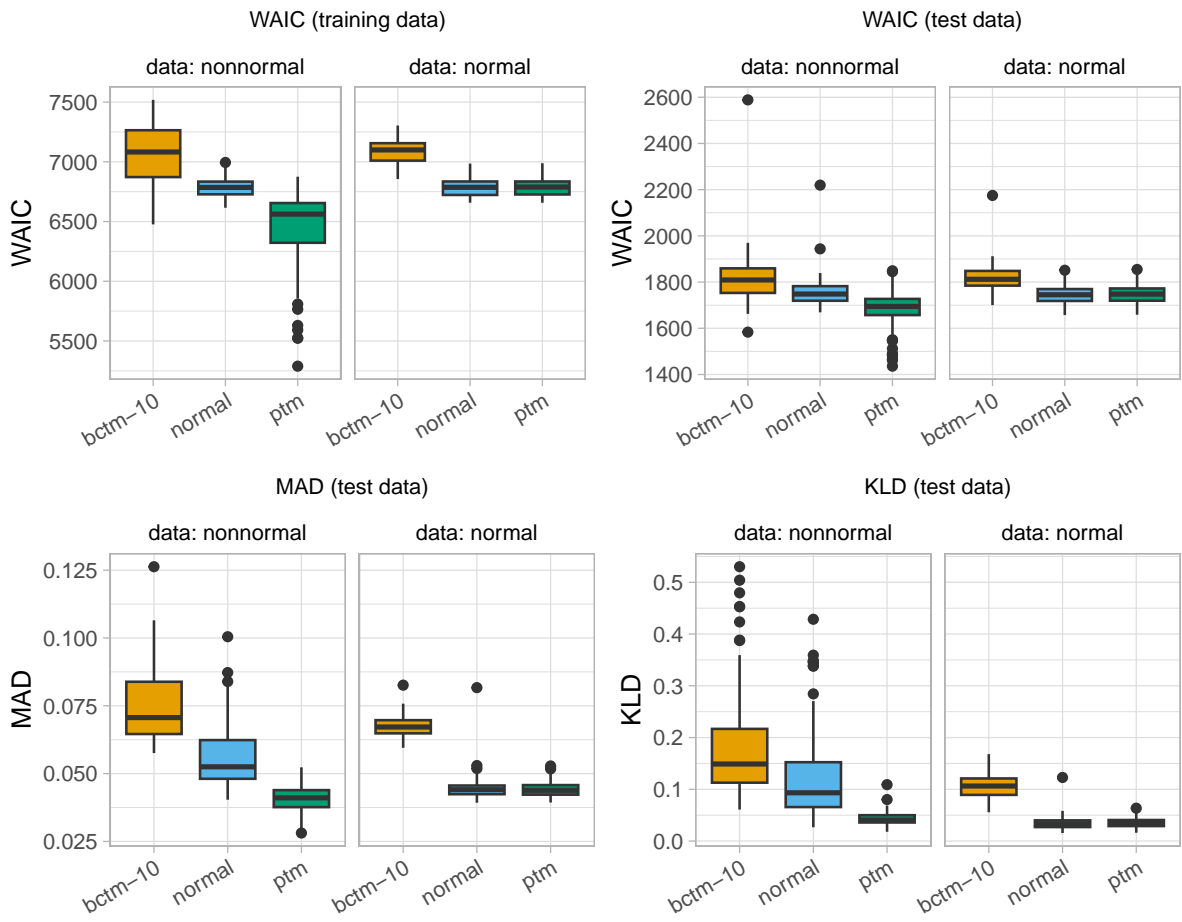


**Figure A7** Performance criteria for comparison of PTMs with the normal location-scale model and the BCTM. The plots depict results for  $N_{\text{obs}} = 2000$ . MAD and KLD are averaged over all  $T = 20,000$  samples for each seed.

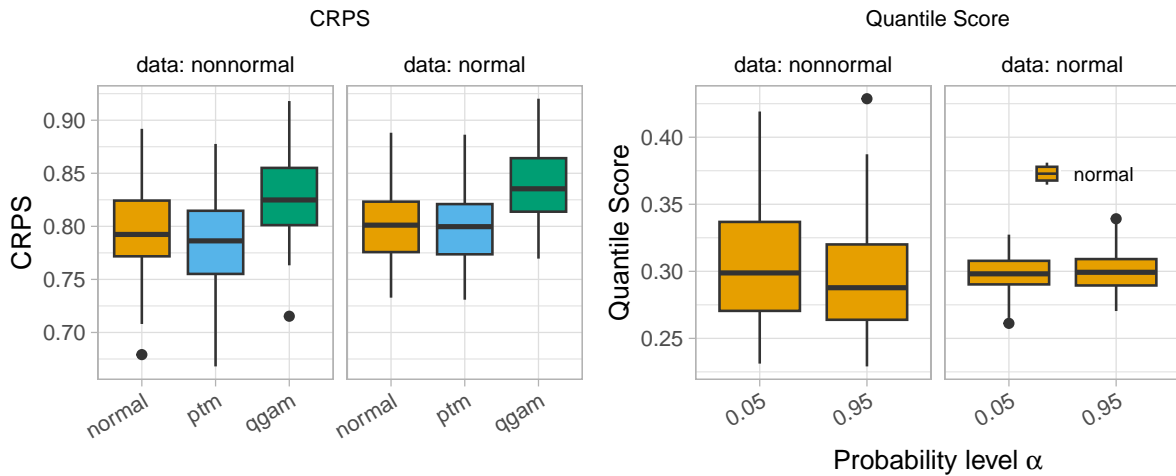


**Figure A8** The left panel shows the continuously ranked probability score for comparison of PTMs with the normal location-scale model and quantile regression. The right panel shows individual quantile score evaluations for the two tail probability levels  $\alpha = 0.05$  and  $\alpha = 0.95$ . The plots depict results for  $N_{\text{obs}} = 500$ .

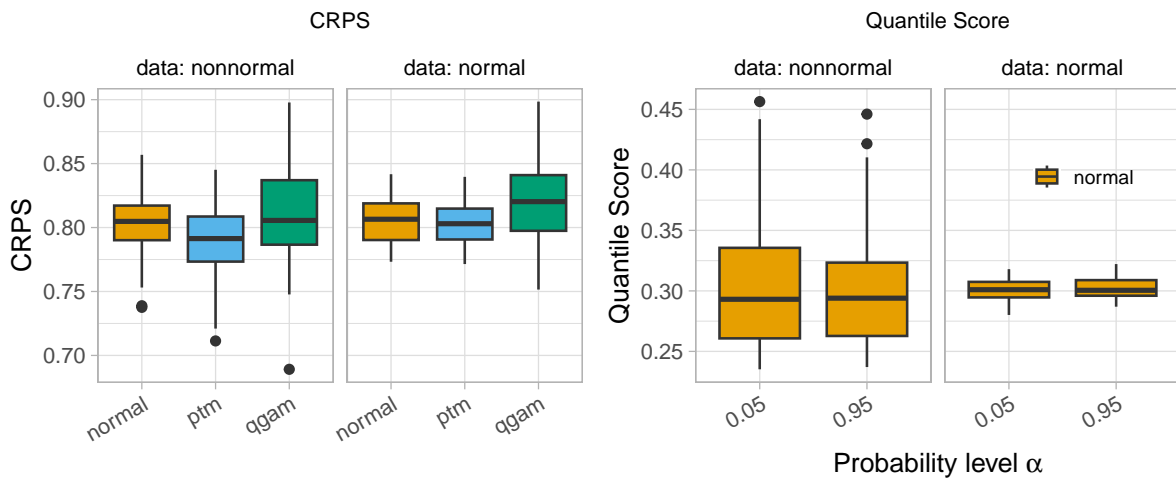


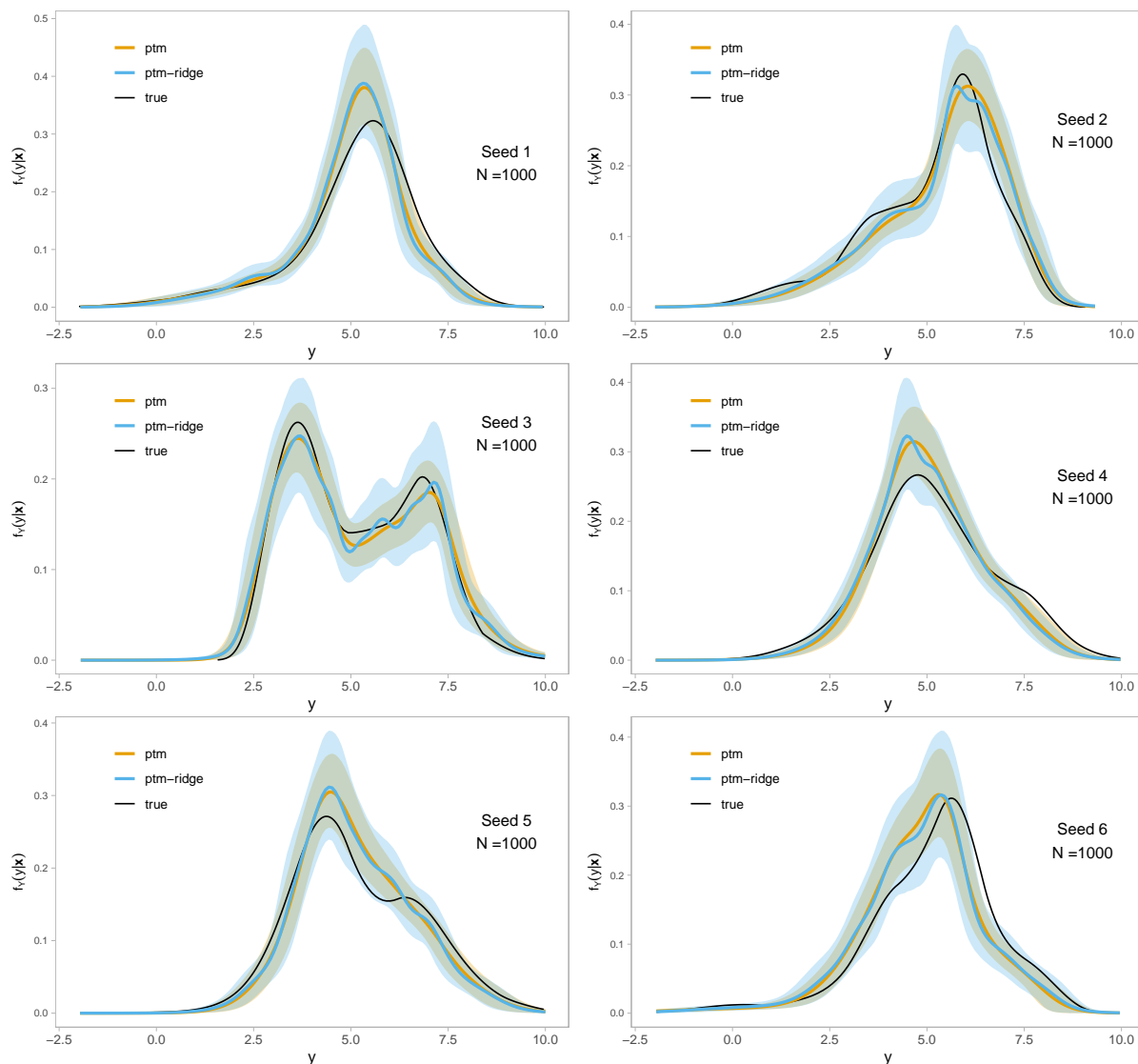
**Figure A9** The left panel shows the continuously ranked probability score for comparison of PTMs with the normal location-scale model and quantile regression. The right panel shows individual quantile score evaluations for the two tail probability levels  $\alpha = 0.05$  and  $\alpha = 0.95$ . The plots depict results for  $N_{\text{obs}} = 2000$ .

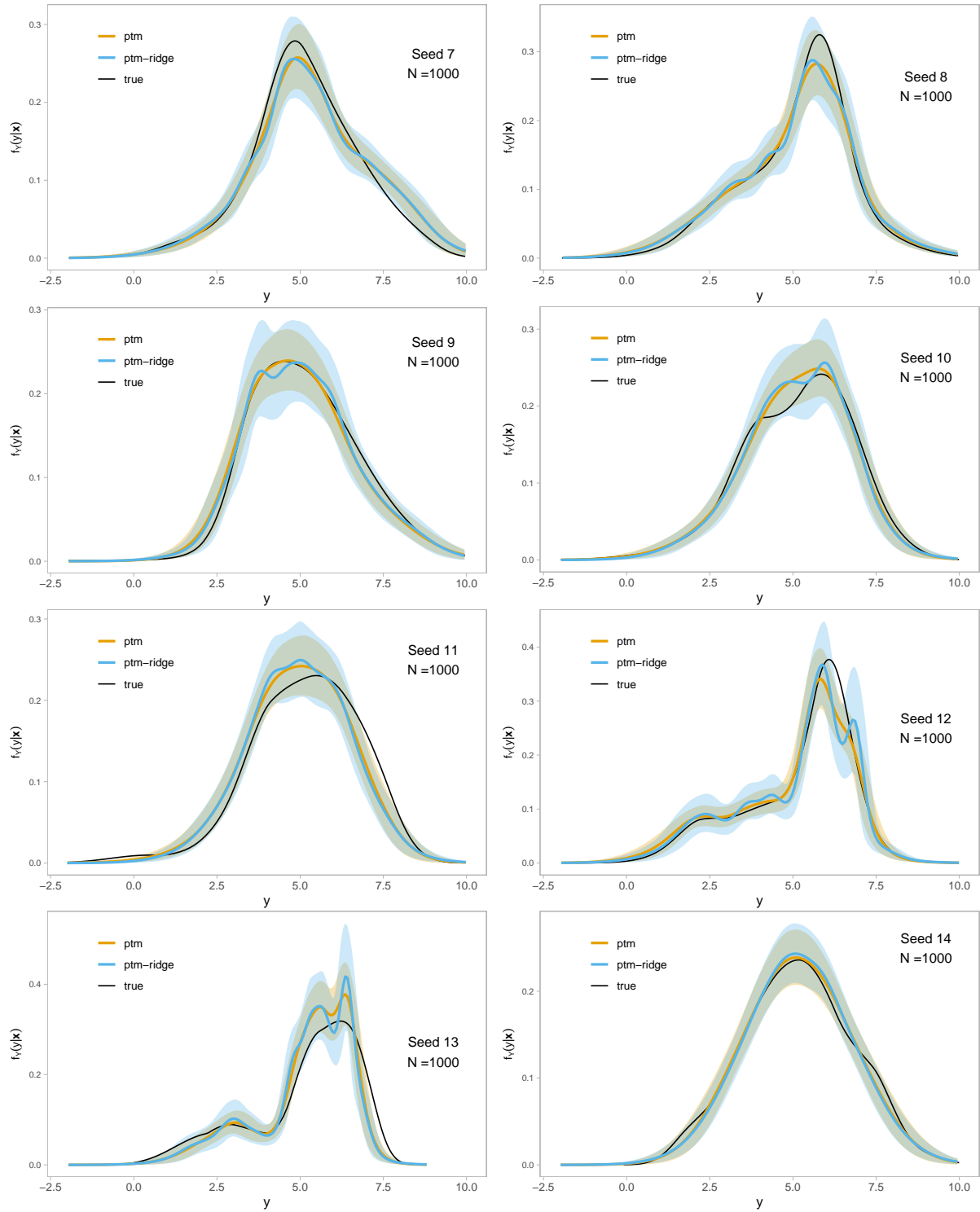
## E.6. Conditional densities

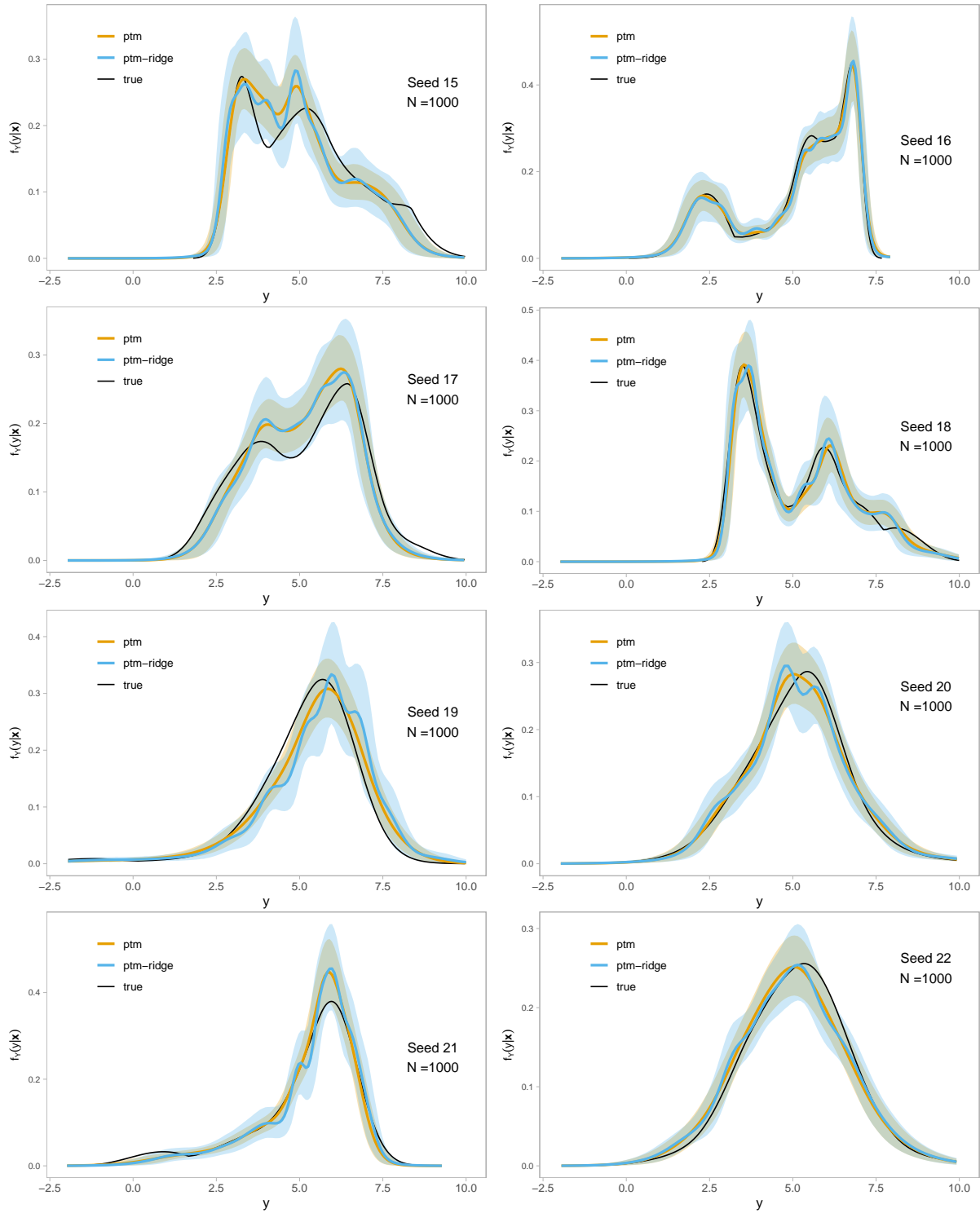
The following plots show the conditional densities at

$$x_1 = x_2 = x_3 = x_4 = 0$$

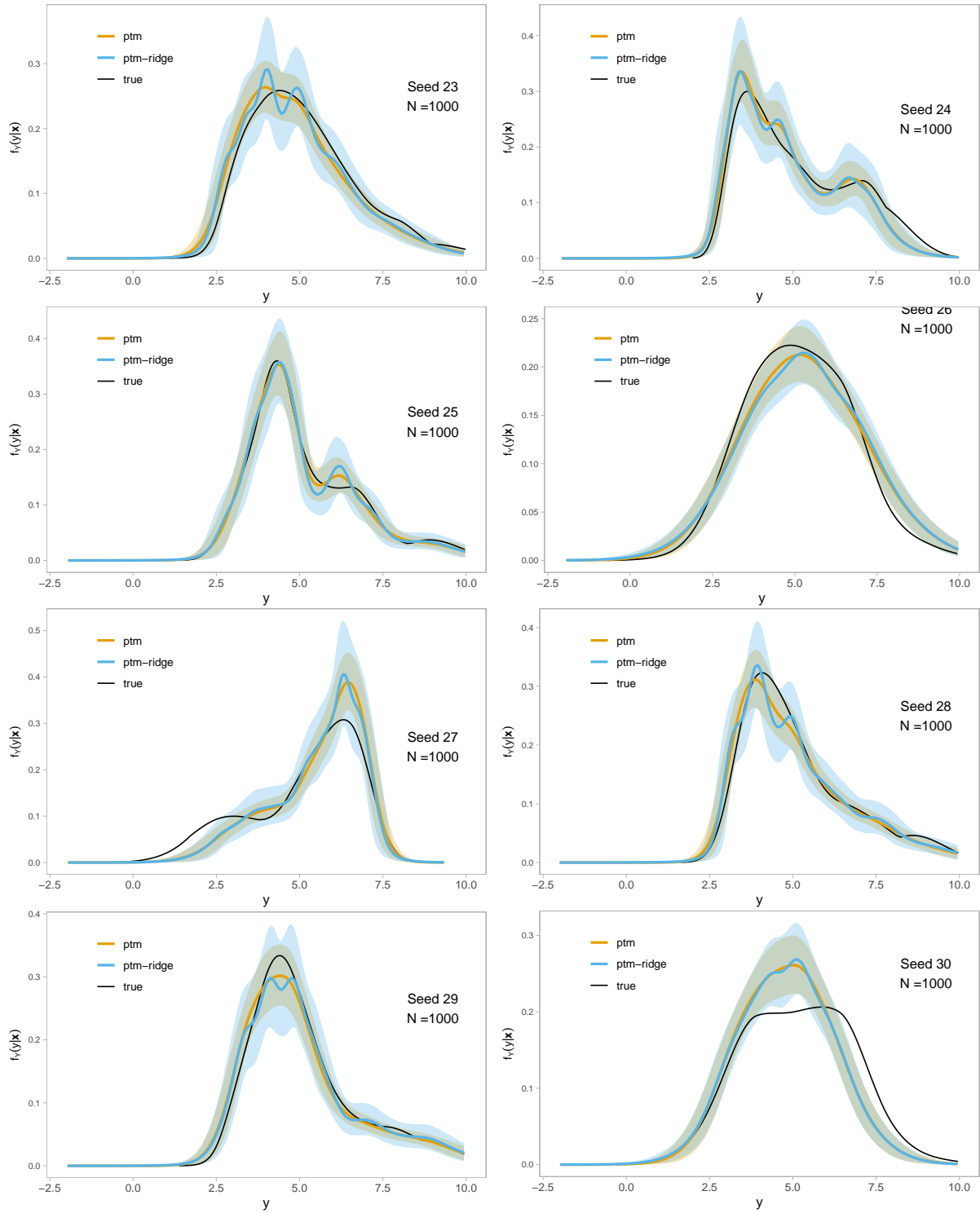
for the models `ptm-bounded` and `ptm-ridge` next to the true density. The shaded areas show posterior quantiles at levels  $\alpha_{\text{low}} = 0.1$  and  $\alpha_{\text{high}} = 0.9$ . Note that this is not equal to the residual density; it is the conditional response density including the location and scale model parts. However, the plots allow us to visually inspect how well the models fit the true densities. The comparison between the model with random walk prior on  $\delta$  (`ptm-bounded`) to the model with ridge prior (`ptm-ridge`) reveals the regularizing effect of the random walk prior. The difference is especially striking in seeds 31, 57, 64, 73, 77, 88, 91. Generally, the difference is evident in much narrower posterior quantiles obtained with the random walk prior.

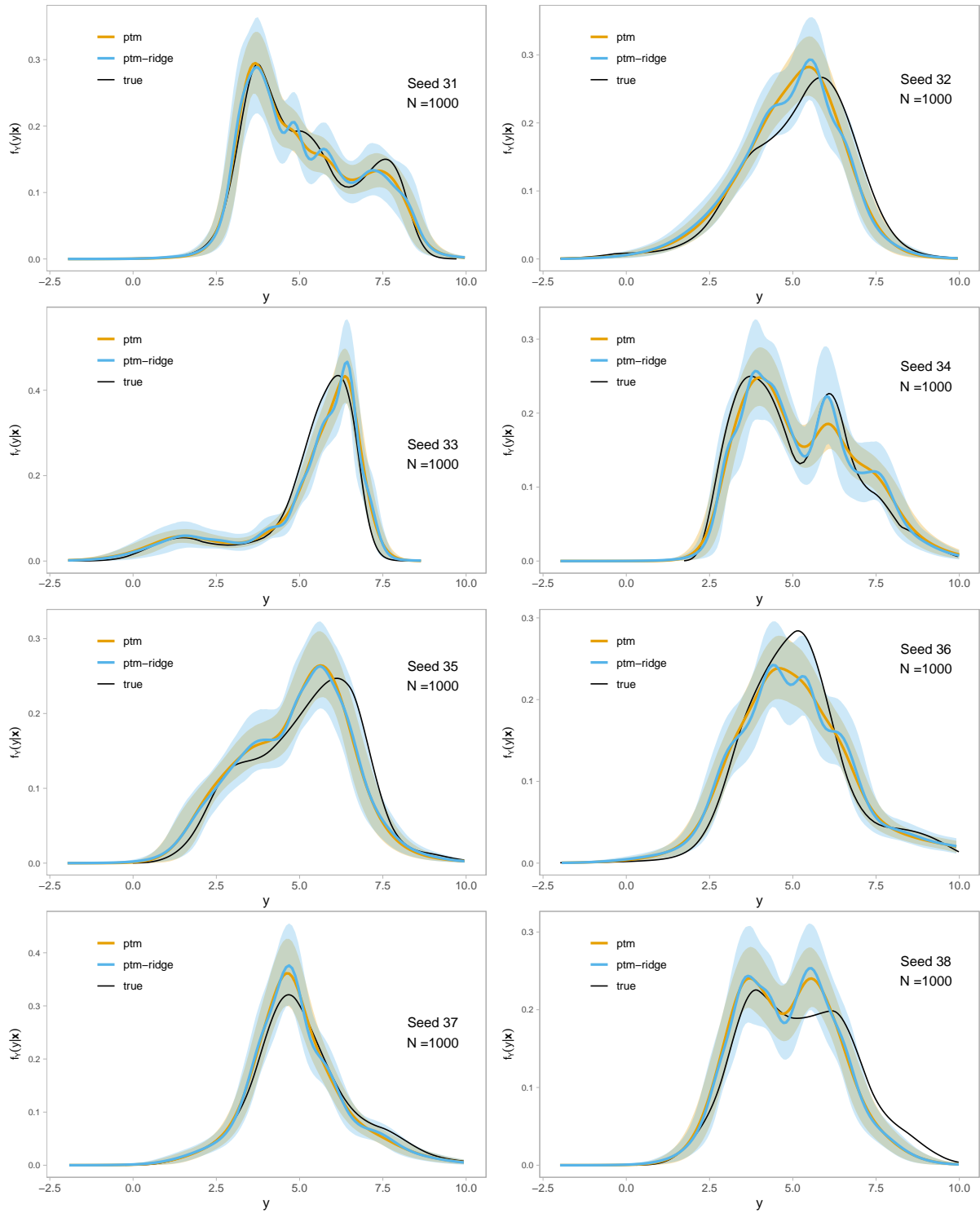


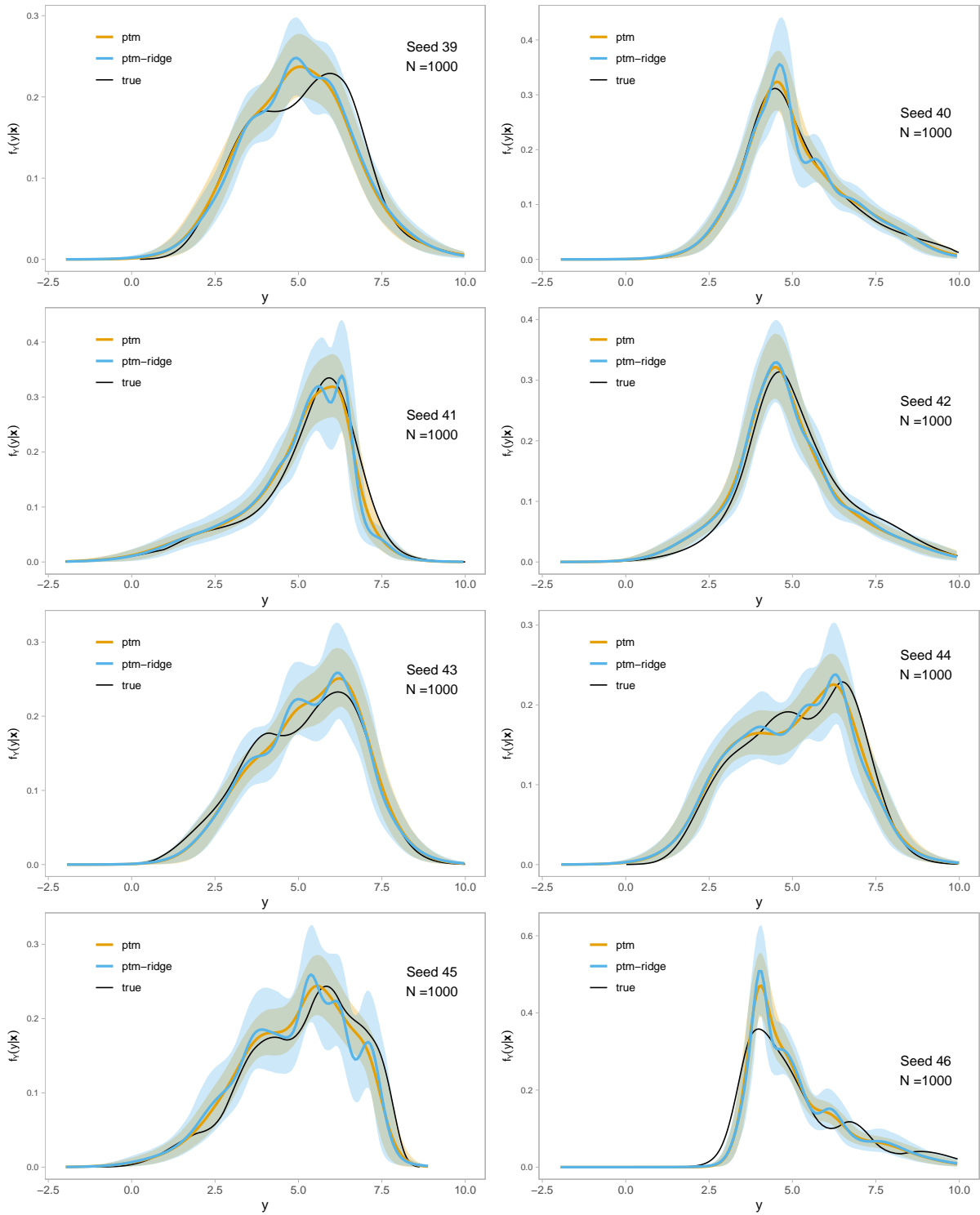


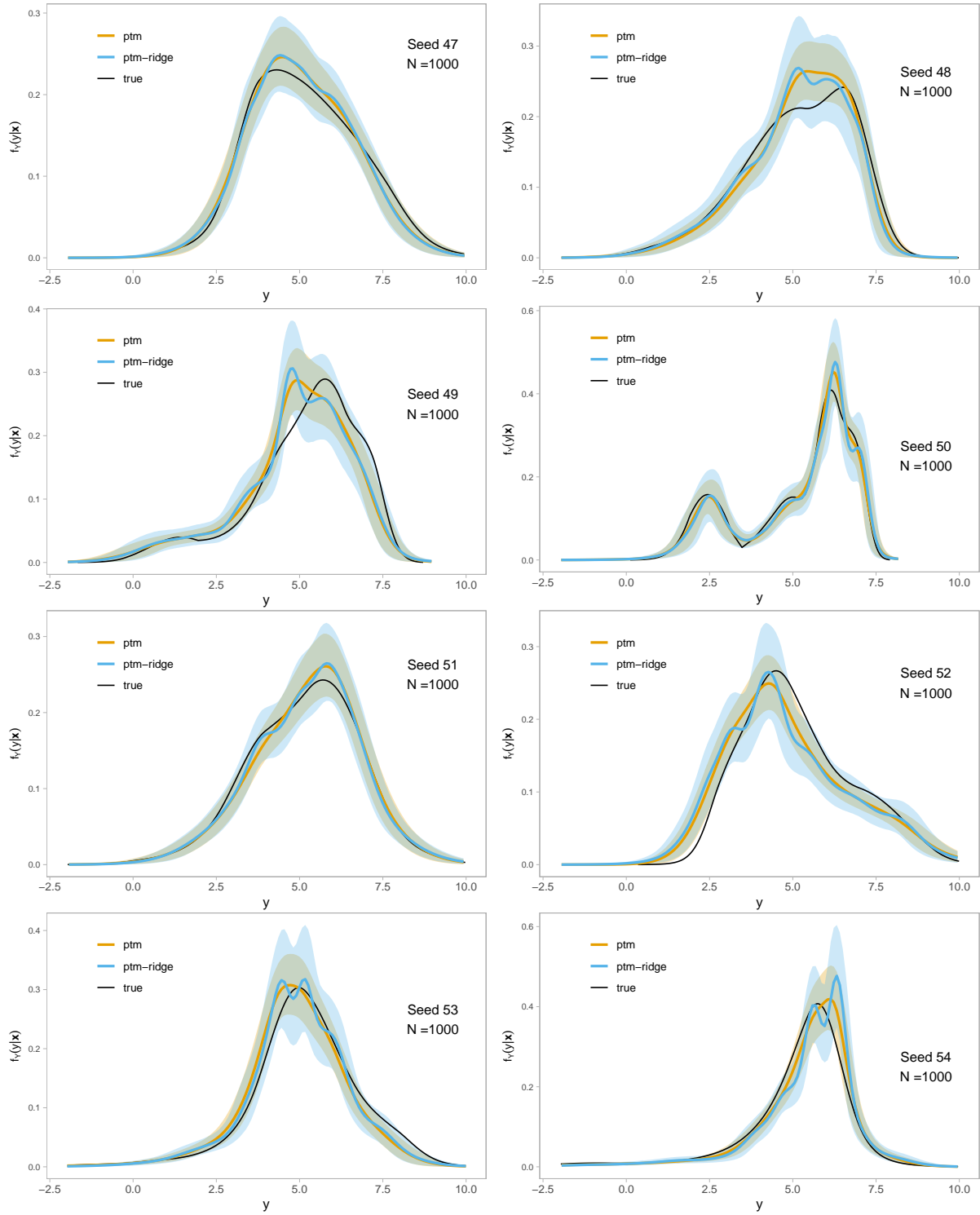


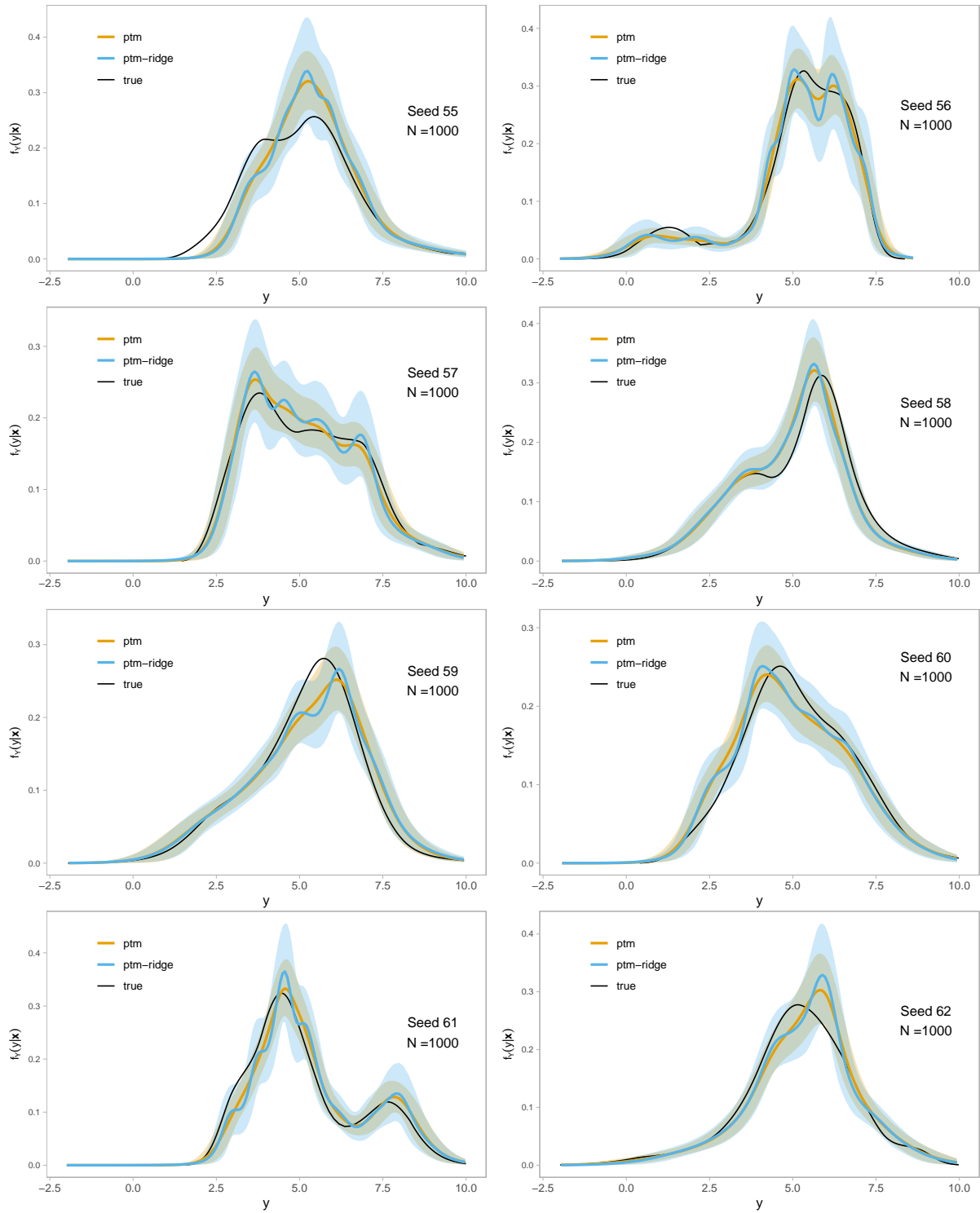


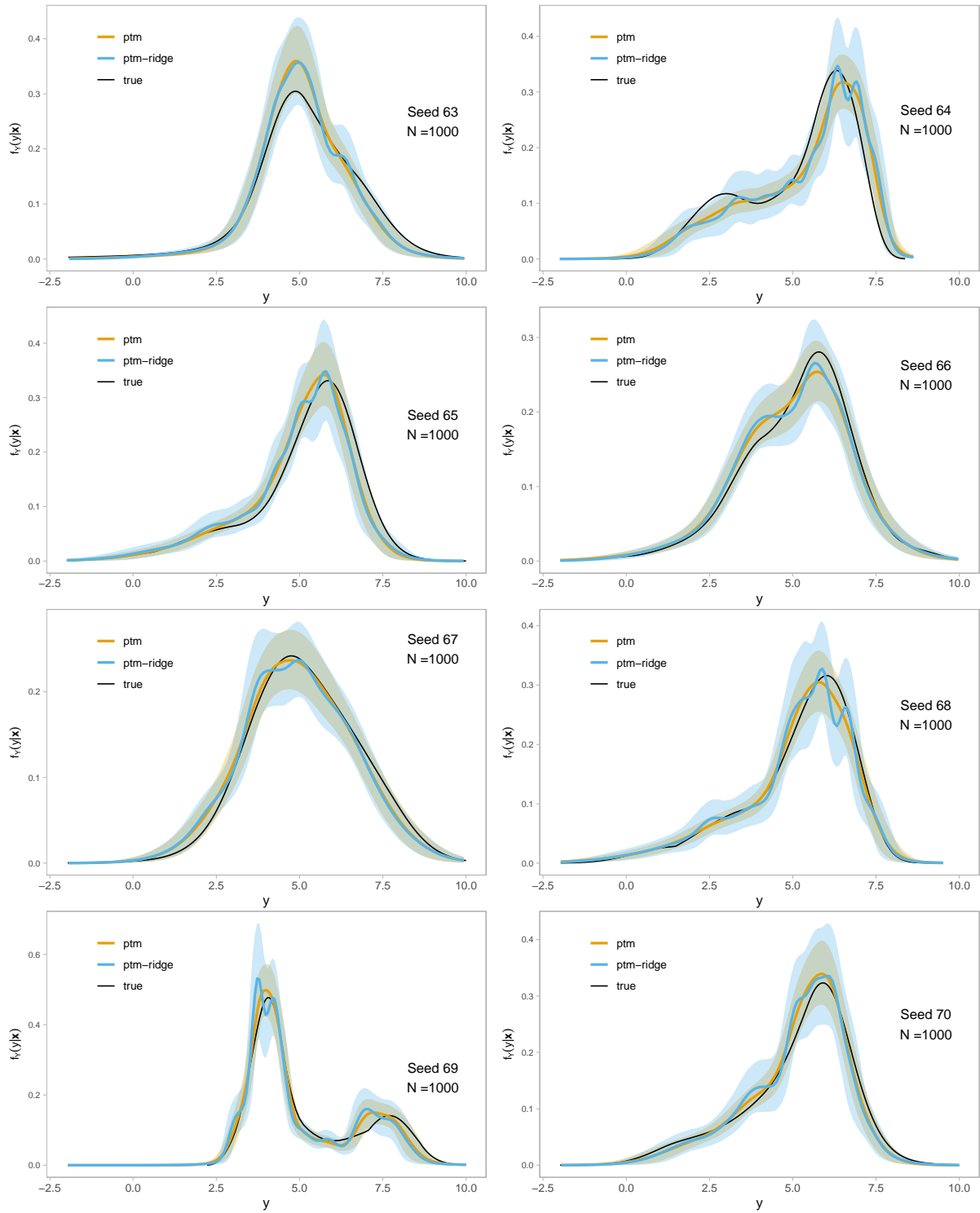


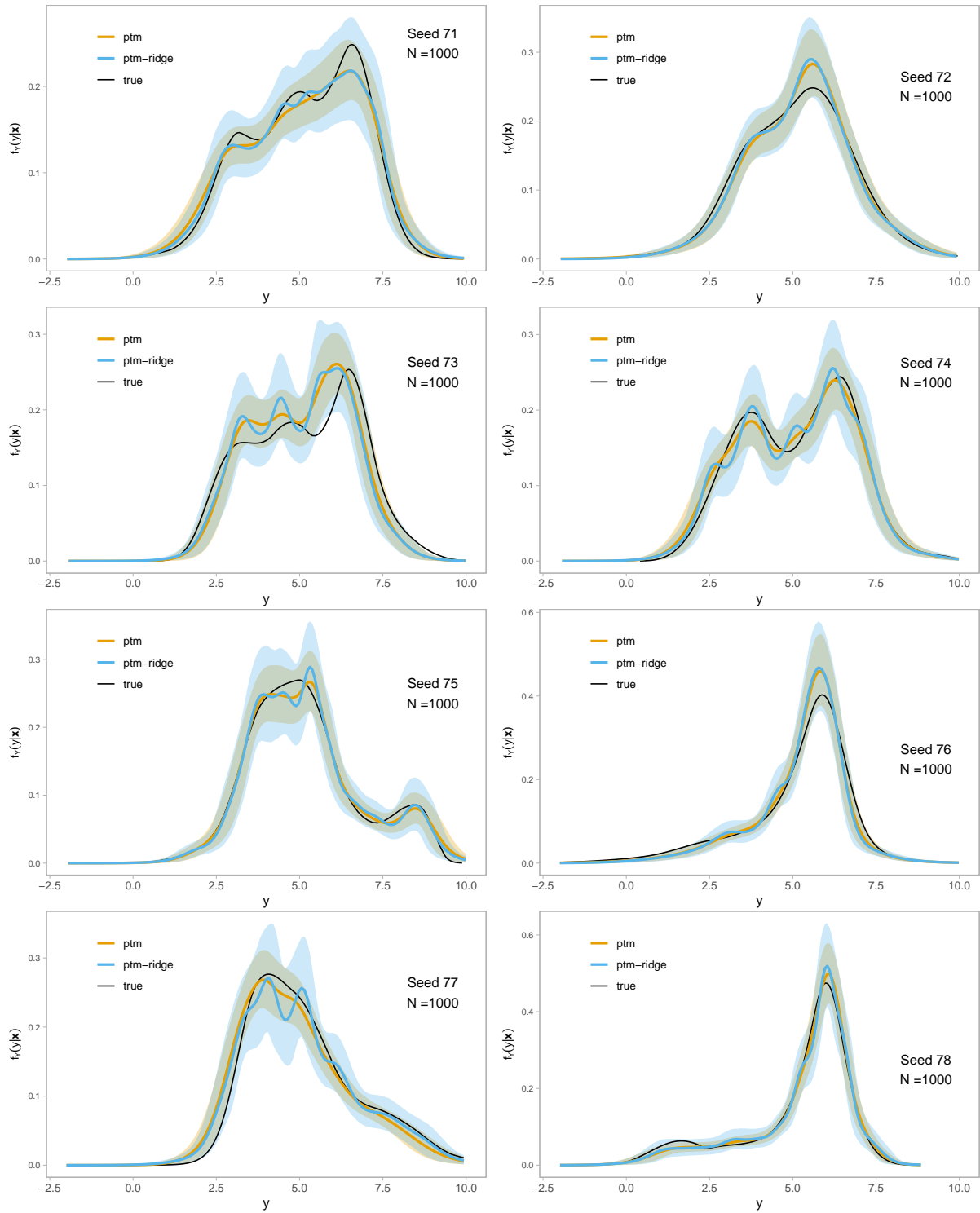


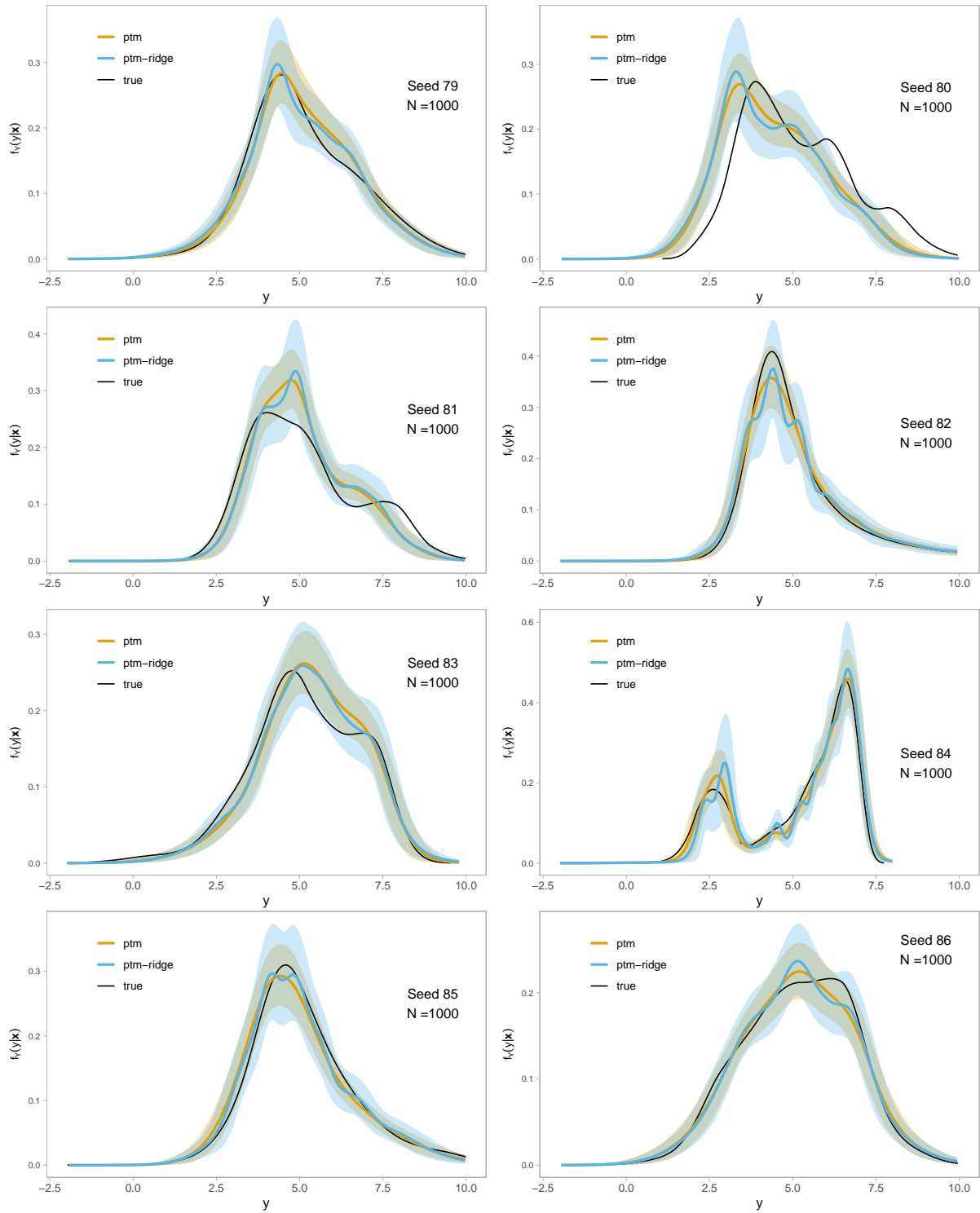




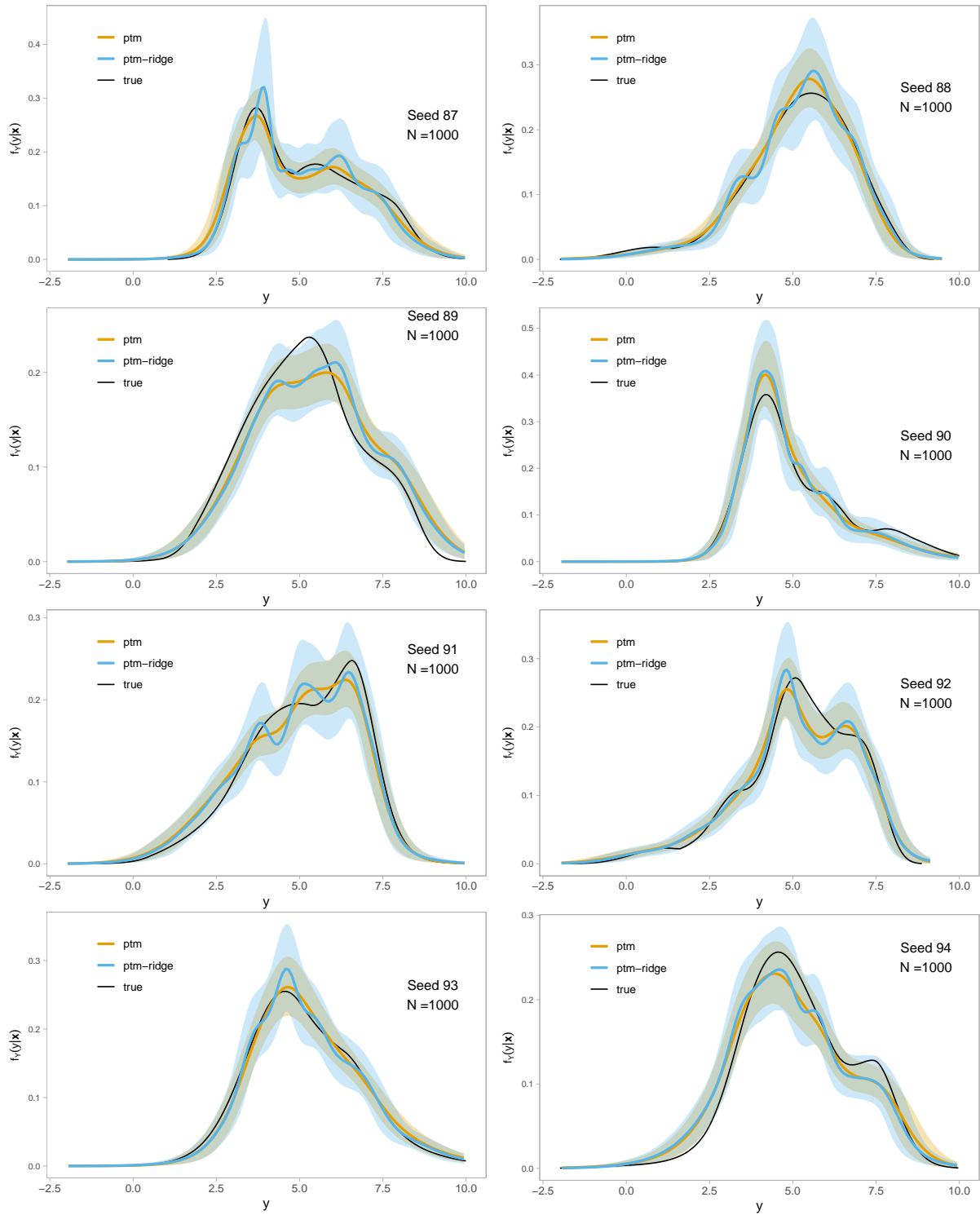


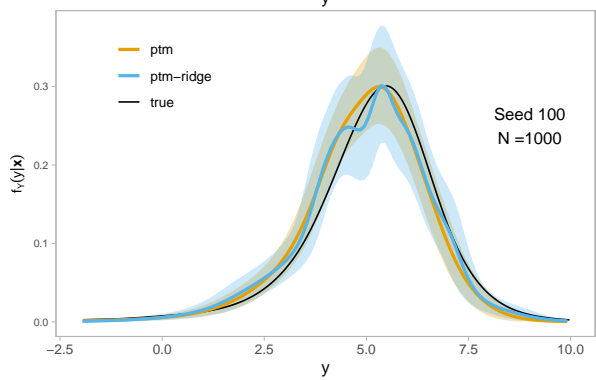
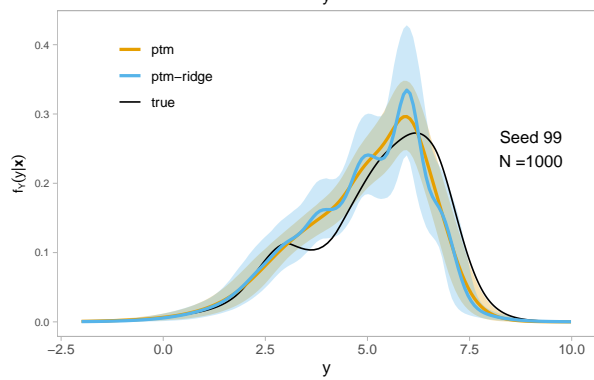
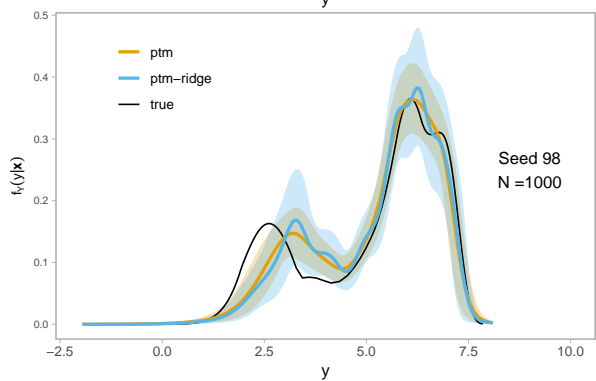
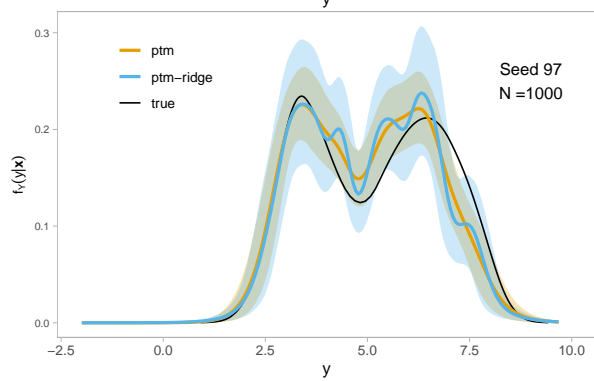
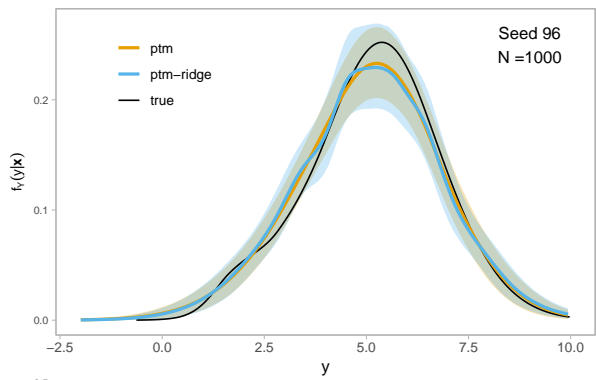
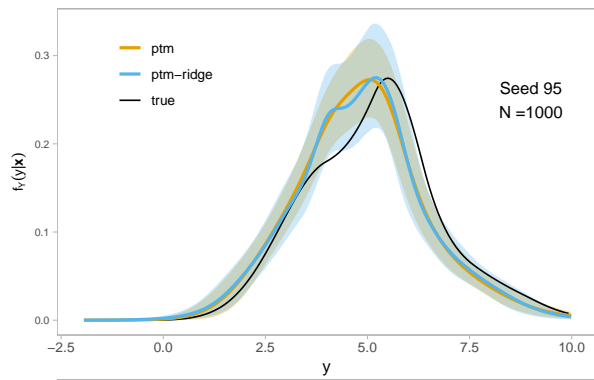












## F. Application: Dutch boys

### F.1. Model diagnostics

**Table A2** Assignment of parameters to kernels.

model	variable	kernel
ptm	age_loc_coef	kernel_00
ptm	age_loc_tau2	kernel_01
ptm	age_scale_coef	kernel_02
ptm	age_scale_tau2	kernel_03
ptm	normalization_shape_transformed	kernel_04
ptm	normalization_tau2_root_transformed	kernel_05
ptm	scaling_factor_unit_transformed	kernel_04
normal	age_loc_coef	kernel_00
normal	age_loc_tau2	kernel_01
normal	age_scale_coef	kernel_02
normal	age_scale_tau2	kernel_03

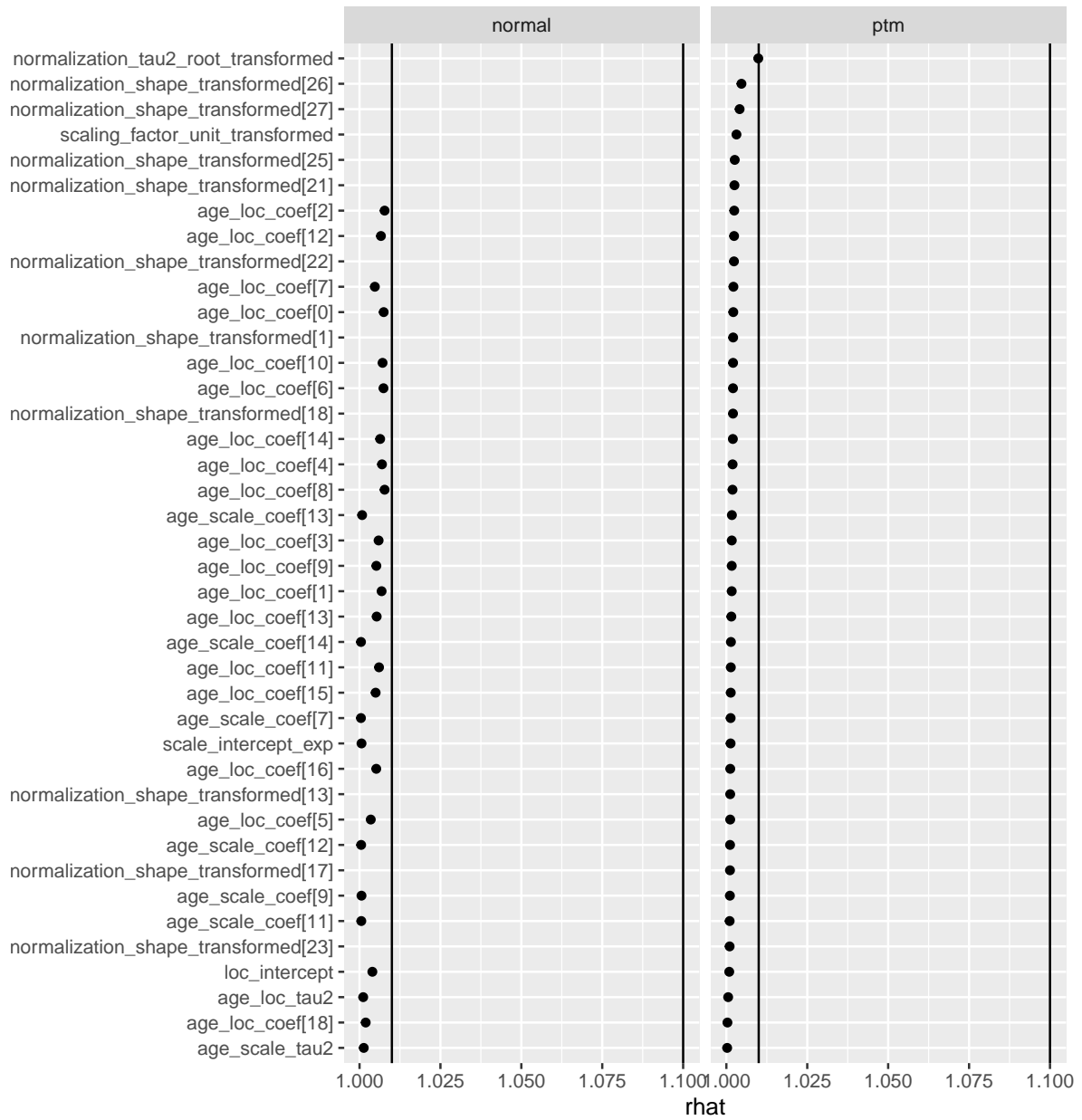
**Table A3** MCMC error overview for errors during posterior sampling.

model	kernel	error_msg	count	relative
ptm	kernel_00	divergent transition	0	0.0000000
ptm	kernel_00	maximum tree depth	0	0.0000000
ptm	kernel_02	divergent transition	3	0.0002500
ptm	kernel_04	divergent transition	0	0.0000000
ptm	kernel_05	divergent transition	0	0.0000000
normal	kernel_00	divergent transition	0	0.0000000
normal	kernel_00	maximum tree depth	0	0.0000000
normal	kernel_02	divergent transition	44	0.0036667

### Convergence: rhat statistic

Vertical lines indicate  $\text{rhat} = 1.01$  and  $\text{rhat} = 1.1$

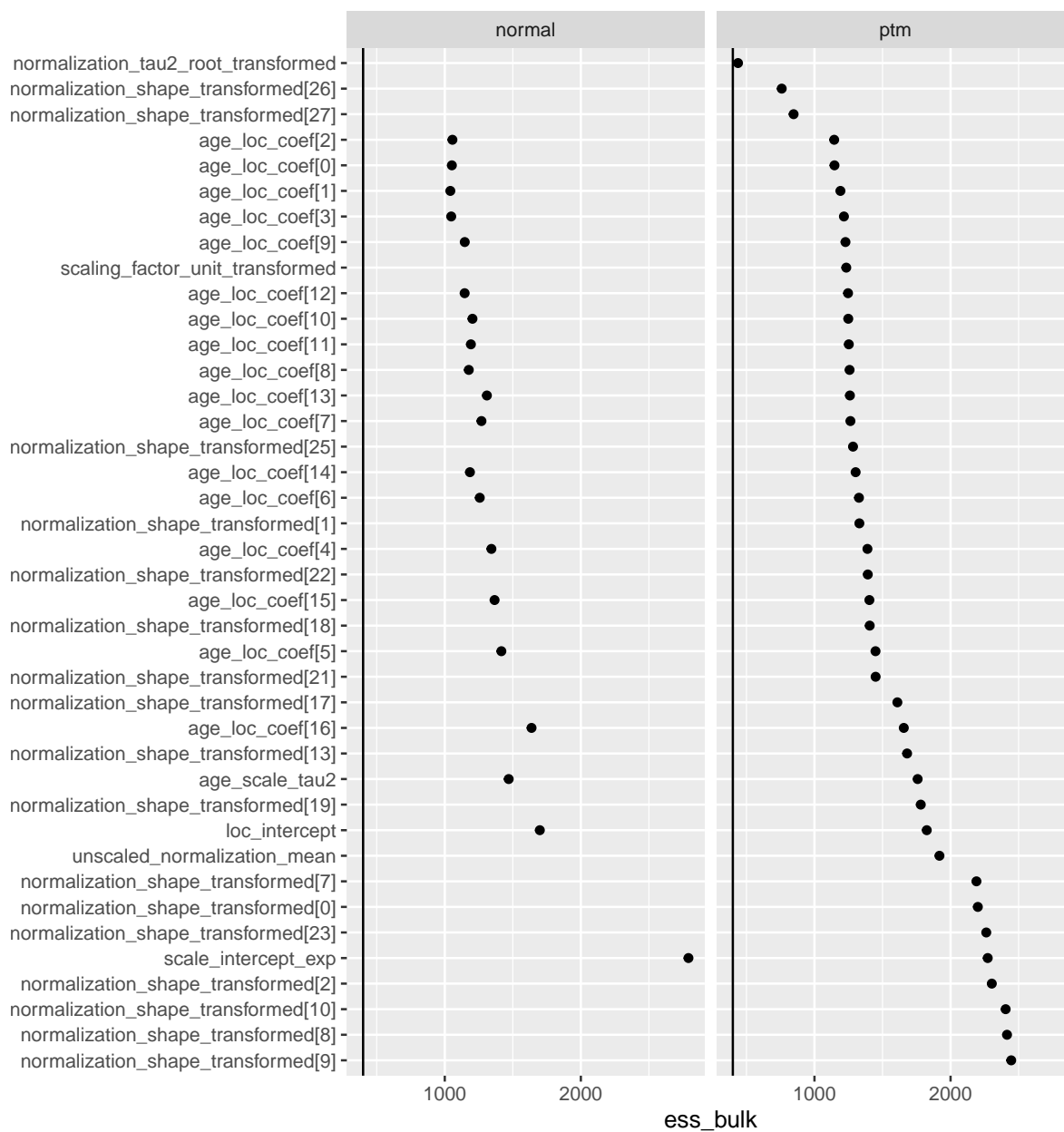
Showing 40 parameters with highest rhat, sorted by PTM



## Effective sample size

Vertical line indicates a value of 400.

Showing 40 parameters with lowest ess\_bulk, sorted by PTM



# G. Application: Framingham heart study

## G.1. Model diagnostics

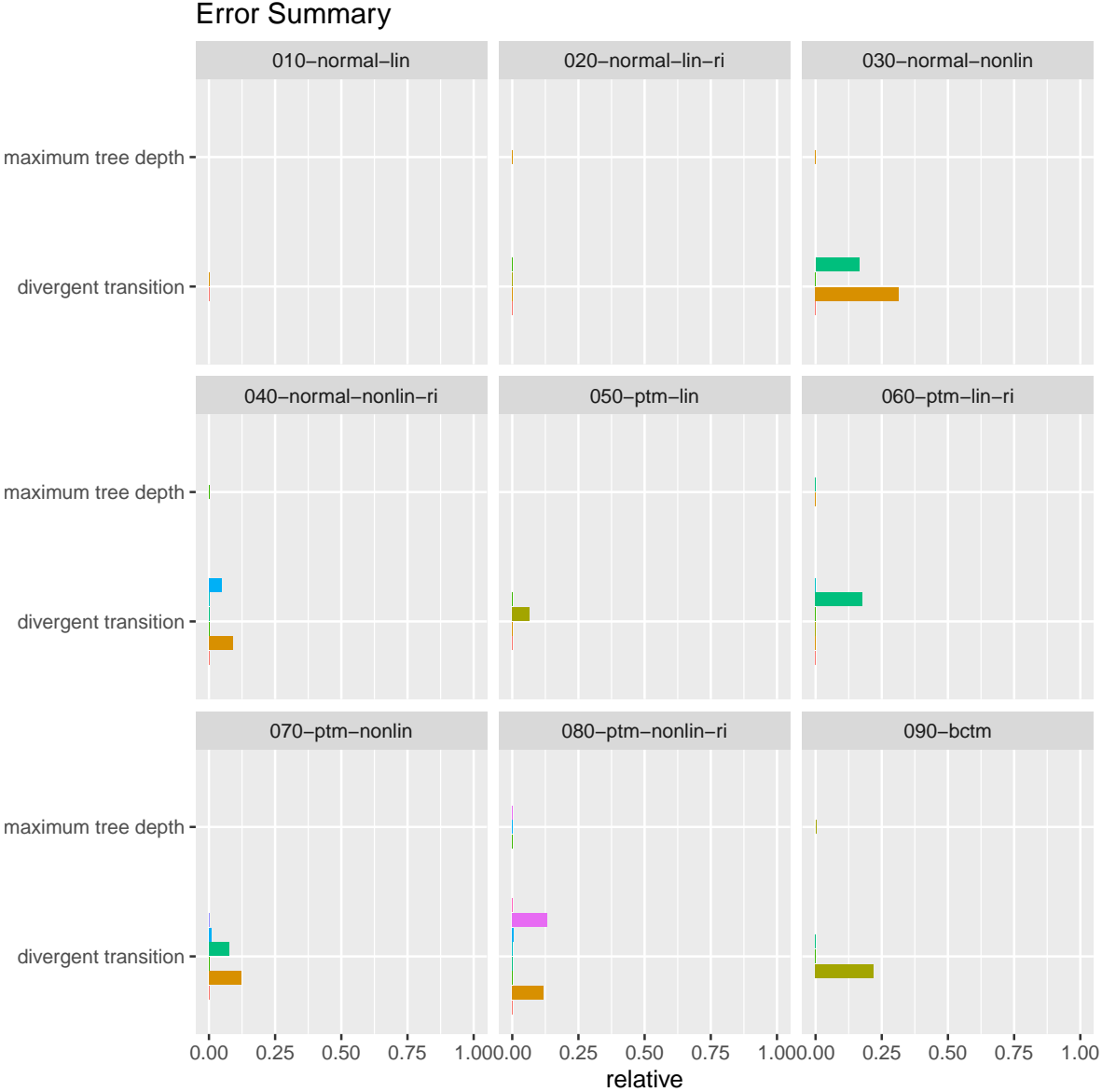


**Table A4** Maximum and mean of the Gelman-Rubin  $\hat{r}$  statistic for all fitted models, rounded to 3 decimals.

Model	Max. $\hat{r}$	Mean $\hat{r}$
010-normal-lin	1.000	1.000
020-normal-lin-ri	1.001	1.000
030-normal-nonlin	1.001	1.000
040-normal-nonlin-ri	1.003	1.000
050-ptm-lin	1.002	1.000
060-ptm-lin-ri	1.003	1.001
070-ptm-nonlin	1.001	1.000
080-ptm-nonlin-ri	1.009	1.001
090-bctm	1.039	1.003

**Table A5** Minimum and mean effective sample size (ESS) for all fitted models, rounded to one decimal.

Model	Min. ESS (bulk)	Mean ESS (bulk)	Min. ESS (tail)	Mean ESS (tail)
010-normal-lin	7182.2	7895.0	7577.5	7764.5
020-normal-lin-ri	2438.9	6150.5	4066.2	7180.5
030-normal-nonlin	1351.7	5049.7	1741.7	4922.6
040-normal-nonlin-ri	1285.1	5182.4	2411.3	6602.0
050-ptm-lin	2174.7	7083.9	4169.8	7117.2
060-ptm-lin-ri	1009.4	5352.1	753.2	6642.3
070-ptm-nonlin	1115.6	5402.5	2494.4	5764.7
080-ptm-nonlin-ri	435.0	4711.6	169.5	6115.4
090-bctm	92.9	4990.1	283.7	5564.2

## G.2. Details on the marginal WAIC

### Models with random intercepts

For the random intercept PTM and normal baseline, we add an i.i.d. random intercept to the location model:

$$\mu_{ij} = \beta_0 + \beta_1 \text{age}_{ij} + \beta_2 \text{year}_{ij} + \beta_3 \text{sex}_{ij} + \zeta_i,$$

where  $i = 1, \dots, 200$  identifies the individual participants and  $j = 1, \dots, n_i$  identifies the observations available for each participant. The random intercept is given by  $\zeta_i$ , with prior structure

$$\begin{aligned} \zeta_i &\sim \mathcal{N}(0, \psi^2) \\ \psi^2 &\sim \text{Weibull}(0.5, 0.05). \end{aligned} \tag{20}$$

The scale model part remains as in the models without random intercepts:

$$\ln \sigma_{ij} = \gamma_0 + \gamma_1 \text{age}_{ij} + \gamma_2 \text{year}_{ij} + \gamma_3 \text{sex}_{ij}.$$

The BCTM with random intercept is

$$\mathbb{P}(\text{cholst} \leq \text{cholst}_{ij}) = \Phi\left(\gamma_0 + (\mathbf{a}(\text{cholst}_{ij})^\top \otimes \mathbf{b}(\text{age}_{ij})^\top)^\top \boldsymbol{\gamma}_1 + \gamma_2 \text{year}_{ij} + \gamma_3 \text{sex}_{ij} + \zeta_i\right),$$

where the prior for  $\zeta_i$  is defined as in (20).

### Marginal and conditional likelihood

For the following exposition, let  $\boldsymbol{\vartheta}$  denote all regression coefficients of the respective models from above, except for the random intercept  $\boldsymbol{\zeta} = [\zeta_1, \dots, \zeta_n]^\top$ . Further, we write  $y$  for the response instead of cholst to shorten the notation. Treating the random intercept as a parameter, we get the conditional likelihood

$$f_c(\mathbf{y}|\boldsymbol{\vartheta}, \boldsymbol{\zeta}) = \prod_{i=1}^N f_c(\mathbf{y}_i|\boldsymbol{\vartheta}, \zeta_i), \tag{21}$$

with the joint conditional density of observations for person  $i$  given by

$$f_c(\mathbf{y}_i|\boldsymbol{\vartheta}, \zeta_i) = \prod_{j=1}^{n_i} f_c(y_{ij}|\boldsymbol{\vartheta}, \zeta_i)$$

under the assumption of conditional independence. Now, assuming an i.i.d. prior  $\zeta_i \sim \mathcal{N}(0, \psi^2)$ , and letting  $\mathcal{N}(\zeta_i|\psi^2)$  denote the corresponding prior probability density function, we can inte-



grate out the random intercept of (21) to obtain the marginal likelihood

$$f_m(\mathbf{y}|\boldsymbol{\vartheta}, \psi^2) = \prod_{i=1}^N \int f_c(\mathbf{y}_i|\boldsymbol{\vartheta}, \zeta_i) \mathcal{N}(\zeta_i|\psi^2) d\zeta_i.$$

with cluster-contributions

$$f_m(\mathbf{y}_i|\boldsymbol{\vartheta}, \psi^2) = \int f_c(\mathbf{y}_i|\boldsymbol{\vartheta}, \zeta_i) \mathcal{N}(\zeta_i|\psi^2) d\zeta_i. \quad (22)$$

This likelihood is marginal with respect to the random intercept, but of course not with respect to  $\boldsymbol{\vartheta}$  and  $\psi^2$ .

### Conditional WAIC

The basis for the WAIC is the assessment of predictive accuracy via the log posterior predictive density for a new observation  $y^*$ , given by

$$\ln f_{c, \text{post}}(y^*) = \ln \int f_c(y^*|\boldsymbol{\vartheta}, \zeta) p(\boldsymbol{\vartheta}, \zeta|\mathbf{y}) d\boldsymbol{\vartheta} d\zeta, \quad (23)$$

where  $f_c$  is the (conditional) likelihood (21) and  $p(\boldsymbol{\vartheta}, \zeta|\mathbf{y})$  is the posterior distribution given a vector of observed data  $\mathbf{y}$ . The expectation of the log posterior predictive density with respect to the true distribution of the new data is called the *expected log predictive density* and given by

$$\text{elpd}(y^*) = \int \ln f_{c, \text{post}}(y^*) \cdot f_{\text{true}}(y^*) dy^*.$$

Assuming independence given the model parameters, the joint elpd for a sample of new data points  $\{y_i^*\}_{i=1}^n$  is given by the *expected log pointwise predictive density*

$$\text{elppd} = \sum_{i=1}^n \text{elpd}(y_i^*).$$

The WAIC aims to estimate the elppd from the same data that were used to fit the model. It is given by

$$\text{WAIC}_{\text{elppd}} = \text{lppd} - p_{\text{WAIC}},$$

where the *log pointwise predictive density* lppd is obtained from taking the log of the average posterior predictive density

$$\text{lppd} = \sum_{i=1}^N \ln \left( \frac{1}{T} \sum_{t=1}^T f_c^{[t]}(\mathbf{y}_i|\boldsymbol{\vartheta}, \zeta_i^{[t]}) \right) \quad (24)$$

and the *effective number of parameters* is the sum of pointwise sample variances of the log posterior predictive density over the posterior parameter samples

$$p_{\text{WAIC}} = \sum_{i=1}^N \widehat{\text{Var}}_{t=1}^T (\ln f_c^{[t]}(\mathbf{y}_i | \boldsymbol{\vartheta}^{[t]}, \zeta_i^{[t]})).$$

To get the WAIC on the deviance scale, we multiply by  $-2$ :

$$\text{WAIC}_{\text{deviance}} = -2(\text{lppd} - p_{\text{WAIC}}). \quad (25)$$

We call this the conditional WAIC because it uses the conditional likelihood (21) to compute the lppd. It assumes that we know the cluster-membership (here: the person) for which we want to make predictions, and that this cluster (here: person) was a part of the data used to fit the model.

### Marginal WAIC

The goal of the marginal WAIC is to provide a measure of predictive accuracy for the case that we do not know the cluster-membership of new observations, or that the cluster of new observations was not part of the data used to fit the model. To this end, the conditional likelihood is replaced by the marginal likelihood (22) in the computation of both the lppd (24) and the effective number of parameters (25). The lppd is then given by

$$\text{lppd}_m = \sum_{i=1}^N \ln \left( \frac{1}{T} \sum_{t=1}^T f_m(\mathbf{y}_i | \boldsymbol{\vartheta}^{[t]}, \psi^2 [t]) \right) \quad (26)$$

and the effective number of parameters is given by

$$p_{m,\text{WAIC}} = \sum_{i=1}^N \widehat{\text{Var}}_{t=1}^T (\ln f_m(\mathbf{y}_i | \boldsymbol{\vartheta}^{[t]}, \psi^2 [t])),$$

such that the marginal WAIC is

$$\text{WAIC}_{m,\text{deviance}} = -2(\text{lppd}_m - p_{m,\text{WAIC}}).$$

Note that this marginalized version of the WAIC assumes that the random intercept is normally distributed, since we integrate over its normal prior to obtain the marginal likelihood (22). Posterior sampling information about the random intercept only enters the marginal WAIC via its variance  $\psi^2$ . Note also that, by using the joint marginal likelihood for each cluster, we still take the clustering of observations into account here.

## Evaluating the marginal WAIC

To evaluate the marginal WAIC, we follow the approach of Merkle et al. (2019) and evaluate the marginal likelihood contribution (22) by numerical integration. Namely, we implement the adaptive Gauss-Hermite quadrature produce described in Appendix C of Merkle et al. (2019).

### G.3. Parameter estimates

Table A6 shows parameter estimates for the covariates included with linear effects in the linear normal model, the linear PTM model, and the BCTM. Note that the sign of the parameter estimates in the BCTM is reversed, i.e. a negative coefficient means that the corresponding covariate has a positive association with the response's location. However, also note that the coefficients in the BCTM cannot be interpreted directly. Rather than operating on the response level, like in the normal model and the PTM, these coefficients reflect associations on the *latent* level, after normalization. Specifically, the BCTM

$$\mathbb{P}(\text{cholst} \leq \text{cholst}_{ij}) = \Phi\left(\gamma_0 + (\mathbf{a}(\text{cholst}_{ij})^\top \otimes \mathbf{b}(\text{age}_{ij})^\top)^\top \boldsymbol{\gamma}_1 + \gamma_2 \text{year}_{ij} + \gamma_3 \text{sex}_{ij}\right),$$

can be written as

$$\mathbb{P}(\text{cholst} \leq \text{cholst}_{ij}) = \Phi(h(\text{cholst}_{ij}|\mathbf{x}_{ij})),$$

where  $\mathbf{x}_{ij}$  collects the covariate observations for observation  $ij$  and the transformation function  $h$  is given by

$$h(\text{cholst}_{ij}|\mathbf{x}_{ij}) = \gamma_0 + h_1(\text{cholst}_{ij}|\text{age}_{ij}) + \gamma_2 \text{year}_{ij} + \gamma_3 \text{sex}_{ij}.$$

The partial transformation function  $h_1$  is

$$h_1(\text{cholst}_{ij}|\text{age}_{ij}) = (\mathbf{a}(\text{cholst}_{ij})^\top \otimes \mathbf{b}(\text{age}_{ij})^\top)^\top \boldsymbol{\gamma}_1.$$

We can now observe that the model implies

$$h(\text{cholst}_{ij}|\mathbf{x}_{ij}) \sim \mathcal{N}(0, 1),$$

such that we can also write

$$h_1(\text{cholst}_{ij}|\text{age}_{ij}) \sim \mathcal{N}(\nu_{ij}, 1),$$

where

$$\nu_{ij} = -\gamma_0 - \gamma_2 \text{year}_{ij} - \gamma_3 \text{sex}_{ij}.$$

This offers up a way to understand the BCTM's transformation function. The function  $h_1$  transforms the response  $\text{cholst}$  to follow a normal distribution with scale one and some mean  $\nu_{ij}$ . This transformation is allowed to vary in a flexible way, depending on the age of the participant. The covariates  $\text{year}$  and  $\text{sex}$  then act on the expectation  $\nu_{ij}$  of the *latent*, or *normalized* and scaled response  $h_1(\text{cholst}_{ij}|\text{age}_{ij})$ . While this parameter does have a monotonic relationship with the response's expectation, we have to keep in mind that  $h_1$  is a nonlinear transformation. This means that, apart from the sign of the coefficients in  $\nu_{ij}$ , there is not much we can interpret about them, since the implied conditional response distribution may be affected in hard-to-predict ways.

**Table A6** Parameter estimates for linear regression coefficients in different models fitted to the Framingham dataset. The columns beta refer to parameter estimates in the location model part. The columns gamma refer to parameter estimates in the scale model part. The columns labelled HDI give highest posterior density intervals at the .90 level.

Covariate	Base model				Random Intercept model			
	$\hat{\beta}$	HDI	$\hat{\gamma}$	HDI	$\hat{\beta}$	HDI	$\hat{\gamma}$	HDI
<b>Normal</b>								
Age	0.28	[ 0.23, 0.33]	0.10	[ 0.07, 0.14]	0.26	[ 0.15, 0.35]	0.10	[ 0.06, 0.14]
Year	0.07	[ 0.06, 0.08]	0.02	[ 0.01, 0.03]	0.07	[ 0.06, 0.07]	-0.01	[-0.02, 0.01]
Sex	-0.07	[-0.17, 0.02]	-0.03	[-0.10, 0.05]	-0.03	[-0.23, 0.17]	-0.02	[-0.10, 0.06]
<b>PTM</b>								
Age	0.30	[ 0.25, 0.35]	0.14	[ 0.10, 0.18]	0.26	[ 0.16, 0.35]	0.10	[ 0.06, 0.15]
Year	0.07	[ 0.06, 0.08]	0.02	[ 0.01, 0.03]	0.06	[ 0.06, 0.07]	-0.01	[-0.02, 0.01]
Sex	-0.07	[-0.16, 0.03]	0.02	[-0.06, 0.09]	-0.03	[-0.22, 0.17]	-0.01	[-0.10, 0.08]
<b>BCTM</b>								
Age	-	-	-	-	-	-	-	-
Year	-0.07	[-0.09, -0.06]	-	-	-0.13	[-0.15, -0.12]	-	-
Sex	0.04	[-0.06, 0.15]	-	-	0.12	[-0.29, 0.52]	-	-